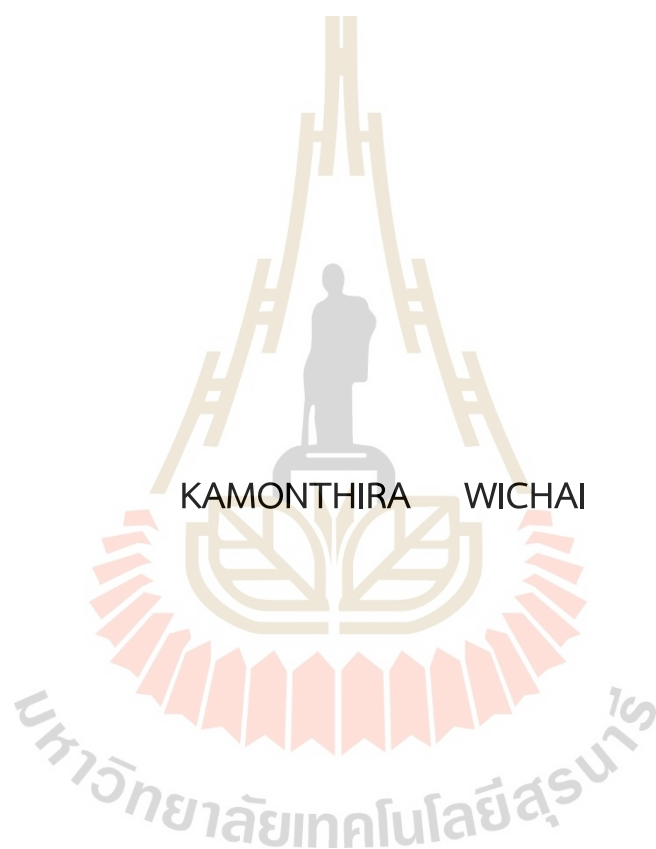


MULTISCALE MOLECULAR SIMULATION AND EXPERIMENTAL
STUDIES OF STRUCTURAL PROPERTIES OF POLYSTYRENE AND ITS
DERIVATIVE



A Thesis Submitted in Partial Fulfillment of the Requirements for the
Degree of Master of Science in Chemistry
Suranaree University of Technology
Academic Year 2021

การจำลองโมเลกุลหลายระดับและการทดลองเพื่อศึกษาสมบัติเชิงโครงสร้าง
ของพอลิไสตรีน

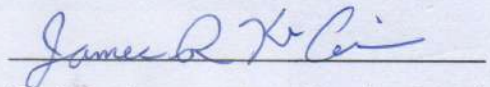


วิทยานิพนธ์นี้เป็นส่วนหนึ่งของการศึกษาตามหลักสูตรปริญญาวิทยาศาสตรมหาบัณฑิต
สาขาวิชาเคมี
มหาวิทยาลัยเทคโนโลยีสุรนารี
ปีการศึกษา 2564

MULTISCALE MOLECULAR SIMULATION AND EXPERIMENTAL STUDIES OF
STRUCTURAL PROPERTIES OF POLYSTYRENE AND ITS DERIVATIVE

Suranaree University of Technology has approved this thesis submitted in
partial fulfillment of the requirements for a Master's Degree.

Thesis Examining Committee



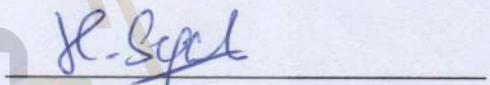
James R. Ketudat-Cairns

(Prof. Dr. James R. Ketudat-Cairns)
Chairperson



Visit Vao-soongnern

(Assoc. Prof. Dr. Visit Vao-soongnern)
Member (Thesis Advisor)



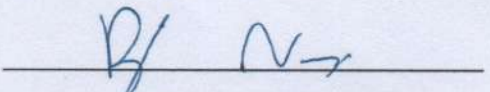
Kritsana Sagarik

(Prof. Dr. Kritsana Sagarik)
Member



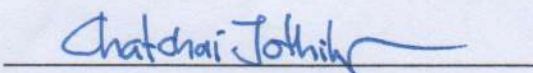
Suwit Suthirakun

(Assist. Prof. Dr. Suwit Suthirakun)
Member



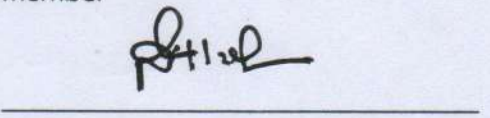
Piyarat Nimmanpipug

(Assoc. Prof. Dr. Piyarat Nimmanpipug)
Member



Chatchai Jothityangkoon

(Assoc. Prof. Dr. Chatchai Jothityangkoon)
Vice Rector for Academic Affairs
and Quality Assurance



Santi Maensiri

(Prof. Dr. Santi Maensiri)
Dean of Institute of Science

กมลธิรา วิชัย : การจำลองโมเลกุลหลายระดับและการทดลองเพื่อศึกษาสมบัติเชิงโครงสร้างของพอลีสไตรีน (MULTISCALE MOLECULAR SIMULATION AND EXPERIMENTAL STUDIES OF STRUCTURAL PROPERTIES OF POLYSTYRENE AND ITS DERIVATIVE) อาจารย์ที่ปรึกษา : รองศาสตราจารย์ ดร.วิศิษฐ์ แวสูงเนิน, 85 หน้า

คำสำคัญ: พอลีสไตรีน, ซัลโฟเนตพอลีสไตรีน, การจำลองในหลากหลายระดับ, การจัดเรียง, การจำลองแบบมอนติคาร์โล, โคพอลิเมอร์สุ่ม, फिल्์มบาง, โครงสร้างการล้อมรอบ, MD-EXAFS

วิทยานิพนธ์เล่มนี้ประกอบด้วยสามหัวข้อหลัก หัวข้อแรกคือการศึกษาสมบัติทางด้านโครงสร้างและพลวัตของพอลีสไตรีนที่มีการจัดเรียงโครงสร้างกึ่งต่างกันโดยใช้วิธีการจำลองในหลากหลายระดับขั้นแรก สายโซ่พอลีสไตรีนจะถูกทำให้เป็นโครงสร้างแบบหยาบแล้วนำไปใส่ในกล่องการจำลองที่มีการบรรจุแบบชิดสุดโดยมีแรงที่เกี่ยวข้องสองแรงคือแรงภายในโมเลกุลและแรงระหว่างโมเลกุล โดยแรงภายในโมเลกุลจะศึกษาโดยวิธีสถานะไอโซเมอร์แบบหมุน (RIS) ส่วนแรงระหว่างโมเลกุลจะศึกษาโดยวิธีของเลนนาร์ดโจนส์ (Lennard-Jones potential function) โครงสร้างพอลีสไตรีนจะถูกทำให้สมดุลโดยวิธีการจำลองของมอนติคาร์โล (Monte Carlo simulation) จากนั้นได้มีการคำนวณสมบัติเชิงโครงสร้างบนกล่องซึ่งประกอบด้วยไดนามิกซ์ของสายโซ่ ขนาดโมเลกุล และสถิติเชิงโครงสร้าง ผลลัพธ์พบว่าไดนามิกซ์ของโมเลกุลสามารถจัดเรียงได้ดังนี้ $sPS \gg aPS > iPS$ การแพร่ของโมเลกุลสอดคล้องกับการจัดเรียงแบบชิดสุดโดยแรงระหว่างโมเลกุลมากกว่าเกี่ยวข้องกับขนาดและความแข็งของโมเลกุล จากนั้นทำการแปลงสายโซ่แบบหยาบกลับมาเป็นแบบละเอียดที่แสดงทุกอะตอมในโมเลกุล แล้วศึกษาสมบัติเชิงโครงสร้างของสารซึ่งประกอบด้วยการกระจายมุมบิด ฟังก์ชันการกระจายในแนวรัศมี ความเข้มของการกระเจิงนิวตรอน และพารามิเตอร์การละลายของพอลีสไตรีนที่มีการจัดเรียงกึ่งแตกต่างกัน

หัวข้อที่สองคือการใช้การจำลองเชิงไดนามิกซ์ของโมเลกุล (MD simulation) และเอกซเรย์ดูดกลืนแสงโครงสร้างละเอียดแบบขยาย (EXAFS) เพื่อศึกษาโครงสร้างล้อมรอบของซัลโฟเนตพอลีสไตรีนที่เติมเกลือแคลเซียม โซเดียม และโพแทสเซียม จากผลลัพธ์ของการจำลองพบว่าไอออนแคลเซียมถูกล้อมรอบด้วยอะตอมออกซิเจน 6 อะตอม ในขณะที่ไอออนโซเดียมและโพแทสเซียมถูกล้อมรอบด้วยอะตอมออกซิเจน 5-6 อะตอม จากนั้นทำการเทียบสเปกตรัม EXAFS ของสาร CaSPS จากการทดลองกับโครงสร้างมาตรฐาน $CaCO_3$ เพื่อหาโครงสร้างล้อมรอบของสาร CaSPS ผลลัพธ์พบว่าโครงสร้างล้อมรอบของโครงสร้างนี้ประกอบด้วยออกซิเจน 5 อะตอมล้อมรอบอะตอมกลาง ซึ่งไม่สอดคล้องกับรายงานก่อนหน้าและยังมีค่า R-factor สูง จากนั้นได้ลองเทียบสเปกตรัมของสารจากการทดลองด้วยผลจากการจำลอง ผลพบว่ามีออกซิเจน 5 อะตอมจากหมู่ซัลโฟเนต และออกซิเจน 1

อะตอมจากน้ำล้อมรอบอะตอมกลาง ซึ่งผลนี้ค่อนข้างใกล้เคียงกับผลการรายงานก่อนหน้านี้และมีค่า R-factor ต่ำ ดังนั้นผลการวิจัยนี้บ่งชี้ให้เห็นว่าโครงสร้างล้อมรอบของไอโอโนเมอร์สามารถหาได้โดยวิธีการจำลองทางคอมพิวเตอร์และการทดลอง EXAFS

สำหรับหัวข้อที่สามคือการศึกษาสมบัติระดับโมเลกุลและโครงสร้างของฟิล์มบางแบบสุ่มของพอลิเมอร์ร่วมโดยวิธีการจำลองแบบมอนทีคาร์โล ซึ่งพอลิเมอร์ร่วมแบบสุ่มนี้ประกอบด้วยโมเลกุลที่ถูกตัดแปลงแรงอันตรกิริยาระหว่างโมเลกุลอยู่ 50 เปอร์เซ็นต์ การตัดแปลงแรงอันตรกิริยาระหว่างโมเลกุลนี้ดำเนินการโดยการแปลงพารามิเตอร์ศักย์ของเลนนาร์ด-โจนส์ให้หลากหลายค่า ส่วนแรงอันตรกิริยาภายในโมเลกุลจะเป็นไปตามแบบจำลองสถานะไอโซเมอร์การหมุน (RIS) ของพอลิเอทิลีน (PE) ผลลัพธ์เชิงสมบัติของสารซึ่งประกอบด้วยความหนาแน่น การจัดเรียงของพันธะ ขนาดและรูปร่างของโมเลกุล การจัดเรียงของโมเลกุล และพลังงานของโมเลกุลจะถูกตรวจสอบและเปรียบเทียบผลที่ได้ระหว่างค่าพารามิเตอร์ของเลนนาร์ด-โจนส์ที่หลากหลาย ($\epsilon/k = 100, 185, 250, 300, \text{ and } 350 \text{ K}$)



สาขาวิชาเคมี
ปีการศึกษา 2564

ลายชื่อนักศึกษา กมลธรี อึ้ง
ลายชื่ออาจารย์ที่ปรึกษา Toykumporn

KAMONTHIRA WICHAJ : MULTISCALE MOLECULAR SIMULATION AND EXPERIMENTAL STUDIES OF STRUCTURAL PROPERTIES OF POLYSTYRENE AND ITS DERIVATIVE. THESIS ADVISOR : ASSOC. PROF. VISIT VAO-SOONGNERN, Ph.D.
85 PP.

Keyword: polystyrene, sulfonated polystyrene, multiscale simulation, tacticity, Monte Carlo simulation, random copolymer, thin-film, coordination structure, MD-EXAFS

There are three main parts to this thesis. For the first part, a multiscale simulation was adapted to study the structural and dynamic properties of glassy PS with different tacticity. PS chains were coarse-grained and then mapped onto the second nearest neighbor diamond lattice (2nd lattice) incorporating short- and long-range interactions from the modified rotational isomeric state (RIS) model and the discretized Lennard-Jones (LJ) potential function, respectively. The PS bulk structures were generated and then equilibrated by using Monte Carlo (MC) simulation. The on-lattice properties were calculated including chain dynamics, molecular size, and conformational statistics. The dynamics of PS chains were qualitatively ordered as *sPS* \gg *aPS* $>$ *iPS*. The diffusion of PS melts was related to intermolecular packing more than molecular size and chain stiffness. The reverse-mapping procedure was performed by converse from the coarse-grained bead to a fully atomistic PS model. After energy minimization, molecular and material properties including torsional angle distribution, radial distribution function, neutron scattering intensity, and solubility parameter for amorphous PS with different tacticities were investigated.

In the second part, Molecular Dynamics (MD) simulation and Extended X-ray Absorption Fine Structure (EXAFS) spectroscopy were employed to investigate the detailed coordination structure of the cation neutralized with a sulfonated group of polystyrene ionomers (M-SPS with M = Na, K, and Ca). From MD results, the first coordination shell of Ca^{2+} ions was surrounded by 6 oxygen atoms, while Na^+ and K^+ ions were surrounded by 5-6 oxygen atoms. EXAFS fitting procedure of CaSPS samples was tried using both the atomic coordinates from standard CaCO_3 crystal structure and the selected snapshot from the MD trajectory. The coordination structure of CaSPS

fitting with CaCO_3 contains 5 oxygen atoms, which does not agreed with previous reports and had a high R-factor. However, the fitting result of CaSPS and the MD trajectory was better, the Ca^{2+} ion was surrounded by 5 oxygen atoms from sulfonation groups and 1 oxygen atom from water. Our findings suggest that the coordination structure of ionomers can be done by a combination method including MD simulation and EXAFS.

For the third part, molecular and structural properties of random copolymer thin films were determined by Monte Carlo simulation of the coarse-grained copolymer model on the high coordination lattice. The random copolymer contains 50% of modified non-bond interaction strength of comonomer units, which is operated by varying Lennard-Jones potential parameters (ϵ/k). The intramolecular interaction was based on Flory's rotational isomeric state (RIS) model of polyethylene (PE). The results of density profiles, bond orientation, chain size and shape, chain orientation, and energetics were investigated and compared with varied LJ parameter ($\epsilon/k = 100, 185, 250, 300, \text{ and } 350 \text{ K}$).



มหาวิทยาลัยเทคโนโลยีสุรนารี

School of Chemistry
Academic Year 2021

Student's Signature

กมลธิรา วิชัย

Advisor's Signature

วิชัย วิชัย

ACKNOWLEDGEMENTS

This research can be finished because of the helping from my collaborators. I would like to thank my advisor, Assoc. Prof. Visit Vao-soongnern, for giving me the opportunity to study at Suranaree University of Technology and join his laboratory. I appreciate the contribution of his research resources, financial support, and guidelines of many others. He helped me put ideas for this thesis and gave helpful discussions. His guidance and advice carried me through all the stages of my Master's thesis. I would like to thank my friends in Visit's laboratory members for giving me discussion, teaching me how to use the tools, and making a good environment.

Besides Suranaree University of Technology advisors, I would like to thank Assist. Prof. Khongvit Prasitnok from Mahasarakham University, who gave me advice and helpful discussion about MD simulation. I would like to thank the Synchrotron Light Research Institute (Public Organization) for EAXFS measurements.

I am very much thankful to the Development and Promotion of Science and Technology Talents Project (DPST) scholarship, the National Research Council of Thailand (NRCT) research grant, Japan Student Services Organization (JASSO) scholarship, Suranaree University of Technology, and Osaka University for financial support and research resource.

Finally, I would like to thank my family and friends for encouraging me and pointing me in the right direction.

Kamonthira Wichai

CONTENTS

	Page
ABSTRACT IN THAI.....	I
ABSTRACT IN ENGLISH.....	III
ACKNOWLEDGEMENTS.....	V
CONTENTS.....	VI
LIST OF TABLES.....	IX
LIST OF FIGURES.....	X
LIST OF ABBREVIATIONS.....	XII
CHAPTER	
I INTRODUCTION.....	1
1.1 Research objectives.....	3
1.2 Scope and limitations.....	3
II LITERATURE REVIEWS.....	5
2.1 Computer simulation of amorphous polystyrene.....	5
2.2 Structural investigation of sulfonated polystyrene.....	7
2.3 Monte Carlo simulation of random copolymer.....	10
III RESEARCH METHODOLOGY.....	12
3.1 Multiscale simulations of polystyrene with different tacticities.....	12
3.1.1 Model and Method.....	12
3.1.2 Moves in the simulation.....	14
3.1.3 Simulation of polystyrene on 2nd lattice.....	16
3.1.4 Fully atomistic model.....	17
3.2 Atomistic local structure of salt dope sulfonated polystyrene.....	17
3.2.1 Molecular simulation of sulfonated polystyrene dope with cation salts.....	17
3.2.2 EXAFS measurements and data analysis.....	18

CONTENTS (Continued)

		Page
	3.2.3 MD-EXAFS fitting.....	19
	3.3 SPS thin film by coarse-grained random copolymer models.....	19
	3.3.1 Random copolymer model.....	20
	3.3.2 Monte Carlo simulation.....	22
	3.3.3 Film formation.....	23
IV	RESULTS AND DISCUSSION.....	24
	4.1 Multiscale simulations of polystyrene with different tacticities.....	24
	4.1.1 Structure relaxation.....	24
	4.1.2 Chain dimension.....	26
	4.1.3 Structure.....	27
	4.1.4 Conformation.....	28
	4.1.5 Radial distribution function and neutron scattering.....	29
	4.1.6 Solubility parameters.....	32
	4.2 MD simulation of Cation-ionomer benchmark model.....	34
	4.2.1 Bivalent calcium-ionomer (Ca-SPS) model.....	34
	4.2.2 Monovalent sodium-ionomer (Na-SPS), and potassium-ionomer (K-SPS) models.....	39
	4.2.3 Solvation structure of calcium neutralized sulfonated polystyrene (Ca-SPS) by EXAFS.....	44
	4.2.4 Solvation structure of calcium neutralized sulfonated polystyrene (Ca-SPS) by MD-EXAFS fitting.....	49
	4.3 SPS thin film by coarse-grained random copolymer models.....	53
	4.3.1 Equilibration.....	53
	4.3.2 Density profiles.....	55
	4.3.3 Bond arrangement.....	61
	4.3.4 Chain properties.....	62
	4.3.5 Energetics.....	67
V	CONCLUSION.....	69

CONTENTS (Continued)

	Page
REFERENCES.....	72
APPENDICES.....	80
APPENDIX A INTERNATIONAL CONFERENCE I.....	81
APPENDIX B INTERNATIONAL CONFERENCE II.....	83
CURRICULUM VITAE.....	85



LIST OF TABLES

Table	Page
3.1 Non-bonded interaction parameter (kJ/mol) for copolymer model: C..C, X..X, and C..X beads at 473 K ($\sigma = 4.4 \text{ \AA}$ with different ϵ/k).....	22
4.1 Chain dimension, chain stiffness, and chain diffusion.....	27
4.2 Distribution of the C-C-C-C torsion angles with different tacticity of Polymer chains before and after energy minimization.....	29
4.3 Cohesive energy density and solubility parameter calculated from atomistic PS models.....	33
4.4 Parameter characterizing the RDF from MD simulation of Ca-ionomer.....	37
4.5 Parameter characterizing the RDF from MD simulation of Na-ionomer.....	42
4.6 Parameter characterizing the RDF from MD simulation of K-ionomer.....	43
4.7 Fitting parameters of the first solvation shell: coordination number (CN), the amplitude reduction factor (S_0^2), the shift of energy (E_0), the shift of distance (ΔR), and the first-shell oxygen Debye-Waller factors of Ca-SPS.....	48
4.8 Atomic coordinates from MD snapshot of Ca-SPS.....	52
4.9 Density profile parameters of random copolymer thin films as a function of monomer interaction strength.....	58
4.10 Root mean square radius of gyration $\langle R_g^2 \rangle^{1/2}$ and root mean square end-to-end vector $\langle R_e^2 \rangle^{1/2}$ for copolymer thin films.....	63
4.11 The comparison of the principal components of the mean square radius of gyration and normalized average acylindricity and asphericity values for various LJ interaction parameters.....	65

LIST OF FIGURES

Figure		Page
2.1	Multiscale simulation with the coarse-grained and reverse-mapped method.....	7
3.1	Single bead move on 2nd lattice.....	14
3.2	Schematic representation of two-bead pivot move. Two middle red beads change their positions after moving, (a) old-conformation, (b) change sequence of bond vector, (c) new-conformation.....	15
3.3	Two kinds of unphysical collapses. <i>i</i> is intramolecular collapse, and <i>k</i> is intermolecular collapse. <i>i</i> and <i>k</i> are occupied in the same lattice site after reverse-mapping.....	16
3.4	Calcium sulfonated polystyrene repeating unit.....	19
4.1	(a) The orientation autocorrelation functions (OACF), (b) the average mean square displacements of the center-of-mass (MSD) of polymer chains with different tacticity in 90 million Monte Carlo Step (MCS). (c) the relative diffusion as a function of different amounts of <i>meso</i> diads from 0.0 to 1.0.....	26
4.2	The pair correlation function (chain packing) of <i>i</i> PS, <i>s</i> PS, and <i>a</i> PS pure melts.....	28
4.3	Distribution of the C-C-C-C torsion angle of reversed mapping <i>a</i> PS before and after minimization from selected snapshot.....	29
4.4	The radial distribution function for three different pairs of elements (a) C-C, (b) H-H, and (c) C-H.....	30
4.5	Neutron scattering vector for <i>a</i> PS, <i>i</i> PS, <i>s</i> PS from the calculation, and <i>a</i> PS from an experiment.....	32

LIST OF FIGURES (Continued)

Figure	Page
4.6 Ca-SPS ionomer with water (a) initial- and (b) final-structure from MD simulation (The simulation box on the left-hand side is larger than right side). The green sphere = Ca^{2+} ion, red = oxygen atom, yellow = sulfur atom, gray = carbon atom, and white = hydrogen atom.....	35
4.7 The radial distribution function (RDF) of Ca^{2+} --O interaction calculated from the MD simulation.....	36
4.8 Ca-SPS model (a) bulk system and (b) hydrated system from MD simulation, the green sphere = Ca^{2+} ion, red = oxygen atom, yellow = sulfur atom, gray = carbon atom, and white = hydrogen atom. Solvation model of (c) bulk system and (d) hydrated system of Ca-SPS.....	38
4.9 RDF curve of (a) Na-SPS and (b) K-SPS from MD simulation analysis.....	41
4.10 TGA curve of Ca-SPS sample. At 70°C – 120 °C weight-loss stage represented to the loss of absorbed water in ionomers. For 460°C – 550°C weight loss stage could be the decomposition of the polystyrene backbone.....	44
4.11 EXAFS spectra expressed in (a) k -space and (b) r -space for Ca-SPS ionomers.....	45
4.12 Fitting the first coordination shell of the calcium carbonate with CaCO_3 crystal Structure (a) $k^2\chi$ and (b) radial structure function.....	47
4.13 Fitting the first coordination shell of the Ca-SPS using CaCO_3 model (a) $k^2\chi$ and (b) radial structure function.....	49
4.14 Fitting the first coordination shell of the Ca-SPS using MD snapshot model (a) $k^2\chi$ and (b) radial structure function.....	51
4.15 Equilibration of random copolymer thin film structure as illustrated by (a) the mean square displacement for the center of mass (MSD) and (b) the decorrelation function of the end-to-end vector of copolymer chains as a function of Monte Carlo Step.....	55

LIST OF FIGURES (Continued)

Figure	Page
4.16	Example snapshots of random copolymer thin film structure for different LJ interaction parameters (ϵ/k) of 100, 185, 205, 300 and 350 K.....56
4.17	Density profile of random copolymer thin film structure for different LJ interaction parameters (ϵ/k) of 100, 185, 205, 300 and 350 K.....57
4.18	Density profile parameters of random copolymer thin film structure given by fitting the density profile curve with the hyperbolic equation.....58
4.19	Normalized radial density profiles of the end beads (solid line) and the middle beads (dashed line) as a function of distance from the center of mass of the films.....59
4.20	(a) center of mass and (b) cumulative chain center of mass distribution of random copolymer thin film structure for different LJ interaction parameters (ϵ/k) of 100, 185, 205, 300, and 350 K.....60
4.21	The orientation of bond vectors with respect to the distance from the center of mass of the films (a) middle bonds. (b) end bonds.....61
4.22	(a) The normalized principal moments (L_1 , L_2 , and L_3) of individual chains and (b) the normalized asphericity and acylindricity as a function of distance from the center of mass of thin film for various LJ interaction parameters.....64
4.23	The components of the mean-squared radius of gyration in random copolymer thin films for various LJ interaction parameters.....66
4.24	The orientation of the first and third principal axis of copolymer molecule (open symbol – L_3 , filled symbol – L_1).....67
4.25	The average short-range, long-range, and total energy of polymer molecule (in 6 Å) with $\epsilon/k = 100, 185, 250, 300,$ and 350 K along the Z-axis of thin film.....68

LIST OF ABBREVIATIONS

PS	Polystyrene
<i>i</i> PS	<i>isotactic</i> polystyrene
<i>s</i> PS	<i>syndiotactic</i> polystyrene
<i>a</i> PS	<i>atactic</i> polystyrene
T_g	Glass transition temperature
°C	Degree celcius
SPS	Sulfonated polystyrene
Ca ²⁺	Calcium ion
Na ⁺	Sodium ion
K ⁺	Potassium ion
2nd	the second nearest neighbor diamond lattice
MC	Monte Carlo
RIS	Rotational isomeric state
LJ	Lennard-Jones
MD	Molecular dynamic
EXAFS	Extend X-ray Absorption Fine Structure
<i>L</i>	principal component
<i>c</i>	acylindricity
<i>b</i>	asphericity
ϵ/k	Well-depth Lennard Jones parameter
nm	nanometer
η	The first order interaction expressing the <i>trans</i> state
τ	The first order interaction expressing the <i>gauche</i> state
ω	The second order interaction between CH _x -CH _x
ω'	The second order interaction between CH _x -Phenyl
ω''	The second order interaction between Phenyl-Phenyl
μ	The absorption coefficient

LIST OF ABBREVIATIONS (Continued)

eV	electron volt
E	energy
N_j	the number of atoms of type j in the j^{th} shell
$S_0^2(k)$	the amplitude reduction factor
$F_j(k)$	the backscattering amplitude from the N_j atom
R_j	the root mean square distance between the central atom and the j^{th} atom
σ_j	the Debye-Waller factor
λ_j	the electron mean free path
ϕ_{ij}	the phase shift experienced by the photoelectron
PCFF	the polymer consistent force-field
OPLS-AA	the optimized potentials for liquid simulations-all atom
PME	the particle mesh ewald
RDF	the radial distribution function
RSF	the radial structure-function
Å	Angstroms
MCS	Monte Carlo step
MSD	mean square displacement of the center of mass
OACF	the normalized orientation autocorrelation functions
$\langle \mathbf{m}(t) \cdot \mathbf{m}(0) \rangle$	Orientalional autocorrelation function of bond vector
$\langle \mathbf{R}(t) \cdot \mathbf{R}(0) \rangle$	Chain end-to-end vector orientational autocorrelation
PP	polypropylene
NMR	Nuclear magnetic resonance
C_n	Characteristic ratio
$\langle R_g^2 \rangle^{1/2}$	The mean square radius of gyration
$\langle R_e^2 \rangle^{1/2}$	The mean square end-to-end vector
D	Diffusion
PCF	Pair correlation function
g^+	<i>gauche</i> plus

LIST OF ABBREVIATIONS (Continued)

g	<i>gauche</i> minus
t	<i>trans</i>
$S(Q)$	neutron elastic structure factor
Q	Scattering vector magnitude
δ	Solubility parameter
CE_D	Cohesive energy density
U_{coh}	Cohesive energy
CN	Coordination number
R_0	Peak position
WAXS	Wide-angle x-ray scattering
ρ_{bulk}	bulk density
Z	z-dimension
R	Film thickness
W	Surface thickness
K	Kelvin
S	Orientation
θ	Angle between z-axis and surface plan

CHAPTER I

INTRODUCTION

Polystyrene (PS) is an aromatic hydrocarbon polymer that is made from the styrene monomer and is one of the most widely used plastics (Scheirs, 2003). There are three different stereochemical configuration of phenyl side chain or tacticity; (1) *isotactic*, *syndiotactic* and *atactic* PS, denoted by *iPS*, *sPS* and *aPS*, with the two consecutive phenyl groups located on the same side, alternating direction and randomly placement, respectively. Difference in chain tacticity has significant influence on various physical properties of polystyrene. In general, *aPS* is the only one produced in commercial form, while *sPS* can be produced recently by Ziegler-Natta polymerization (Pasztor, 1991). However, *iPS* is difficult to prepare. Physical properties of *aPS* and *sPS* are quite different. *aPS* is amorphous with the glass transition temperature (T_g) about 100°C, while *sPS* has high crystalline content with the melting temperature around 270°C (Pasztor, 1991). It might be better if we knew more about the properties of *iPS*, *sPS*, and *aPS* that the experiments could not tell. Here, we are interested to study the structural and dynamics properties of PS with three different tacticities (*iPS*, *sPS*, and *aPS*) by using a development multiscale simulation method.

It is possible to functionalize polystyrene to have new properties for application. Sulfonation of polystyrene is a well-known and effective way to increase the value of original polystyrene by converting its hydrophobic structure to hydrophilic structure (Kim, 2002 and Barra, 2004). Sulfonation of polystyrene can be prepared by incorporated sulfonic acid group to polystyrene chain through aromatic electrophilic substitution. The practical application of sulfonated polystyrene (SPS) can be used as water softening resin and membrane for proton exchange fuel cell. SPS consists of hydrophilic sulfonated group and hydrophobic polymer backbone. The sulfonated groups at the phenyl group of PS chain can change thermal, mechanical, and charge

transport properties of this material such as the case of proton conductive perfluorosulfonic acid membrane. The ionic transportation in the membrane, a novel concept regarding high ability of the membrane to transport the ionic molecules, is anxiously desired in a fabrication of high-performance energy sources, *i.e.*, fuel cell, lithium-ion battery, and so forth. In particular, the morphology control at the nanometer scale has attracted much attention regarding the formation of molecular pathways for faster transport (Kawahara, 2009). Studying the inside domain structure is extremely important in ionomer research, since this information is necessary to understand the thermodynamics and mechanism of phase separation in these materials (Grady, 1994).

There are many factors that affect the rapid transportation of ions in a polymer matrix. Castagna *et al.* (Castagna, 2010; 2011; 2011) studied the effects of degree of sulfonation, degree of neutralization, and cation type on structural and dynamic properties of sulfonated polystyrene. It was found that the ionic aggregated sizes are independent of the sulfonation levels, but significantly changes with increasing neutralization levels. The sulfonated polystyrene with different types of cations exhibit slight increases in the aggregated sizes with cation. The relaxation time of chain motion is increased with increasing degree of sulfonation and neutralization, due to the reduced mobility of chain segment in the aggregates. For different ion valency, the monovalent cations give only one broad segmental process, while divalent cations exhibit two distinct segmental processes. Although the aggregated sizes of SPS with different cation types are not different, there are different relaxation processes. In this thesis, the morphology of SPS neutralized with different cations is investigated by the combined methods of molecular simulation and experiment.

The sulfonation level of SPS can affect the aggregated size, the relaxation time of chain motion and macroscopic properties of bulk materials. As in most applications these polymers are normally fabricated as thin film, the presence of the sulfonate groups with attractive interaction should affect the molecular and surface properties of these materials. Understanding of polymer surfaces at the molecular level provides great capability to modify the membrane for specific purposes (Stamm, 1992). Computer simulation is a powerful method to study properties and design polymeric

materials at the molecular level (Monnerie, 1994). In principle, fully atomistic simulation should provide more details and specific characteristics of these copolymer chains. However, atomistic simulation requires formidable computational resources to completely relax the structure and equilibration, especially for large macromolecule (Mansfield, 1990; Misra, 1995). To overcome this difficulty, coarse-grained copolymer model has been developed to simulate the larger system size and longer time scale. As the monomer structure of styrene and sulfonated styrene units are quite similar, SPS may be treated as the coarse-grained copolymer chains with similar bead size with different intermolecular interaction parameter. In this work, the coarse-grained SPS is proposed as the “polyethylene-like” copolymer model to study the physics of random copolymer chains as the general behavior. This simple random copolymer model was proposed and applied to study the free surfaces of random copolymer thin film and nanoparticle (Baschnagel, 2000; Doruker, 1998; Vao-soongnern, 1999; 2001).

1.1 Research objectives

- 1.1.1 To investigate structural, dynamic and material properties of polystyrene with different tacticities (*iPS*, *sPS*, and *aPS*) by multiscale molecular simulation.
- 1.1.2 To investigate the solvation structure and morphology of sulfonated polystyrene neutralized by some cations (CaSPS and KSPS) by the combined method of synchrotron X-ray absorption spectroscopy and molecular dynamic simulation.
- 1.1.3 To investigate the general characteristics of molecular, structural, and surface properties of SPS thin film by means of molecular simulation of coarse-grained random copolymer model.

1.2 Scope and limitations

This thesis research is divided into 3 main topics:

- 1.2.1 Multiscale simulations of polystyrene with different tacticities

Three polystyrene chains with different tacticity (*iPS*, *sPS*, and *aPS*) are coarse-grained and then mapped onto the second nearest neighbor diamond ($2nd$) lattice. Structural equilibration is performed by Monte Carlo (MC) simulation incorporating short- and long-range interactions from the modified rotational isomeric state (RIS) model and the discretized Lennard-Jones (LJ) potential function, respectively. Then, the coarse-grained model is reverse-mapped back to the fully atomistic model of amorphous structures. Some molecular and material properties are determined including torsional angle distribution, solubility parameter, radial distribution function and neutron scattering intensity.

1.2.2 Atomistic local structure of salt doped sulfonated polystyrene

The solvation and aggregated structure of Ca^{2+} , Na^+ and K^+ ions by SPS are studied by MD simulation. The distance and coordination number between the central and the surrounded atoms were determined. Next, Extended X-ray Absorption Fine Structure (EXAFS) spectroscopy is employed in combination with MD simulation to validate the simulated structures. In addition, dynamic properties of SPS neutralized by cations are also investigated by MD simulation.

The atomistic structure of CaSPS was determined using EXAFS analysis. The EXAFS spectrums of sample were fitted with EXAFS spectrum of reference to determine the distance and coordination number of probed atoms in polymer electrolytes. Moreover, the hypothetical EXAFS scattering path from MD simulation also used to fit with EXAFS spectra from experiment.

1.2.3 SPS thin film by coarse-grained random copolymer models

SPS is represented as “polyethylene-like” copolymer model with different non-bonded interaction by varying the LJ interaction parameter of ethylene bead (ϵ/k). Density profiles, beads, bonds and chain properties are determined.

CHAPTER II

LITERATURE REVIEWS

2.1 Computer simulation of amorphous polystyrene

At the present, the advancement in computer hardware greatly benefits polymer modeling and simulation. The development of new methods and algorithms is important for simulations, which are based on physical and chemical science. Each method is used in different length and time scales that are appropriate for structures and dynamics occurring in polymeric materials. Currently, multiscale modeling and simulation, involving a combination of atomistic (< 10 nm), mesoscopic (10-1000 nm), and macroscopic methods, are generally accepted as a successful solution for materials design (Kotelyanskii, 2008).

Computer simulation of polymeric materials with coarse-grained lattice models has been considered as an efficient simulation approach for the time and length scale of these systems. Monte Carlo simulation of coarse-grained polymer model on a high coordination lattice such as the second-nearest-neighbor diamond (*2nd*) has the key advantage because this method can keep the detailed chemistry of polymer species and suitable for the study of large polymer systems with more efficiency, while atomistic simulation may not be able to fully equilibrate the large molecular system within the appropriated computation time (Antoniadis, 1998 and 1999; Logotheti, 2007). The effect of the stereochemistry of side groups in vinyl polymer chains on various properties can also be studied using the simulation technique. Unlike enantiomer of small molecules, computer simulation studies on stereochemical effects on dynamic properties of polymer materials are still not well understood. It is therefore important to have a more comprehensive study for the influence of different stereochemical sequences on the dynamics of the vinyl polymer such as polystyrene in this research.

Polystyrene is a vinyl polymer with a large atomic side chain, which requires large simulation resources for generating and relaxing structures. It is challenging to find ways

to reduce the computational costs for molecular simulations but still maintain reasonable results. In many research, there have been developed the molecular simulation of polymeric materials with a coarse-grained model. This is a model that involves grouping multiple atoms into coarse-grained beads. Each coarse-grain model's bead interacts with others by potential interaction, which is determined to match the thermodynamics properties of the polymer (Hatakeyama, 2007; Marrink, 2003 and 2007; Monticeli, 2008 and Wallace, 2007). However, it still has its shortcoming about reproduction and accuracy, the same method cannot be used for different polymer models. Here, we are interested to develop multiscale simulations to study structures, dynamics, and material properties of amorphous PS. This multiscale simulation can be divided into three steps as shown in figure 2.1. The first step is mapping atomistic polymer into the coarse-grained bead on the second nearest neighbor diamond lattice. Then, Monte Carlo (MC) simulation was performed with known intra- and inter-molecular interaction in the second step. From the literature, intra-molecular interaction was obtained by Flory's Rotational Isomeric State (RIS) model (Rehan, 1997) with the set of parameter interaction $(\eta, \tau, \omega, \omega', \omega'')$. While the method of Lennard-Jones (LJ) potential was used to describe inter-molecular interaction (Cho, 1997) with σ and ϵ parameters. For the third step, a reverse mapping from the coarse-grained model to the atomic level was determined. This method has been worked well with other polymeric systems such as poly(ethylene oxide), polyethylene, polyvinylchloride, and polypropylene (Doruker, 1997 and 1999; Jang, 2000; Vao-soongnern, 1999 and 2000). For amorphous PS, there was a report about the simulation of surface properties of thin-film atactic PS in previous (Clancy, 2001). However, there has been no report about the simulation of bulk PS with different stereochemical sequences yet. Thus, we are interested to use coarse-grained and reverse-mapped methods to determine structural and dynamics properties of *i*PS, *a*PS, and *s*PS.

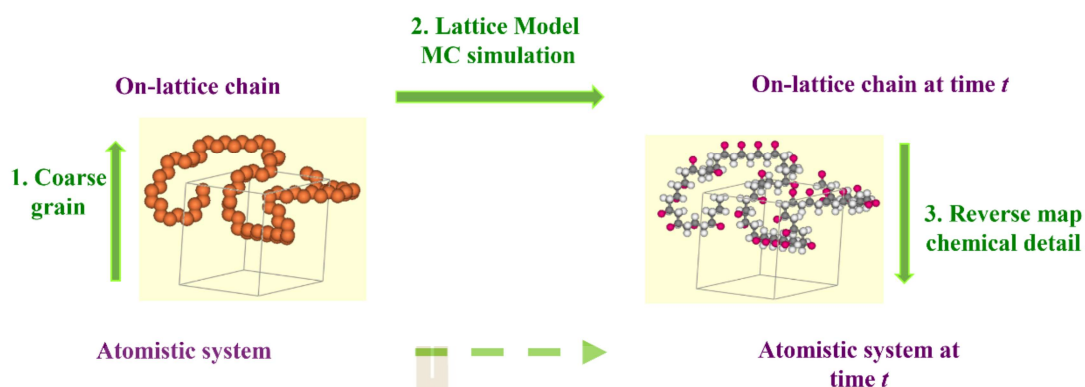


Figure 2.1 Multiscale simulation with the coarse-grained and reverse-mapped method.

2.2 Structural investigation of sulfonated polystyrene

Sulfonated polystyrene, polystyrene containing ionic functionality with a maximum ionic group content of about 15 mol% (Eisenberg, 1998 and Tant, 1987), has been a significant research focus over the past 5 decades (Grady, 2008). It is one of the interesting polymer electrolytes because it composes of high mechanical polystyrene group and high ionic conductivity sulfonated group. The sulfonic acid groups on a phenyl ring may contribute to the rapid transportation of protons, as in the case of proton conductive perfluorosulfonic acid membrane, such as Nafion. Investigation the structure inside these domains is extremely important in ionomer research since this information is essential to understanding the thermodynamics and mechanism of phase separation in these materials (Grady, 1994). Moreover, the percentage of sulfonation is also the important key for ion transport in this electrolyte material. Safronova et al studied the effect of amounts of a cross-linking agent and degree of polystyrene grafting on both mechanical and transport properties of sulfonated cation-exchange membranes, and also compare the results with commercial membranes (*i.e.* Nafion) (Safronova, 2016). They found that the mechanical property (tensile strength) increases with increasing amounts of cross-linker. At the state of no cross-linking agent, the conductivity of membranes showed high value with high relative humidity at 25°C. The conductivity value at high relative humidity decreased when the amount of the cross-linking agent increased. However, the associated cation transport numbers of

cross-linking polystyrene exhibit a high value compare with commercial Nafion membrane, and the calculated power of reverse electro dialysis batteries of this best membrane also shows a higher value up to 10% than commercial membrane.

Sulfonated polystyrene enhanced properties such as elastic modulus, glass transition temperature, viscosity, melt strength, fatigue resistance, transport properties (Eisenberg, 1998). These property enhancements arise from the microphase separation of ionic species into aggregates due to strong electrostatic interactions, which behave as thermoreversible cross-links (Grady, 2008). Extensive investigation of the morphology of these ionic rich domains, dynamic, and mechanical properties of these materials have been performed (Grady and Cho, 2008; Chi, 1989). However, the coordination structure, the relationship between ionic cation and sulfonated group, is not well defined. One of the most famous techniques to study the local structural information of metal ions is the extended X-ray absorption fine structure or EXAFS technique. EXAFS measurements have been employed to determine the near-neighbor environment of the neutralized cation in many ionomer systems. The analyzed structure was compared with the structure in analogous low-molecular-weight crystalline salts.

In recent years, many works have been published on the microstructure of ionomers, polymers that predominantly hydrophobic character but contain small amount of bound ionic functionality (Holliday, 1975; Eisenberg, 1979; Lee, 1981). However, there has been a lot of controversy over the interpretation of some of the data, and no clear picture of the morphology has emerged. In recent years, the interpretation of the internal structure of ionomers can be described by EXAFS measurements, which are uniquely suited to determine the near-neighbor environment of the cation in ionomers. In particular, it provides information about the types of near-neighbor atoms and their coordinated distances. It is expected that there are at least two distinct environments for the cations in ionomers, which correspond to ions in aggregates and that are related to ionic groups dispersed in the matrix (Yarusso, 1983). To interpret EXAFS data, the coordination environment in the ionic aggregates should be very well ordered compared to the unaggregated ions, and therefore should dominate the EXAFS signal.

Technically, EXAFS corresponds to the oscillating part of the spectrum as displayed in the absorption coefficient (μ) of a given material versus energy between 50 and 1000 eV above the atomic absorption edge. The X-ray absorption spectroscopy (XAS) process is started when an X-ray beam is applied to a probed atom and then the electron has been ejected from the core shell, normally the ejection electron corresponds to the $1s$ electron in the K-edge. This process leaves a vacancy in the core shell and make the relaxation of outer electrons to fill that hole. The outer electron can release some energies when go to fill electron hole in the core shell. The released photoelectron can also be interacted with electron in the surrounding non-excited atoms and generated the backscattering waves. The interference between the outgoing and backscattered waves is represented in the EXAFS oscillation. The shape and period of the oscillations can be qualitatively expressed with the distance, coordination number, and type of neighboring atom. In General, the distance between the probing atom and the backscattering atom must be less than 6 Å for the interference to be significant. Stern *et al.* (Stern, 1975) developed the simplest correct theory to describe this phenomenon and labeled single-electron single-scattering theory. This theory assumes that multiple-scattering paths are insignificant and that both thermal and static disorders are small. From this simple theory, EXAFS oscillation of a completely isotropic sample can be explained following equation:

$$\chi(k) = \frac{\mu(E) - \mu_0(E)}{\mu_0(E)} = \sum_j N_j S_0^2(k) \frac{F_j(k)}{kR_j^2} e^{2\sigma_j^2 k^2} e^{-\frac{2R_j}{\lambda_j}} \sin[2kR_j + \phi_{ij}(k)]$$

where $\mu(E)$ and $\mu_0(E)$ are the measurement and average absorption coefficients at the energy E , respectively. N_j is the number of neighboring atoms in the j^{th} shell, $S_0^2(k)$ is the amplitude reduction factor caused by the excitations of electrons other than K-edge electrons in the X-ray absorbing atom, $F_j(k)$ is the amplitude function of backscattering wave from the N_j atom, R_j is the root mean square distance from the probing atom to the neighboring atom in j^{th} shell, λ_j is the electron mean free path, σ_j is the Debye-Waller factor which measures the variation in R_j about its mean, and ϕ_{ij} is the phase shift. The k dependence of the amplitude reduction factor is usually quite small and was treated as a constant. k is called the wavevector because $\frac{2\pi}{k}$ is the wavelength of the ejected photoelectron.

2.3 Monte Carlo simulation of random copolymer

Random copolymers consist of two chemically distinct monomer units covalently bonded together with statistical arrangement. The random copolymers were purposed to improve some properties of macromolecular material that homopolymer cannot provide. Recently, many interesting random copolymers were used as commercial products such as styrene-butadiene rubber and polymer resins made from methacrylic acid or styrene-acrylic derivatives (Overberger, 1985). Compared with the improved material properties through the block or graft copolymer, the random copolymer can be prepared conveniently and provides advantages over other chain structures for commercial usage (Shaffer, 1995). SPS is one kind of random copolymer, it is mixed between styrene and sulfonated styrene side-chain units. The sulfonated group attached to the phenyl ring of styrene units exhibits stronger interaction than original styrene units, due to electrostatic force. The ratio of sulfonated styrene unit per styrene unit is called percentage of sulfonation. It is an important key of distinct macromolecular properties, for example, viscoelastic property and ionic conductivity. Here, we would like to observe the effect of sulfonation level on the structural property at the molecular scale. However, it is difficult to simulate the fully atomistic model of the sulfonated polystyrene with various sulfonation levels due to large polymer molecules. We have conceptualized a modified coarse-grained PE model with various non-bond interactions. We start with observing the effect of non-bond interactions, both repulsive and attractive, on the structural interface property. Previously, Doruker (Doruker, 1998) and Mattice (Mattice, 1994) used the model of coarse-grained PE beads to study the surface property of the thin film. The PE films were generated with the different numbers of chains, 9, 36, 72, and 108 chains. The density profile of these films exhibited similar behavior as a hyperbolic structure with end beads being more abundant than the middle beads. The difference in chain number does not indicate any difference of local and global structure, it shows different only the thickness of the film. There are some reorient of bonds and whole chains of polymer near the film interface. In addition, they also studied the mobility of the surface and interior of amorphous PE thin film. They found that the mobility of both beads and chains PE increased toward the free surfaces due to the decrease in

density. The chain diffusion trended to increase parallel with the interface as the film thickness decreased, while the diffusion in the perpendicular direction to the surface decreased as the film thickness decreased. This behavior occurred generally because of the confinement of the chains between the surfaces. In the next few years, Jang and co-workers also used PE coarse-grained model to study the effect of chain-end modification on freely standing thin films. They observed the modified beads at the end chain, the bead with changing the well-depth (ϵ) parameter of LJ potential equation, compared to the middle beads. They found that the end beads with $\epsilon_{end} \gg \epsilon_{middle}$ shown segregation in the bulklike region, while the end beads with $\epsilon_{end} \leq \epsilon_{middle}$ prefer to stay near the free surface. The distribution of chain ends is mainly affected by entropy and enthalpy factors. For the attractive chain end case ($\epsilon_{end} > \epsilon_{middle}$), the isotropic region could be observed as the entropic effect prefer to the free surface and the enthalpic effect prefer to the bulk region. The chain ends show faster dynamics in the middle region for the case of repulsive interaction, $\epsilon_{end} < \epsilon_{middle}$.

CHAPTER III

METHODOLOGY

3.1 Multiscale simulations of polystyrene with different tacticities

3.1.1 Model and Method

The coarse-grained model of amorphous polystyrene (*i*PS, *s*PS, *a*PS) can be prepared by grouping one repeating unit of polystyrene into one bead. The difference in stereochemical sequence can be distinguished by different energy parameters. The position of each bead is defined by *x*, *y*, and *z* planes on the second nearest neighbor diamond (2nd) lattice. Three consecutive beads *i*, *j*, and *k* were made up to represent as moving beads on 2nd lattice. Twelve possible nearest neighbor sites bead *i* on coordinated x_i, y_i, z_i can connect to bead *j*. Then, bead *k* can be connected to bead *j* in eleven possibilities at the nearest neighbor site. Therefore, all the non-reversal methods in which bead *i* and *k* are connected to bead *j* are 132 ways. The coarse-grained bead can be connected to another by a 2.5 Å unit spacing C-C bond with denoted vector + for +1 and – for -1. The vector component from bead *i* to bead *j*, and from bead *j* to bead *k*, can be represented by using 12x12 matrix (equation 3.1), which represented the reverse mapped C-C bond in the positive *z*-direction.

$$\begin{bmatrix} A & B & A & B \\ B & A & B & A \\ A & B & A & B \\ B & A & B & A \end{bmatrix} \text{ where } A = \begin{bmatrix} a & b & c \\ c & a & b \\ b & c & a \end{bmatrix}, B = \begin{bmatrix} b & c & d \\ c & d & b \\ d & b & c \end{bmatrix} \quad \text{Equation 3.1}$$

a is *tt* or g^+g^+ state. *b* and *c* are $tg^+, tg^-, g^+t, g^-t, g^+g^+, g^-g^+$ and *col.* *d* is *rev* or g^-g^- . Each coarse-grained bead interacts with each other by two types of interaction, intra- and inter-chain interactions. The intra-chain interaction was used to describe the interaction between beads in the short-range distance, which can be determined from the RIS model. For polystyrene, the RIS model can be represented by six statistical weight matrices for each kind of side chain configuration as follows:

$$\begin{aligned}
 U'_i &= \begin{bmatrix} \eta & \tau & 1 \\ \eta & \tau & \omega \\ \eta & \tau\omega & 1 \end{bmatrix} & U'_d &= \begin{bmatrix} \eta & 1 & \tau \\ \eta & 1 & \tau\omega \\ \eta & \omega & \tau \end{bmatrix} \\
 U''_{ii} &= \begin{bmatrix} \eta\omega'' & 1 & \tau\omega' \\ \eta\omega' & \omega' & \tau\omega\omega'' \\ \eta & \omega & \tau\omega' \end{bmatrix} & U''_{id} &= \begin{bmatrix} \eta & \tau\omega'' & \omega' \\ \eta\omega'' & \tau\omega'\omega' & \omega \\ \eta\omega' & \tau\omega & 1 \end{bmatrix} \\
 U''_{dd} &= \begin{bmatrix} \eta\omega'' & \tau\omega' & 1 \\ \eta & \tau\omega' & \omega \\ \eta\omega' & \tau\omega\omega'' & \omega' \end{bmatrix} & U''_{dl} &= \begin{bmatrix} \eta & \omega' & \tau\omega'' \\ \eta\omega' & 1 & \tau\omega \\ \eta\omega'' & \omega & \tau\omega'\omega' \end{bmatrix}
 \end{aligned} \quad \text{Equation 3.2}$$

Where the statistical weight matrices U'_i and U'_d represented to $C^\alpha - C$, and $U''_{ii}, U''_{id}, U''_{dd},$ and U''_{dl} represented to $C - C^\alpha$ (Flory, 1969; Yoon, 1975; Mattice, 1994). C^α is the chiral carbon, while d and l are the stereochemistry of the vinyl group for the right and left, respectively. The parameters in the column and row matrix represented bonds i and $i-1$, respectively. The η parameter examined the interaction between $C^\alpha(\text{phenyl})-C^\alpha(\text{phenyl})$, while τ parameter represented $C^\alpha-CH_2$ interaction in the first order. For the second-order, the $\omega, \omega', \omega''$ parameter represented the CH_2-CH_2 , $CH_2\text{-phenyl}$, and phenyl-phenyl interactions, respectively. In this work, we used the RIS energy parameter in which calculated by Yoon's method (Yoon, 1975) as $E_\eta = -1.7, E_\omega = 8.4, E_{\omega'} = 8.4, E_{\omega''} = 9.2$ kJ/mol. The intermolecular interaction can be generated by finding the energetics obtained from the interaction between pairs of chain subsets, using the discretized version of Lennard-Jones (LJ) potential energy function. The molecular interaction on the 2nd lattice is based on similar statistical thermodynamics of the second virial coefficients of real gases as follows:

$$B_2 = -\frac{1}{2} \left[\int \{e^{-\beta u(r)} - 1\} dr \right] = \frac{1}{2} \int f dr \quad \text{Equation 3.3}$$

Where $\beta = 1/kT$; k is the Boltzman constant (1.38×10^{-23} m² kg s⁻² K⁻¹). While f is the Mayer function and $u(r)$ is the inter-particle LJ potential, which is defined as in equation 3.4

$$u = \begin{cases} \infty & r < 2.5 \text{ \AA} \\ 4\varepsilon \left[\left(\frac{\sigma}{r}\right)^{12} - \left(\frac{\sigma}{r}\right)^6 \right] & r \geq 2.5 \text{ \AA} \end{cases} \quad \text{Equation 3.4}$$

Where ε and σ are the well depth (epsilon) and finite distance at the inter-particle potential is zero (sigma), respectively. r is the distance between two beads, which is defined by the contour length of the polymer. In this work, the LJ-

potential parameters of styrene monomers were obtained from Clancy's (Clancy, 2001) calculation, $\varepsilon/k_B = 377$ K and $\sigma = 5.932$ Å at simulated temperature 600 K. The interaction between polystyrene units for the first three shells on the 2nd lattice are 86.4, 11.53, and -1.15 kJ/mol. We used only three shells of interaction to speed up the simulation time, and these parameters give the bulk density close to the database 1.06 g/cm³ (Mattice, 1994).

3.1.2 Moves in the simulation

In this lattice MC simulation, two types of motion are involved. The first one is the movement of the single bead as shown in Figure 3.1. Every bead will have the chance to move to nearest unoccupied neighbors under the restriction of bond length and energetics. Single bead motion can change the position of 2 or 3 consecutive carbon atoms on the underlying fully atomistic diamond lattice. Another type of move is the multiple bead pivot move. In a pivot move, bond vectors of a short sub-chain are reversed from old conformation to new one and 2-6 beads in pivot moves are applied in the simulation, as illustrated in Figure 3.2.

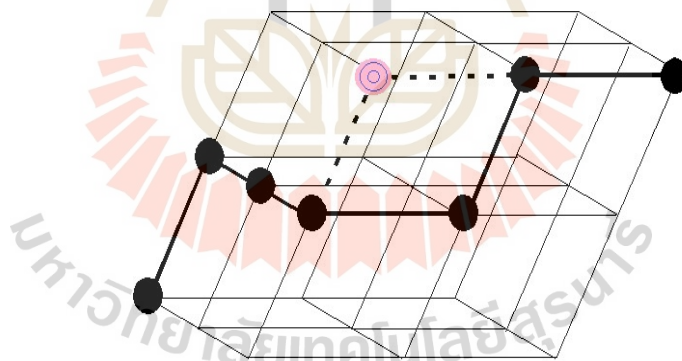


Figure 3.1 Single bead move on 2nd lattice.

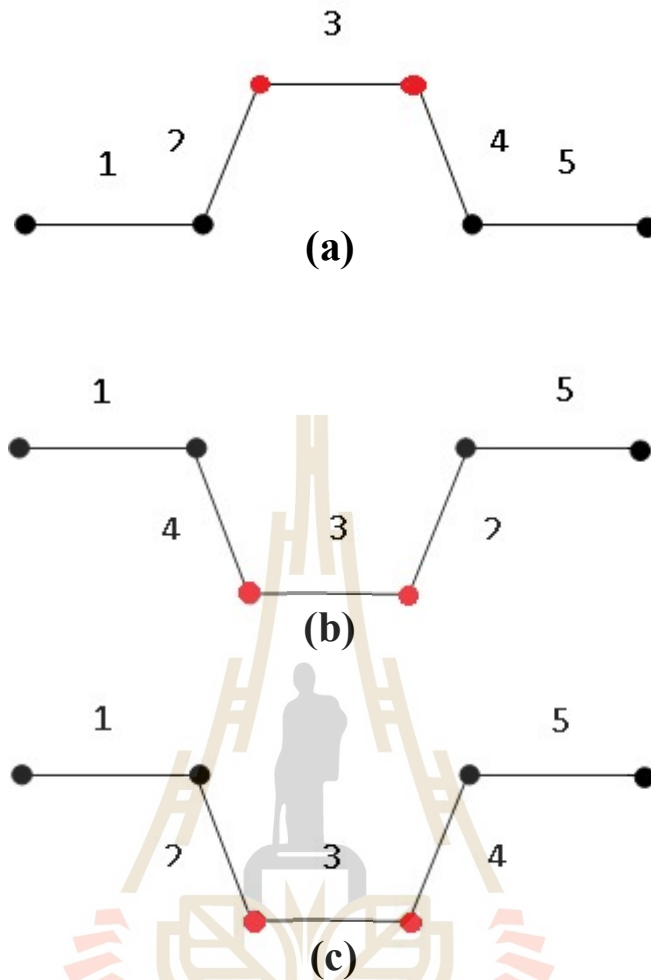


Figure 3.2 Schematic representation of two-bead pivot move. Two middle red beads change their positions after moving, (a) old-conformation, (b) change sequence of bond vector, (c) new-conformation.

For every Monte Carlo Step (MCS), single bead and multiple bead pivot moves will be tried randomly, and every bead will be attempted for both moves. Therefore, one MCS will correspond to single and pivot moves in each bead, on average. Moved to double occupancy and collapse is prohibited (Figure 3.3). In this work, Metropolis criteria with the following formalism are applied to determine whether the move is made or not (Metropolis, 1953).

$$P = \begin{cases} \exp\left(-\frac{\Delta E}{RT}\right) & \Delta E > 0 \\ 1 & \Delta E \leq 0 \end{cases} \quad \text{Equation 3.5}$$

where ΔE is the energy difference between the new and old conformation, which includes both short- and long-range interactions. R is the universal gas constant and T is the absolute temperature. If $\Delta E \leq 0$, the move is accessed. Otherwise, a random number is generated uniformly from 0 to 1 is used to determine whether the move is successful or not.

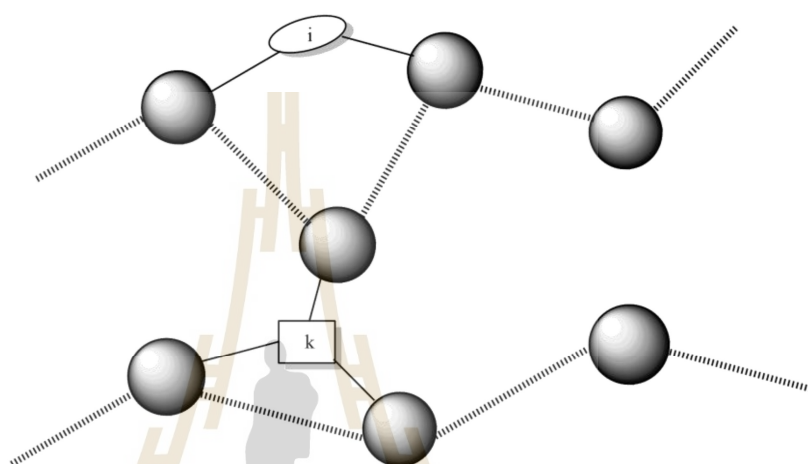


Figure 3.3 Two kinds of unphysical collapses. *i* is intramolecular collapse, and *k* is intermolecular collapse. *i* and *k* are occupied in the same lattice site after reverse-mapping.

3.1.3 Simulation of polystyrene on 2nd nearest neighbor diamond lattice.

In this work, a coarse-grained polystyrene model was developed and used in the simulation. The coarse-grained bead consists of a styrene unit with two backbone carbon atoms on the second nearest neighbor diamond (2nd) lattice which is a cubic-like structure with the angles of 60 degrees ($\alpha = \beta = \gamma = 60^\circ$). The distance between each bead is constant at 0.25 nm, which is calculated from the C-C bond length (0.154 nm) and C-C-C bond angle (109.5°).

This research is based on a coarse-grained polymer model with a length of 42 beads which is equivalent to 84 carbon backbone atoms. There are 14 polystyrene chains in the simulation box to reflect the experimental bulk density (1.06 g/cm^3). The size of simulation box used is $20 \times 20 \times 20$ units (equal to $5.0 \times 5.0 \times 5.0 \text{ nm}$). The density

of the lattice box is 1.080 g/cm^3 with only 7.35% bead occupancy. The temperature used in the simulation is 600 K to increase the simulation efficiency. Statistical analysis is based on an average of 90,000,000 MCS, in which a snapshot will be taken every 10,000 MCS.

3.1.4 Fully atomistic model

The fully atomistic model of amorphous polystyrene can be obtained by reverse mapped back from the coarse-grained model (Figure 3.4). The hydrogen and carbon atomic coordination have been created onto the diamond lattice. Then, the energy minimization has been performed using Xenoview (molecular mechanics and dynamics simulation free software) for fully atomistic polystyrene (Xenoview, 2002). The PCFF force field was used in this simulation with the Steepest descent and conjugate gradient methods until the gradient is less than 0.1 kcal/mol. In some cases, we also used short dynamics simulation for minimized structures to lower potential energy. The dynamics run was performed with an *NVT* ensemble for 500 ps. Therefore, we will obtain a low total potential energy structure from molecular dynamics simulation, and then the potential energy of this structure will be minimized again.

3.2 Atomistic local structure of salt doped sulfonated polystyrene

3.2.1 Molecular simulation of sulfonated polystyrene doped with cation salts

Molecular dynamic (MD) simulation was carried out using GROMACS version 2018.1 software package with OPLS-AA force field. The optimized structure and force field parameter of sulfonated styrene unit and cation (Ca^{2+} , Na^+ , and K^+) was generated using LigParGen (Jorgensen, 2005; Dodda, 2017 and Dodda, 2017) web server, while water model was spc216.gro configuration from standard GROMACS package. A bulk amorphous system of sulfonated styrene units and cations was built using the cubic cell with periodic boundary conditions. Charges of each component were calculated by the *ab initio* calculation and the negative charge of sulfonated styrene was neutralized by cations. The effect of system size on the solvation structure was also studied by varying the number of cation and ionomer. Both dried and hydrated Cation-ionomer were studied. Energy minimization of these amorphous models was performed by the Steepest Descent method with a tolerance of $0.1 \text{ kcal.mol}^{-1} \text{ nm}^{-1}$.

The system was compressed at an artificially high pressure of 30 atm to adjust the box volume for a 10 ns NPT-MD run. Then, the equilibrium density can be obtained from NPT-MD at 298 K and 1.0 atm for another 5 ns run until there is no change in the simulation box dimension. The Berendsen thermostat and Berendsen barostat were used to control the temperature and pressure during the simulation, respectively. The Particle Mesh Ewald (PME) was used to treat the long-range electrostatic interaction. The equilibrated structure can be determined when the density and potential energy of the system reached constant values. Finally, the trajectory of the 20-ns NVT-MD run with a time step of 2 fs at 298 K 1 atm was performed. In all simulations, the trajectories were saved every 500 fs for subsequent analysis. For analysis of the structure, radial distribution function (RDF) and coordination number around the ions were calculated from MD trajectories. The RDF of Ca^{2+} , Na^+ , and K^+ ions surrounded by O atom can be determined from:

$$g(r)_{ca--o} = n(r)_o / [dV(r)\rho(r)] \quad \text{Equation 3.6}$$

where $n(r)_o$ is the number of O atoms in a spherical shell at a distance r from the cation, $dV(r)$ is the shell volume, and $\rho(r)$ is the number density of O atoms in the system.

3.2.2 EXAFS measurements and data analysis

The experiment for K-edge EXAFS spectra was performed at X-ray Absorption Spectroscopy beamline (BL-8), Synchrotron Light Research Institute (Public Organization), Thailand. Calcium sulfonated polystyrene (Ca-SPS) or Kalimite (structure shown in Figure 3.4), purchased from Doctoroncall (Doctoroncall, Malaysia), was set on the sample holder. Data were collected in the transmission mode with Ge (220) double crystal monochromator. The 5-eV steps were used in the pre-edge region, while 0.2-eV steps were employed from -20 eV below the edge to 30 eV above the edge. For the EXAFS region (30 eV above the edge to 1500 eV), 0.05-eV steps were employed. Energy calibration can be done by setting the Ca K-edge absorption to 4038.5 eV with the standard anhydrous CaCO_3 compound. A total of 5 scans (each scan lasted approximately 60 min) were collected, and these scans were added after E_0 determination before further data analysis to improve the signal-to-noise ratio.

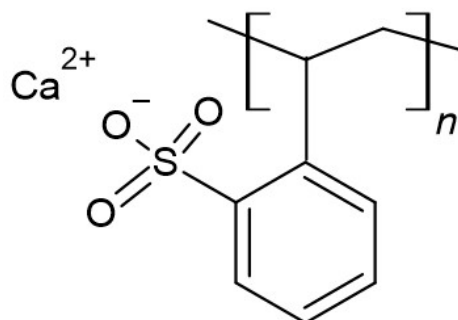


Figure 3.4 Calcium sulfonated polystyrene repeating unit.

ATHENA software (Ravel, 2005) was used for standard analysis procedures such as alignment data, background subtraction, normalization, and spline removal, and to convert the measured EXAFS oscillation from μt vs E to $k^2\chi(k)$ vs k plot. The EXAFS oscillation was Fourier Transformed to give the radial structure-function (RSF). The RSF is similar, but not the same, to the radial distribution function (RDF) because the peaks in RSF usually correspond to distinct coordination shells. The abscissa of the RSF has units of Angstroms (\AA), but the location of the peak is shifted from the real distances. Fourier transformation was performed over the k -range $2-9 \text{ \AA}^{-1}$ without applying a window function.

3.2.3 MD-EXAFS fitting

The hypothetical EXAFS scattering path of the selected snapshot from MD trajectories was generated using ARTEMIS with FEFF6 package (Rehr, 1992). This package determined the EXAFS patterns based on user-supplied XYZ coordinates of the atomic structure by performing *ab initio* calculations and combining single and multiple scattering curved wave paths. In this work, the EXAFS spectra were calculated from the selected atomic coordinates MD configurations in different trajectories. For each snapshot, the atomic group was obtained by separating all species that fell within a 6 \AA radius of the probed Ca^{2+} ion.

3.3 SPS thin film by coarse-grained random copolymer models

Figure 3.5 shows the Monte Carlo simulation outline of coarse-grained copolymer thin film on the $2nd$ lattice. The first step of simulation starts with creating a RIS

model that characterizes the local conformation of PE. Then, the mapping procedure of PE chains was performed with the modified RIS model and discretized version of non-bonded energy which represented the short- and long-range interactions of the random copolymer model at the bulk density, respectively. After the bulk structures were equilibrated, the free-standing thin-film structures were generated by the periodic box expansion technique (Misra, 1995; Doruker, 1998). The Monte Carlo (MC) long simulation run was then performed with the Metropolis algorithm until the system achieves equilibrium. To obtain the simulation trajectories for subsequent data analysis, some additional runs were operated by MD simulation.

3.3.1 Random copolymer model

The simulation systems were based on a coarse-grained PE-like model, which is composed of ethylene (C) and comonomer (X) units in equal numbers. There are three types of interactions between different beads, C-C, X-X, and C-X interactions. Both C and X beads are represented by CH₂-CH₂ unit placed on the high coordination lattice, the second nearest diamond (*2nd*) lattice (Rapold, 1995). There are 128 copolymer chains with 50 monomer beads in the simulation box. The distance between bead *i* and *i*+1 is 2.5 angstrom, which is determined from the contour distance of the C-C-C bond angle and C-C bond length. Two types of interaction parameters were applied to describe the energetic of copolymer models, intra- and inter-molecular interactions. For short-range intramolecular interaction was applied by the rotational isomeric state (RIS) formalism (Flory, 1969; Mattice, 1994). The contour length in the *2nd* lattice of 2.50 angstrom was obtained from 1.53 angstrom bond length and 112° bond angle of PE. Only the first- and second- order interactions of RIS model were accounted in this work. The first-order interactions were used to explain the conformational states of three successive CH₂-CH₂-CH₂ bonds that depend only on one torsion angle. The second-order interactions depended on two degrees of freedom that were used to describe conformational states of four successive bonds, CH₂-CH₂-CH₂-CH₂. The first- and second- order interaction parameters were normally represented in the RIS statistical matrices. For PE coarse-grained polymer, the RIS model was adopted from Abe and co-workers' work that exhibited in six statical matrices (Abe, 1965) as shown in equation 3.7.

$$U_{PE} = \begin{bmatrix} 1 & \sigma & \sigma \\ 1 & \sigma & \sigma\omega \\ 1 & \sigma\omega & \sigma \end{bmatrix} \rightarrow U_{2nnd} = \begin{bmatrix} 1 & 4\sigma & 2\sigma\sigma(1+\omega) \\ 1 & 4a & 2b\sigma(1+\omega) \\ 1 & 4b & 2c(1+\omega) \end{bmatrix} \quad \text{Equation 3.7}$$

Where

$$\sigma = \sigma_0 \exp\left(-\frac{E_\sigma}{kT}\right), \omega = \omega_0 \exp\left(-\frac{E_\omega}{kT}\right), a = \sigma\omega^{1/8}, b = \sigma\omega^{1/4}, c = \sigma^2\omega^{1/2}$$

The σ and ω are the first- and second- order interaction parameters, respectively. The parameter in the column represented the states of bond i th, and the rows are indexed by the states of $i-1$ bond. The orders of indexing are t , g^+ , and g^- . For the remaining long-range intramolecular interaction and all intermolecular interactions, the Lennard-Jones potential function was performed with parameters of ethylene ($\text{CH}_2=\text{CH}_2$): $\varepsilon/k = 185$ K and $\sigma = 4.4$ Å for C-C interaction (Cho, 1997; Poling, 2000). The varying non-bond interaction with $\varepsilon/k = 100, 185, 250, 300, 350$ K and $\sigma = 4.4$ Å were applied for studying the interaction between comonomer (X-X) beads, where the system with beads having $\varepsilon/k = 185$ K was used as a reference bead. For the interaction between different monomer beads C-X, we used the Lorentz-Berthelot mixing rules to obtain σ and ε/k values follow in equation 3.8 (Poling, 2000).

$$\varepsilon_{AB} = (\varepsilon_A \varepsilon_B)^{1/2} \quad \text{Equation 3.8}$$

The discretized shell energies u_1 , u_2 , and u_3 of both X-X and C-X interactions that calculated from σ and ε/k values at 473 K were summarized in Table 3.1. The larger average interaction energies in the first shell (u_1) of all LJ parameters referred to as highly repulsion force, this is because the distance between the two first neighboring beads (2.5 Å) is smaller than the LJ length parameter (4.4 Å). The second shell (u_2) interaction energy is on average between attractive and repulsive force, the value is slightly above zero. Finally, the attractive force represented as a major interaction for the third shell energy (u_3).

Table 3.1 Non-bonded interaction parameter (kJ/mol) for copolymer model: C..C, X..X and C..X beads at 473 K ($\sigma = 4.4 \text{ \AA}$ with different ϵ/k).

ϵ/k (K)					
(C...C)	100	185	250	300	350
and					
(X...X)					
u_1	14.249	15.048	15.245	15.277	15.240
u_2	0.932	0.620	0.298	0.024	-0.265
u_3	-0.329	-0.625	-0.858	-1.042	-1.229
ϵ/k (K)					
(C...X)	136	185	215	235	254
u_1	14.704	15.048	15.167	15.219	15.251
u_2	0.823	0.620	0.477	0.373	0.277
u_3	-0.453	-0.625	-0.732	-0.806	-0.873

3.3.2 Monte Carlo simulation

Dynamic Monte Carlo simulations were performed after mapping the copolymer chains onto coarse-grained $2nd$ lattice. The simulation run is based on the single bead moves which are equivalent to three or four bond movements in the real atomistic chains. This kind of movement avoided repeating the occupancy of any lattice point. Again, the Metropolis rules are used to determine the acceptance or rejection of these single bead moves (Poling, 2000). The trial moves are obtained from the change in energetics between intra- and inter-chain interactions (ΔE). The probability of a bead move (P_{move}) within a chain is given following equation 3.9. The P_{LR} is the probability from the change in the long-range interaction (LJ) energy.

$$P_{move} = \min[1, P_{LR}P_{new}/P_{old}] \quad \text{Equation 3.9}$$

Where

$$P_{LR} = \exp(-\Delta E_{LR}/(RT))$$

$$\frac{P_{new}}{P_{old}} = \frac{Q_{\epsilon\zeta^*;i-2} Q_{\zeta^*\eta;i-1} Q_{\eta\nu^*;i} Q_{\nu^*\kappa;i+1}}{Q_{\epsilon\zeta;i-2} Q_{\zeta\eta;i-1} Q_{\eta\nu;i} Q_{\nu\kappa;i+1}}$$

One Monte Carlo Step (MCS) is defined as the series of one-bead moves randomly selected for the whole chain and all the beads are attempted equally to move. The different moves correspond to the displacement of two or three backbone atoms on the real PE chain. The acceptance rates for bead move in this MC simulation were inversely proportional to the LJ interaction parameter (ϵ/k) in the range of 4.32 to 9.79% for $\epsilon/k = 350$ and 100 K, respectively.

3.3.3 Film formation

For generating the freely thin film, firstly the bulk states are constructed and equilibrated. The bulk states were generated by placing a coarse-grained copolymer chain into the implemented box with periodic boundary conditions. The dimension of the original box for the bulk system is 30x30x30 lattice units, which is equivalent to 75x75x75 Å³. After the bulk system was completely equilibrated, the box was expanded in z-direction to 90 lattice units that were long enough to prevent the original chains interact with their self-replica, whereas the x and y directions were employed in the periodic boundary condition. Then, a Monte Carlo simulation of copolymer thin film was performed to equilibrate the structure within 20 million MCS (Doruker, 1998). To determine the equilibration of each system, the mean distance criterion, such as mean square displacement of the center of mass (MSD), was applied as the chain movement is greater than $2Rg$. Moreover, the normalized orientation autocorrelation functions (OACF) of the end-to-end vector are also used to determine the equilibration of chain conformations. The OACF of this system decays to 0.37 (below $1/e$) within 20 million MCS, this means that the systems reach the equilibrium point for all systems. After that, a subsequent 20 million MCS run was employed to obtain the trajectories for data analysis.

CHAPTER IV

RESULTS AND DISCUSSION

4.1 Multiscale simulations of polystyrene with different tacticities

4.1.1 Structure relaxation

The structural relaxation of the initial structure can be obtained by the orientation autocorrelation functions (OACF) as defined using the end-to-end vector of the polymer chain, $\langle \vec{R}(t) \cdot \vec{R}(0) \rangle$. The result depicted in Figure 4.1(a), the independence run results are quite similar for every tacticity with 90 million Monte Carlo Step (MCS). The rotational motion of *s*PS decay from an initial value to almost zero within 90 million MCS. While *i*PS and *a*PS OACF decay to about 0.6 and 0.3, respectively. Previously, the same simulation method has been applied to study the effect of stereochemical composition on diffusion in linear polypropylene (PP) melts and compared with the results from pulsed-gradient NMR spin-echo experiments (Waheed, 2007; Meerwall, 2009). The result shows good agreement together between experiment and simulation, this suggests that the real-time MCS in picosecond can be estimated in each system. Therefore, we expect that the chain dynamics of amorphous polystyrene with different tacticity can be compared using this Monte Carlo simulation, at least, qualitatively. The translational motion determined by the average mean square displacements of the center-of-mass (MSD) also showed the same trend with OACFS, which is *s*PS chains exhibit faster movement than *i*PS and *a*PS as shown in Figure 4.1(b). The relative diffusion coefficients can be calculated using Einstein's relation *i.e.* $MSD/6t$ (the slope of MSD as a function of MCS). Table 4.1 presents the relative apparent diffusion of polystyrene melts with three tacticity and Figure 4.1(c) shows the apparent diffusion as a function of different amounts of *meso* diads from 0.0 to 1.0. In this notation, *syndiotactic*, *atactic*, and *isotactic* are represented by $P_m=0.0$, $0.1-0.9$, and $P_m=1.0$, respectively. The diffusion rate is increased with decreasing

P_m , the highest diffusion rate is sPS, while the lowest is iPS. The mobility of polystyrene is quite sensitive to the stereochemistry of PS chains especially at $P_m < 0.5$.

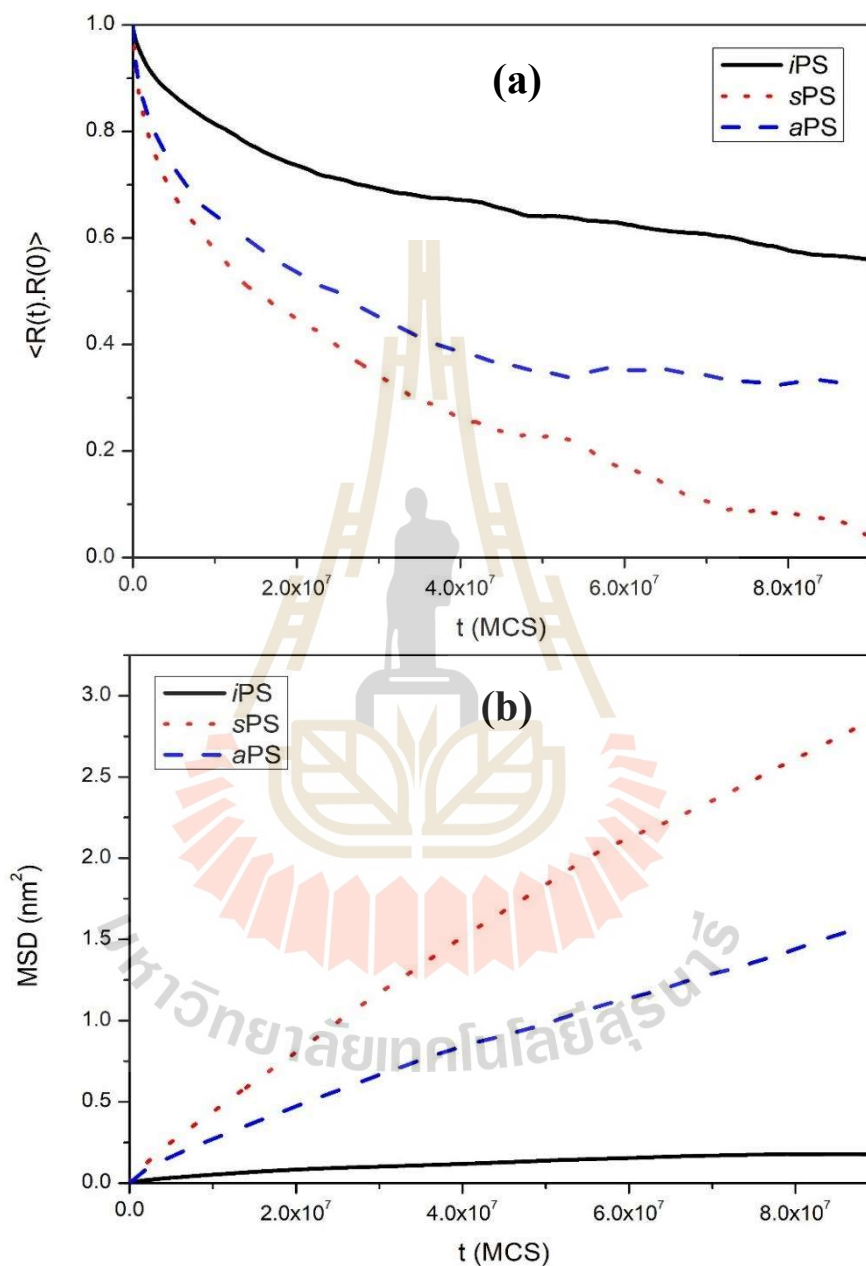


Figure 4.1 (a) The orientation autocorrelation functions (OACF), (b) the average mean square displacements of the center-of-mass (MSD) of polymer chains with different tacticity in 90 million Monte Carlo Step (MCS). (c) The relative diffusion as a function of different amounts of *meso* diads from 0.0 to 1.0.

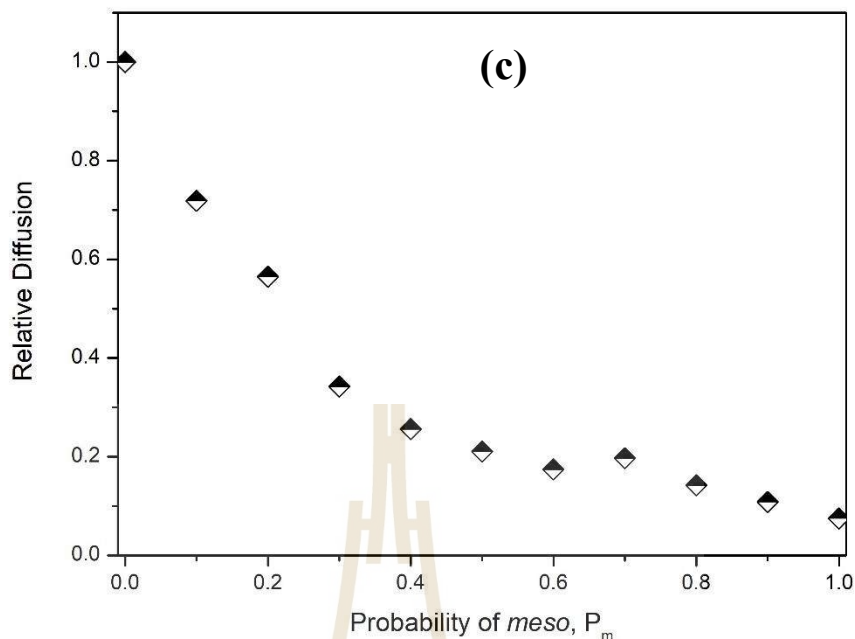


Figure 4.1 (a) The orientation autocorrelation functions (OACF), (b) the average mean square displacements of the center-of-mass (MSD) of polymer chains with different tacticity in 90 million Monte Carlo Step (MCS). (c) The relative diffusion as a function of different amounts of *meso* diads from 0.0 to 1.0 (Continued).

4.1.2 Chain dimension

The chain stiffness and molecular dimension of amorphous polystyrene were determined by the characteristic ratio (C_n) and the mean square radius of gyration ($\langle R_g^2 \rangle^{1/2}$). The results were shown in Table 4.1 that the highest mobility sPS chain exhibits a larger radius of gyration and the characteristic ratio, while the lowest mobility iPS chain has a smaller radius of gyration and characteristic ratio due to fewer *trans* sequences. This smaller molecular size of iPS is also observed by experimental small-angle neutron scattering (Grigoriadi, 2019; Takebe, 2009). In addition, the stiffer chain stiffness of sPS also confirmed by Negash and coworker's study (Negash, 2018). They studied the glass transition temperature (T_g) of thin-film polystyrene with different tacticity by using molecular dynamics simulation. The sPS exhibited higher T_g than iPS as indicated to larger C_n . The ratio of $\langle R^2 \rangle / \langle R_g^2 \rangle$ closed to 6 for each PS system was used for validating our simulation results, this means the results are reasonable following theoretical Gaussian behavior for sufficient long chain (Haliloglu, 1999).

Table 4.1 Chain dimension, chain stiffness, and chain diffusion.

Chain	$\langle R^2 \rangle$ (nm ²)	$\langle R_g^2 \rangle$ (nm ²)	$\langle R^2 \rangle /$ $\langle R_g^2 \rangle$	C_n	D (nm ² /10 ⁷ MCS)	Relative D
<i>i</i> PS	6.92±5.35	1.33±0.59	5.20	3.60±1.92	0.03	0.06
<i>s</i> PS	8.49±6.43	1.53±0.68	5.54	4.42±1.19	0.48	1.00
<i>a</i> PS	7.92±5.50	1.37±0.50	5.79	4.13±1.25	0.27	0.57

4.1.3 Structure

The pair correlation function (PCFs), $g_{AA}(i)$, used to describe the phase behavior of the mixtures, which is often obtained from the probability of finding a particle A at a distance r from another particle A. Because the current study was performed on the discrete space, $g_{AA}(i)$ is defined based on the shell i th, instead of the normal definition based on a continuous distance, r . This discretized form of the pair correlation function can be defined as:

$$g_{AA}(i) = \frac{1}{(10i^2+2)V_A n_s} \sum n_{AA}(i), \quad \text{Equation 4.1}$$

where V_A is the volume fraction of A in systems, n_s is the number of snapshots used in the summary, and $n_{AA}(i)$ is the number occupancy of A in the i th shell from another A, where both A comes from different chains. Thus, the definition of $g_{AA}(i)$ is in terms of intermolecular pairs. The normalization is chosen so that $g_{AA}(i) = 1$ for a random distribution of particles (Haliloglu, 1999).

Figure 4.2 presents the local intermolecular interaction characterized by the intermolecular PCF calculation. The first two shells of PCF are very small as expected from the positive parameter of the discretized intermolecular potential energy function. The third shell exhibits the highest PCF value due to higher attractive interaction. The *i*PS chain shown the highest PCFs for every shell compared to those of *s*PS and *a*PS chains, which is exhibit less efficient intermolecular packing and generally ordered as: *i*PS > *s*PS > *a*PS (however, this order is different from the rate of molecular mobility *i*PS < *a*PS < *s*PS). Based on PCF results, *i*PS chain prefers to interact

with other *i*PS chains more than *s*PS or *a*PS. The effect of intermolecular packing may be the reason why *i*PS chains are more difficult to move. These results imply that intermolecular interaction of different chain packing should be related to the different conformational of PS tacticity.

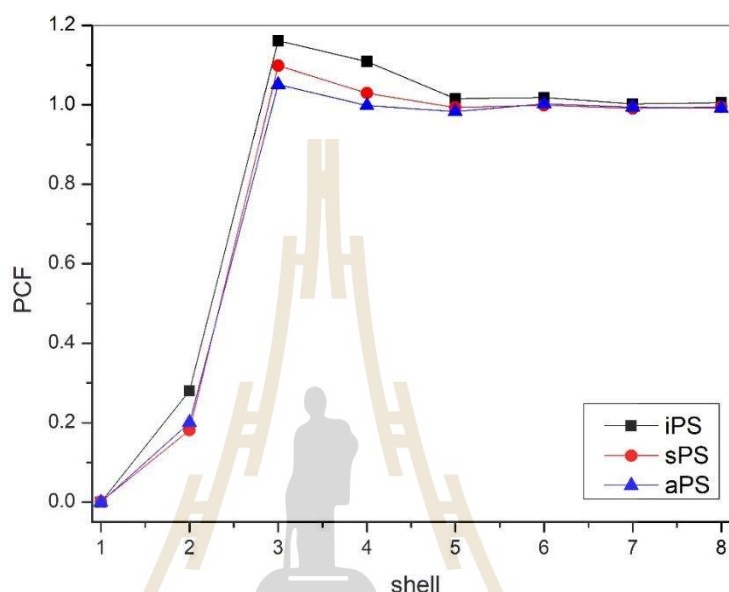


Figure 4.2 The pair correlation function (chain packing) of *i*PS, *s*PS, and *a*PS pure melts.

4.1.4 Conformation

Figure 4.3 represented the C-C-C-C torsion angle of reversed mapping *a*PS before and after minimization. Before the energy minimization, the C-C-C-C torsion angle was distributed into three narrow regions, $g+$ (60°), t (180°), and $g-$ (300°). The torsion angle before energy minimization shown not different with different tacticity, according to the underlying diamond lattice. After minimization, the torsion angle becomes distributed into the various angle as shown histogram in Figure 4.3. The $g+$, t , and $g-$ populations of before and after minimization were compared in Table 4.2 for *i*PS, *s*PS, and *a*PS. Moreover, the theory RIS *a-priori* probabilities were also used to compare with the calculated value after energy minimization for *a*PS (Rapold, 1994). The torsion angle from RIS calculation can be located only in $g+$ state, different from our simulation in which is located by both $g+$ and $g-$ states. This is because of the

consequence non-bond interaction effect from phenyl rings that are not present in the RIS calculations.

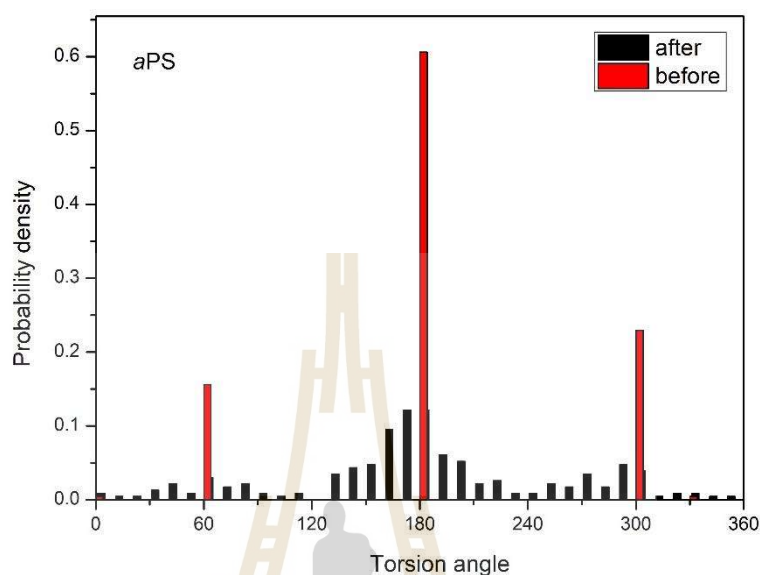


Figure 4.3 Distribution of the C-C-C-C torsion angle of reversed mapping *aPS* before and after minimization from selected snapshot.

Table 4.2 Distribution of the C-C-C-C torsion angles with different tacticity of polymer chains before and after energy minimization.

	Before minimization			After minimization		
	g^+	t	g^-	g^+	t	g^-
<i>iPS</i>	0.17	0.67	0.16	0.20	0.60	0.20
<i>sPS</i>	0.15	0.61	0.24	0.17	0.56	0.27
<i>aPS</i>	0.16	0.61	0.23	0.15	0.63	0.22
RIS				0.29	0.72	0.00

4.1.5 Radial distribution function and neutron scattering

The radial distribution function, the same definition to pair correlation function (PCF) of the bead pair in the coarse-grained model, was used to determine the pair interaction of different elements. The C-C, H-H, and C-H RDFs were calculated as shown in Figure 4.4(a)-(c). The RDF curves of the total correlation function exhibited

a sharp peak at the distance less than 6 Å, and reach over 1.0 RDF in the range from $r > 6$ Å. The inter-molecular interaction increases with increasing separation range and reaches the unity value at a long separation range. There is a weak dependency of tacticity on both interchain and total RDF curves for every interaction. However, the *i*PS has a noticeable higher interchain interaction than other tacticities, *s*PS and *a*PS. These fully atomistic results are consistent with the coarse-grained bead PCF results in that the *i*PS showed the highest intermolecular packing.

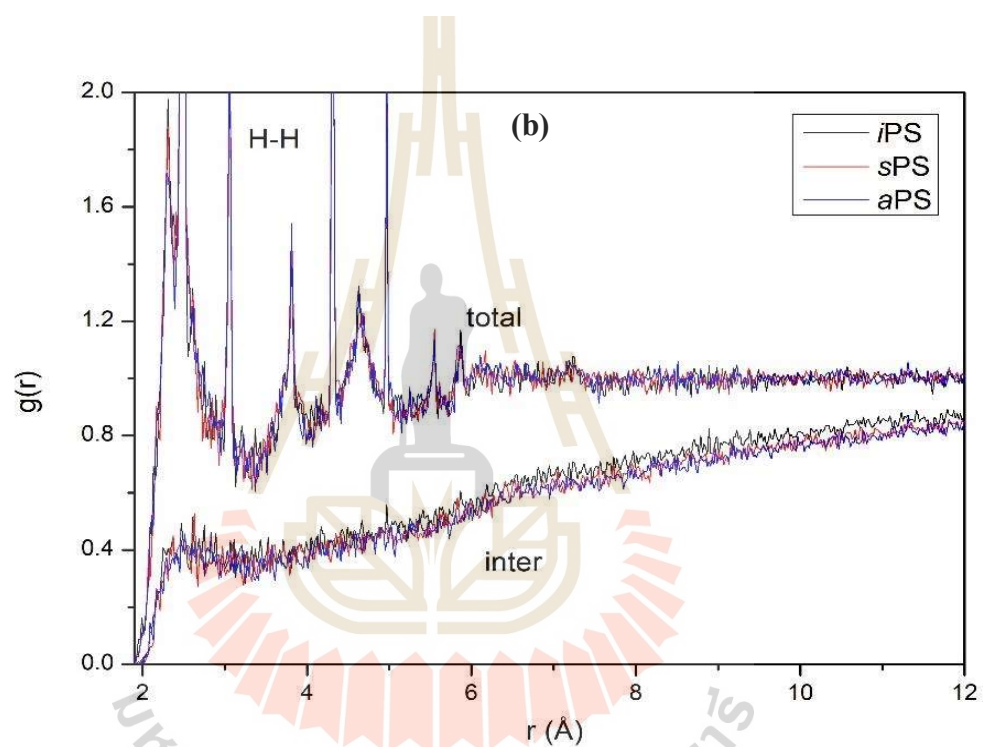


Figure 4.4 The radial distribution function for three different pairs of elements (a) C-C, (b) H-H and (c) C-H.

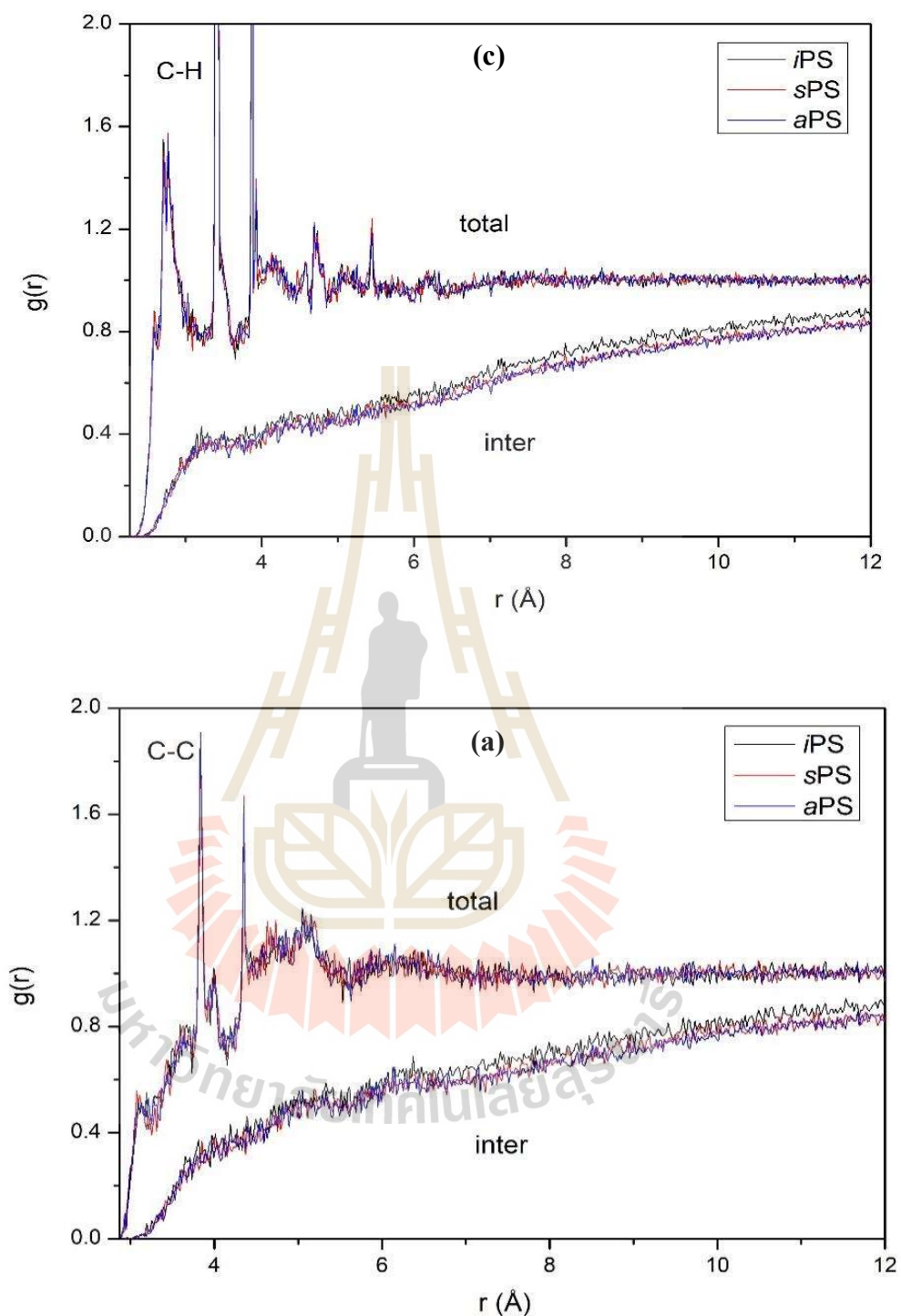


Figure 4.4 The radial distribution function for three different pairs of elements (a) C-C, (b) H-H and (c) C-H (Continued).

The neutron elastic structure factor $S(Q)$ can be calculated as a function of the scattering vector magnitude $Q = \left(\frac{4\pi}{\lambda}\right) \sin \theta$ (Ludovice, 1989). The calculated

structure factor in this work was determined from the atomistic radial distribution function, which has the scattering amplitudes as: $f_c = 6.65$ fermi and $f_H = -3.74$ fermi (Rapold, 1994). The calculated neutron scattering spectrum has three dominant peaks at $Q = 0.9, 1.3,$ and 3.1 \AA^{-1} as shown in Figure 4.5. The calculated and experimental spectrum of *aPS* were fit well together, which the dominant peaks of the experiment shown at $Q = 0.6, 1.33,$ and 3.0 \AA^{-1} . The second peak of an experiment is seeming the major peak, while the first peak is only a shoulder. From our simulation, the neutron scattering at the atomistic level has no significant difference with different tacticity of PS.

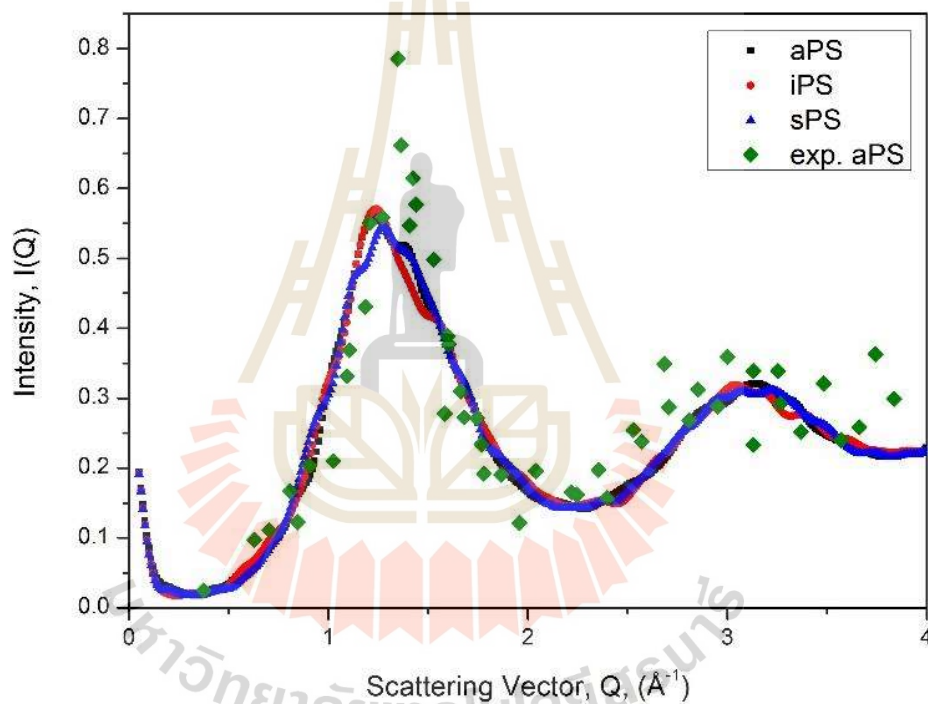


Figure 4.5 Neutron scattering vector for *aPS*, *iPS*, *sPS* from the calculation, and *aPS* from an experiment (Rapold, 1994).

4.1.6 Solubility parameters

The solubility parameter (δ) of polystyrene with different tacticity can be calculated from Hildebrand's equation as in Equation. 4.2.

$$\delta = (CED)^{1/2} = \left[\frac{\Delta E_v}{V_1} \right] \quad \text{Equation. 4.2}$$

Where the CED is the cohesive energy density, ΔE_v is the molar energy of vaporization, and V_1 is the molar volume of liquid. The solubility parameter can be

calculated as the square root of the cohesive energy density of reverse-mapped and energy-minimized snapshots. In general, the molar energy of vaporization is represented by the cohesive energy (U_{coh}), the energy associated with the intermolecular interactions. The U_{coh} can be calculated from the difference the total energy of the microstructure (U_{tot}) and the isolated parent chain (U_{par}) as: $U_{coh} = U_{tot} - U_{par}$. The cohesive energy density and solubility parameter of fully atomistic polystyrene with different tacticity after reverse-mapping and energy minimization has been shown in Table 4.3. Compared with the experimental Hildebrand solubility parameter of commercial PS in the range of 16.6-20.2 $J^{1/2}/cm^{3/2}$ at room temperature (Brandrup, 1989), the calculated solubility parameters have a lower value due to attractive interaction arising from the aromatic ring. In general, the calculated solubility parameters are quite sensitive to the non-bonded interaction. However, the small magnitude of the standard deviations can be indicated that this simulation has a good degree of confidence. It is possible to improve the solubility result by improving the force field parameter in the simulation system. Here, the average values of our simulation are quite close to the experimental range and the prediction provides reasonable estimates.

Table 4.3 Cohesive energy density and solubility parameter calculated from atomistic PS models.

	Cohesive Energy Density (J/cm^3)	Solubility parameter ($J^{1/2}/cm^{3/2}$)
<i>a</i> PS	$2.29 \pm 0.43E08$	15.14 ± 0.14
<i>i</i> PS	$2.44 \pm 0.52E08$	15.62 ± 0.16
<i>s</i> PS	$2.33 \pm 0.47E08$	15.25 ± 0.15

The combination lattice Monte Carlo simulation of coarse-grained model and energy minimization for reverse-mapping to fully atomistic model can be worked well for amorphous PS. The coarse-grained PS bulks were easily equilibrated by lattice Monte Carlo simulation with the mobility order as $sPS \gg aPS > iPS$. The dynamics of

PS chains with different tacticity are more related to intermolecular packing than intramolecular characterization. After reverse-mapped to fully atomistic models, structural and dynamics properties have been determined. The chain dimension and conformational statics are varied with different tacticities of amorphous PS. The calculated neutron scattering spectrum and solubility parameter were in reasonable agreement with those obtained by the experiment.

4.2 MD simulation of Cation-ionomer benchmark model

4.2.1 Bivalent calcium-ionomer (Ca-SPS) model

The solvation structure of the Ca-SPS ionomer can be investigated by MD simulation. The snapshot for the initial and final structure from MD simulation of Ca-SPS ionomer are depicted in Figure 4.6. After equilibrated structure, phase separation can be distinguished between hydrophobic (styrene units) and hydrophilic region (ionic part: Ca^{2+} ion, O and S atom). From the result in Figure 4.6, the crude estimated coordination structure shows that the Ca^{2+} ion can be surrounded by neighbored O atoms from both sulfonated groups and water. The interactions between Ca^{2+} ion and O atom from sulfonated polystyrene and water can be investigated using the radial distribution function (RDF) as shown in Figure 4.7. The solid and dashed lines represented the RDF and coordination number (CN), respectively, of each interaction system. There are two dominant peaks of Ca—O interactions that occurred within 0.6 nm. It is apparent that the first dominant peak occurred at a range of 0.22-0.30 nm represented to Ca-O first shell interaction, and the second peak showed Ca-O second shell in range of 0.38-0.52 nm. In this work, we focus only on the first shell Ca-O interaction. The peak position (R_0) and CN of dried and hydrated systems with various concentrations of water were determined and summarized in Table 4.4. In a dried system, the Ca^{2+} ion is totally coordinated by 5 oxygen atoms from 3 sulfonated groups at the bond distance of 0.22 - 0.30 nm. The coordination numbers are 5.04 and 4.66 for Ca7SPS14 and Ca13SPS26 systems, respectively. Hence, there is no significant difference in the coordination structure between these two systems. For the systems with different amounts of water molecules, the total coordination number of Ca^{2+} is around 6 at the range of 0.22-0.30 nm. It is composed of 5 and 1 oxygen atoms from

the sulfonated group and water, respectively. There is no difference in the coordination number and position of Ca^{2+} -O(total), Ca^{2+} -O- SO_2 , and Ca^{2+} -O-water for different systems. Based on these results, it can be seen that the system size and the ratio of water do not significantly affect the solvation structure of the ionomer.

For the hydrated Ca-SPS, approximately 6 oxygen atoms are surrounding Ca^{2+} ion (5 from the sulfonated group and 1 from water oxygen). This is consistent with the results from EXAFS and Wide-angle x-ray scattering (WAXS) of hydration calcium ion observed by Jalilehvand *et al* (Jalilehvand, 2001), who found that the hydration number of oxygens around the Ca^{2+} ion is 6 to 9 atoms depended on the distance from the center atom. In addition, Megyes *et al.* (Megyes, 2004), found that the Ca^{2+} ion is surrounded by six methanol molecules from X-ray scattering results.

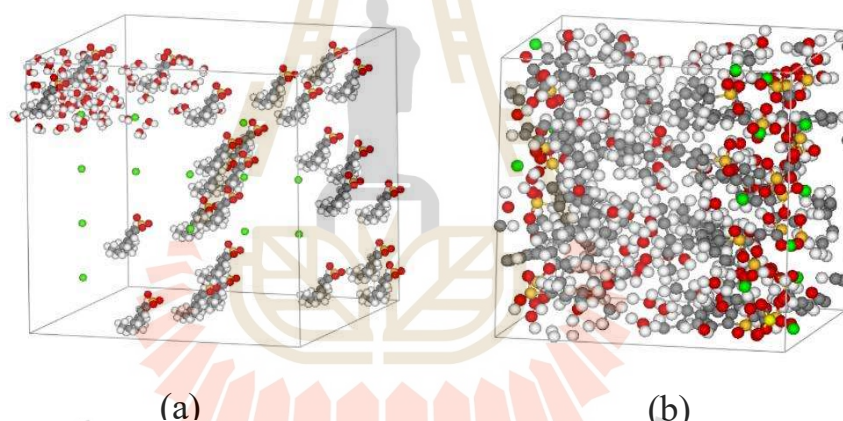


Figure 4.6 Ca-SPS ionomer with water (a) initial- and (b) final-structure from MD simulation (The simulation box on the left-hand side is larger than right side). The green sphere = Ca^{2+} ion, red = oxygen atom, yellow = sulfur atom, gray = carbon atom, and white = hydrogen atom.

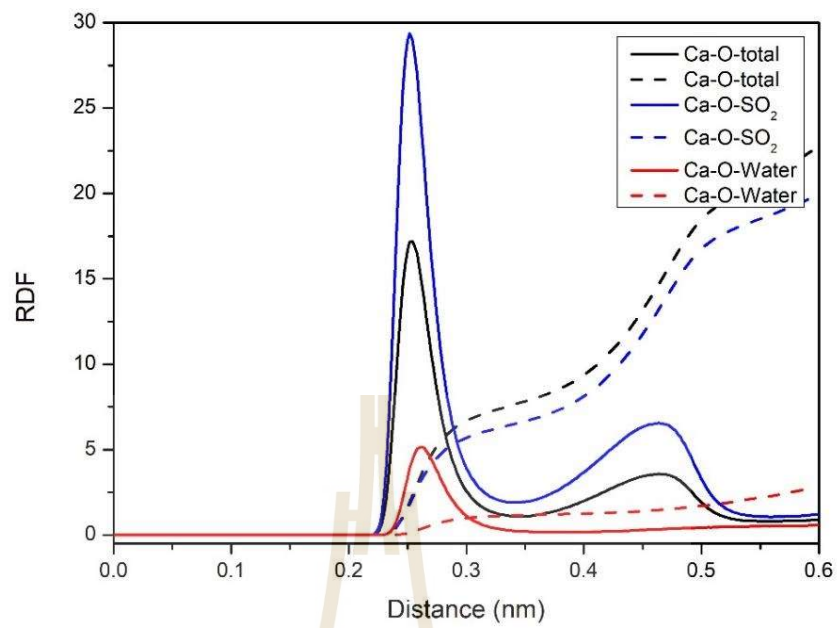


Figure 4.7 The radial distribution function (RDF) of Ca²⁺-O interaction calculated from the MD simulation.

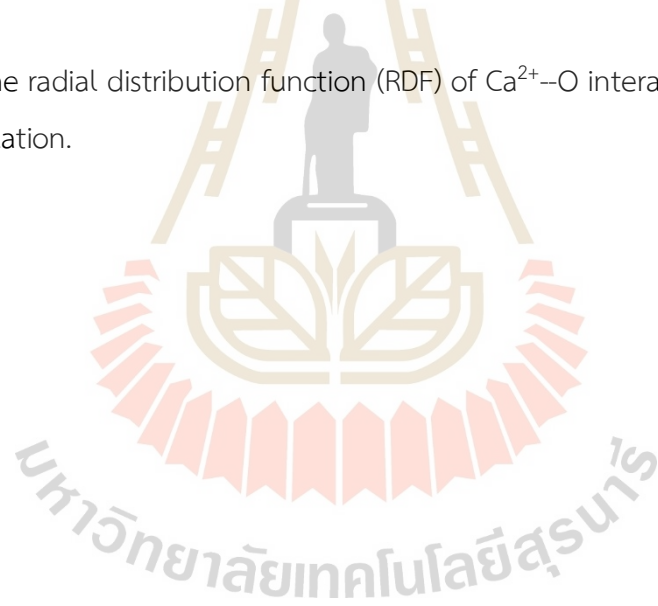
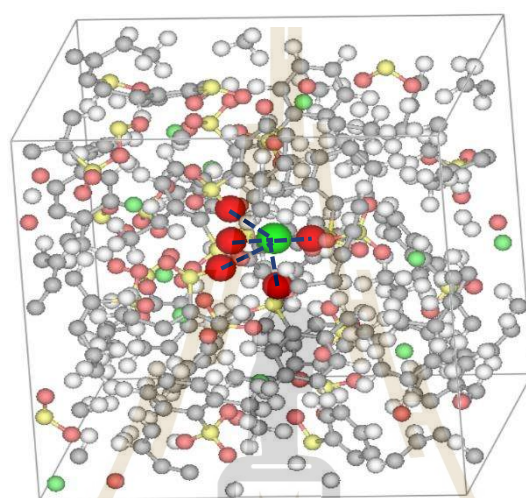


Table 4.4 Parameter characterizing the RDF from MD simulation of Ca-ionomer.

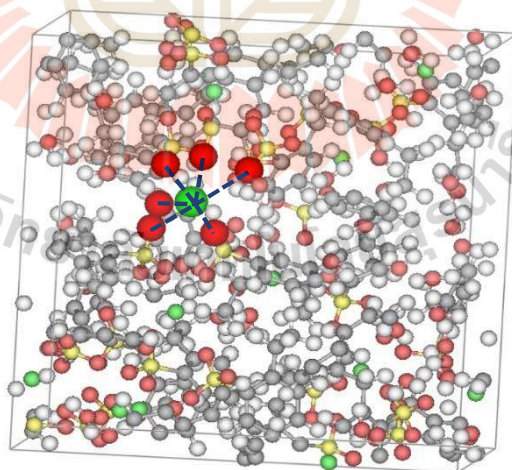
System	interaction	Range (nm)	R ₀ (nm)	CN
Ca7SPS14	Ca ²⁺ -- O-SO ₂	0.22-0.30	0.25	5.04
	Ca ²⁺ --S-O ₃	0.28-0.42	0.38	4.81
Ca13SPS26	Ca ²⁺ -- O-SO ₂	0.22-0.30	0.25	4.66
	Ca ²⁺ --S-O ₃	0.28-0.42	0.38	4.65
Ca7SPS14W14	Ca ²⁺ -- O(total)	0.22-0.30	0.25	6.18
	Ca ²⁺ -- O-SO ₂	0.22-0.30	0.25	5.13
	Ca ²⁺ -- O-water	0.23-0.30	0.26	1.05
	Ca ²⁺ --S-O ₃	0.28-0.42	0.38	4.78
Ca13SPS26W26	Ca ²⁺ -- O(total)	0.22-0.30	0.25	5.81
	Ca ²⁺ -- O-SO ₂	0.22-0.30	0.25	4.68
	Ca ²⁺ -- O-water	0.23-0.30	0.26	1.13
	Ca ²⁺ --S-O ₃	0.28-0.42	0.35	4.32
Ca13SPS26W52	Ca ²⁺ -- O(total)	0.22-0.30	0.25	6.22
	Ca ²⁺ -- O-SO ₂	0.22-0.30	0.25	4.93
	Ca ²⁺ -- O-water	0.23-0.30	0.26	1.29
	Ca ²⁺ --S-O ₃	0.28-0.42	0.35	4.63
Ca13SPS26W78	Ca ²⁺ -- O(total)	0.22-0.30	0.25	6.33
	Ca ²⁺ -- O-SO ₂	0.22-0.30	0.25	4.77
	Ca ²⁺ -- O-water	0.23-0.30	0.26	1.56
	Ca ²⁺ --S-O ₃	0.28-0.42	0.35	4.48

Figure 4.8(a)-(b) shows the example snapshots of dried and hydrated Ca-SPS. From the RDF results in Table 4.4, around 5 sulfur atoms with 5 oxygen atoms are surrounding Ca²⁺ ion in the bulk system. This means that there should be 5 oxygen from 5 different sulfonated groups close to the Ca²⁺ ion. Therefore, the model of the

coordination structure of Ca-SPS bulk in this work can be proposed in Figure 4.8(c) for the dried system and Figure 4.8(d) for the hydrated system. Hence, only one oxygen from each sulfonated group locates near the cation while other oxygen atoms from the same sulfonated group stay away from the nearest Ca^{2+} ion. This is maybe due to the steric hindrance from the backbone chain, only one oxygen can be bound to the central atom.



(a)



(b)

Figure 4.8 Ca-SPS model (a) bulk system and (b) hydrated system from MD simulation, the green sphere = Ca^{2+} ion, red = oxygen atom, yellow = sulfur atom, gray = carbon atom, and white = hydrogen atom. Solvation model of (c) bulk system and (d) hydrated system of Ca-SPS.

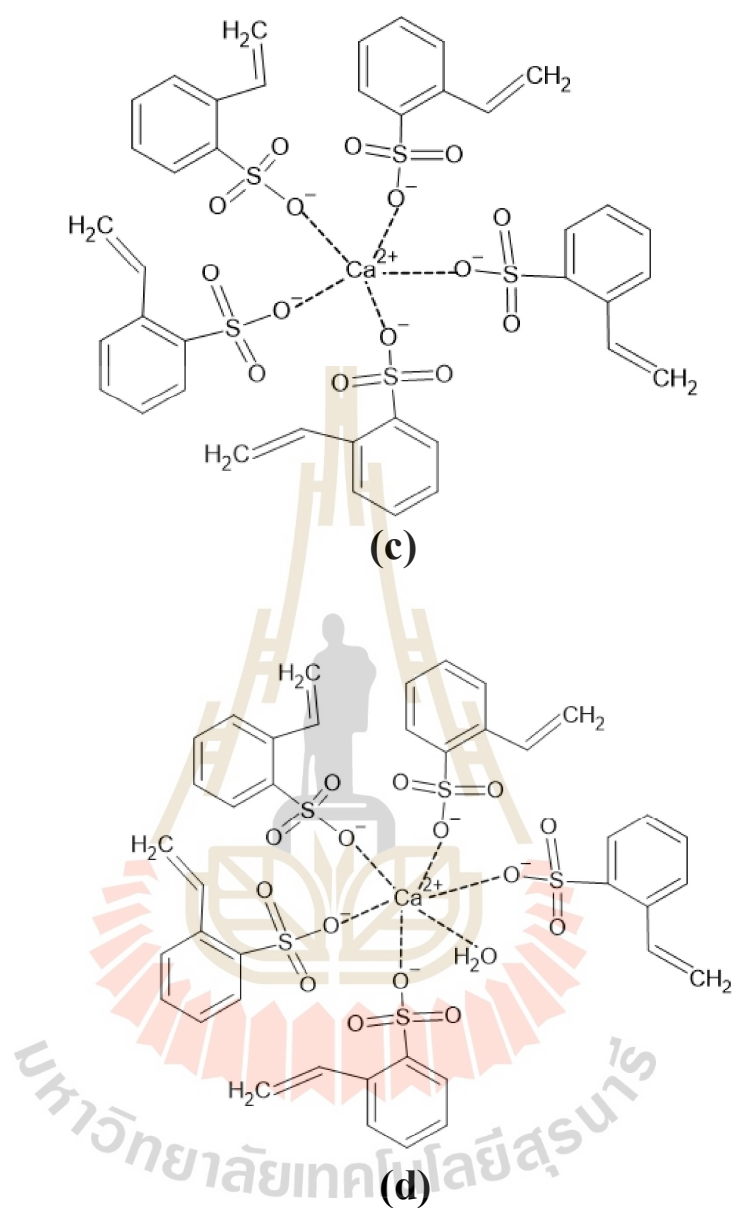


Figure 4.8 Ca-SPS model (a) bulk system and (b) hydrated system from MD simulation, the green sphere = Ca^{2+} ion, red = oxygen atom, yellow = sulfur atom, gray = carbon atom, and white = hydrogen atom. Solvation model of (c) bulk system and (d) hydrated system of Ca-SPS (Continued).

4.2.2 Monovalent sodium-ionomer (Na-SPS), and potassium-ionomer (K-SPS) models

The solvation structure of the monovalent Na-SPS and K-SPS ionomers was also investigated by MD simulation. Figure 4.9 shows the RDF function of Na-SPS (a) and K-SPS (b), the RDF shows two dominant peaks for cation-O interaction and one dominant peak for cation-S interaction at the range within 6 Å. The interaction of Na-O shows the first peak at the range 0.22-0.37 nm and the second peak at the range 0.37-0.54 nm. For the interaction of K-O, the first peak shows at the range of 0.25-0.40 nm and the second peak at 0.30-0.52 nm. The first and the second shells of oxygen that surrounded monovalent metals are close to each other and are not clearly separated, while bivalent metal (calcium ion) from the previous part shows clearly separated. The distance at the maximum first shell of Na-O and K-O are 0.26 and 0.29 nm, which can be seen from Table 4.5 and 4.6, respectively. The maximum first shell of Na and Ca are appeared nearly the same distance, while K appeared at a longer distance. This may be due to the effect of central atomic size and the power of charge.

For bivalent cation in the previous part, the coordination number of Ca^{2+} ions in the hydrate system is around 6 oxygen atoms from 5 sulfonated groups and 1 water. This coordination number is not dependent on the size of the system and the number of waters. However, for monovalent metal, the coordination number depended on both the size of the system and the number of waters. The number of oxygen atoms that surrounded Na^+ ion is around 6 atoms, while the oxygen atoms surrounded to K^+ ion is 5-6 atoms in both bulk and hydrate systems. The number of first shell coordinated oxygen atoms from sulfonated groups and from the water was decreased and increased, respectively, with increasing the water component. These results can imply that the solvation structure of the monovalent cation depended on the ratio of water in the molecule.

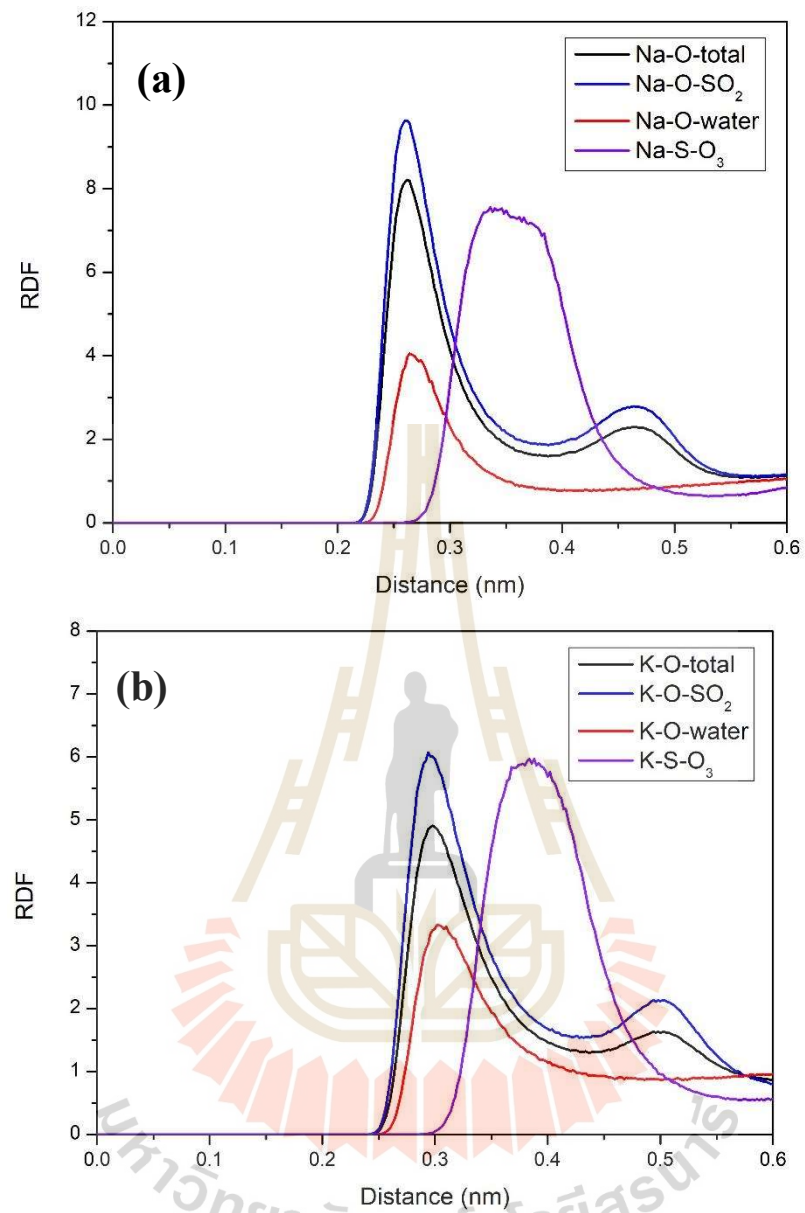


Figure 4.9 RDF curve of (a) Na-SPS and (b) K-SPS from MD simulation analysis.

Table 4.5 Parameter characterizing the RDF from MD simulation of Na-ionomer.

System	interaction	Range (nm)	R ₀ (nm)	CN
Na14SPS14	Na ⁺ -- O-SO ₂	0.22-0.37	0.26	5.35
	Na ⁺ --S-O ₃	0.27-0.50	0.35	3.89
Na26SPS26	Na ⁺ -- O-SO ₂	0.22-0.37	0.26	5.89
	Na ⁺ --S-O ₃	0.27-0.50	0.35	4.43
Na14SPS14W14	Na ⁺ -- O(total)	0.22-0.37	0.26	6.26
	Na ⁺ -- O-SO ₂	0.22-0.37	0.26	5.33
	Na ⁺ -- O-water	0.28-0.35	0.27	0.93
	Na ⁺ --S-O ₃	0.27-0.50	0.35	3.86
Na26SPS26W26	Na ⁺ -- O(total)	0.22-0.37	0.26	6.08
	Na ⁺ -- O-SO ₂	0.22-0.37	0.26	5.32
	Na ⁺ -- O-water	0.28-0.35	0.27	0.76
	Na ⁺ --S-O ₃	0.27-0.50	0.35	3.88
Na26SPS26W52	Na ⁺ -- O(total)	0.22-0.37	0.26	5.82
	Na ⁺ -- O-SO ₂	0.22-0.37	0.26	4.51
	Na ⁺ -- O-water	0.28-0.35	0.27	1.31
	Na ⁺ --S-O ₃	0.27-0.50	0.35	3.25
Na26SPS26W78	Na ⁺ -- O(total)	0.22-0.37	0.26	5.79
	Na ⁺ -- O-SO ₂	0.22-0.37	0.26	4.11
	Na ⁺ -- O-water	0.28-0.35	0.27	1.67
	Na ⁺ --S-O ₃	0.27-0.50	0.35	2.95

Table 4.6 Parameter characterizing the RDF from MD simulation of K-ionomer.

System	interaction	Range (nm)	R ₀ (nm)	CN
K14SPS14	K ⁺ -- O-SO ₂	0.25-0.40	0.29	5.47
	K ⁺ --S-O ₃	0.30-0.52	0.38	3.99
K26SPS26	K ⁺ -- O-SO ₂	0.25-0.40	0.29	5.95
	K ⁺ --S-O ₃	0.30-0.52	0.38	4.27
K14SPS14W14	K ⁺ -- O(total)	0.25-0.40	0.29	5.69
	K ⁺ -- O-SO ₂	0.25-0.40	0.29	4.70
	K ⁺ -- O-water	0.28-0.40	0.30	0.98
	K ⁺ --S-O ₃	0.30-0.52	0.38	3.37
K26SPS26W26	K ⁺ -- O(total)	0.25-0.40	0.29	5.64
	K ⁺ -- O-SO ₂	0.25-0.40	0.29	4.66
	K ⁺ -- O-water	0.28-0.40	0.30	0.98
	K ⁺ --S-O ₃	0.30-0.52	0.38	3.36
K26SPS26W52	K ⁺ -- O(total)	0.25-0.40	0.29	5.65
	K ⁺ -- O-SO ₂	0.25-0.40	0.29	4.05
	K ⁺ -- O-water	0.28-0.40	0.30	1.59
	K ⁺ --S-O ₃	0.30-0.52	0.38	2.91
K26SPS26W78	K ⁺ -- O(total)	0.25-0.40	0.29	5.68
	K ⁺ -- O-SO ₂	0.25-0.40	0.29	3.63
	K ⁺ -- O-water	0.28-0.40	0.30	2.04
	K ⁺ --S-O ₃	0.30-0.52	0.38	2.61

4.2.3 Solvation structure of calcium neutralized sulfonated polystyrene (Ca-SPS) by EXAFS

Figure 4.10 shows the thermograms of sulfonated polystyrene neutralized with calcium cation. There are two weight-loss stages at 70°C - 120°C and 460°C - 550°C were distinguished in this figure. According to *Sloan and co-workers* (Sloan, 2008) work, they found that the neutralized sulfonated polymers usually show two degradation temperatures. One occurred at $453 \pm 3^\circ\text{C}$, which is attributed to the decomposition of the polymer backbone, and another one occurred in the 500-600°C temperature range attributed to the counterion-sulfonic acid complex. Thus, weight loss in the first stage of Ca-SPS may be due to the loss of absorbed water in ionomers and the second stage could be the decomposition of the polystyrene backbone. Water content in Ca-SPS was estimated to be 9% (w/w). While other amounts of a sample should be the combining decomposition of the main chains of the polymer and calcium-sulfonated groups, which would be decomposed in higher than the range of measured temperature.

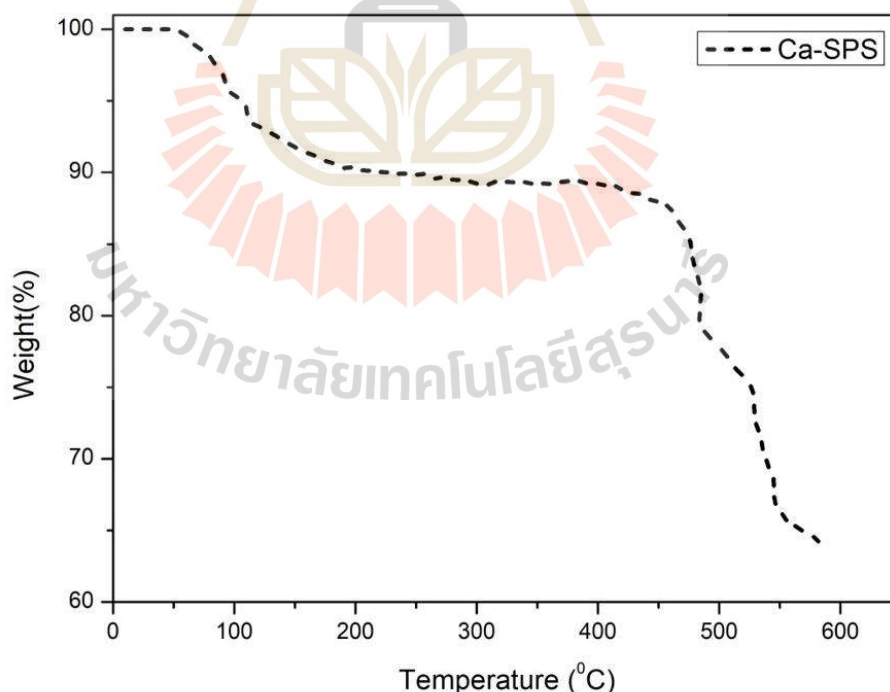


Figure 4.10 TGA curve of Ca-SPS sample. At 70°C - 120°C weight-loss stages represented to the loss of absorbed water in ionomers. For 460°C - 550°C weight loss stage could be the decomposition of the polystyrene backbone.

The atomistic solvation structure of calcium neutralized sulfonated polystyrene (Ca-SPS) can be determined via the EXAFS method. After subtracting background and normalized EXAFS spectra of calcium central atom in Ca-SPS sample, the plot of oscillation pattern (k space) and radial structure function (r space) were determined as shown in Figure 4.11(a) and (b). The data of the Ca-SPS sample shows a distinct oscillation pattern in the 3 - 9 k -range and displays a very noisy pattern in the higher k -range. The radial structure-function (RSF) shown in Figure 4.11(b) can be obtained from the Fourier transform method, which converts data from k to r space. The first prominent coordination shell was observed around 2 Å implying that the neighboring atoms of Ca^{2+} in the first shell are located at a distance of around 2 Å. Next, the oxygen coordination number of Ca^{2+} in the first shell will be evaluated by the fitting procedure using the atomic coordinates from standard crystalline materials and the selected snapshots of the MD trajectory.

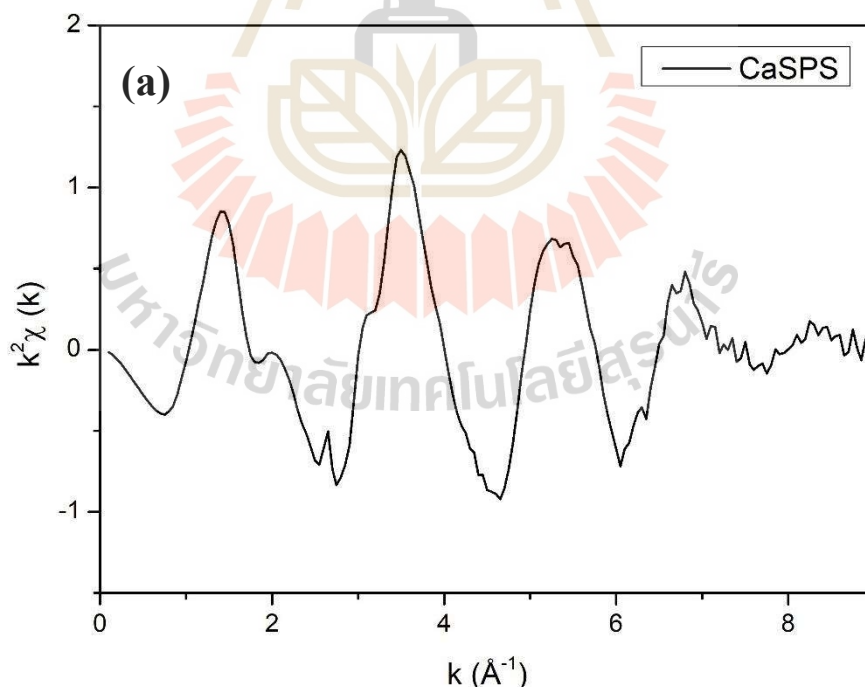


Figure 4.11 EXAFS spectra expressed in (a) k -space and (b) r -space for Ca-SPS ionomers.

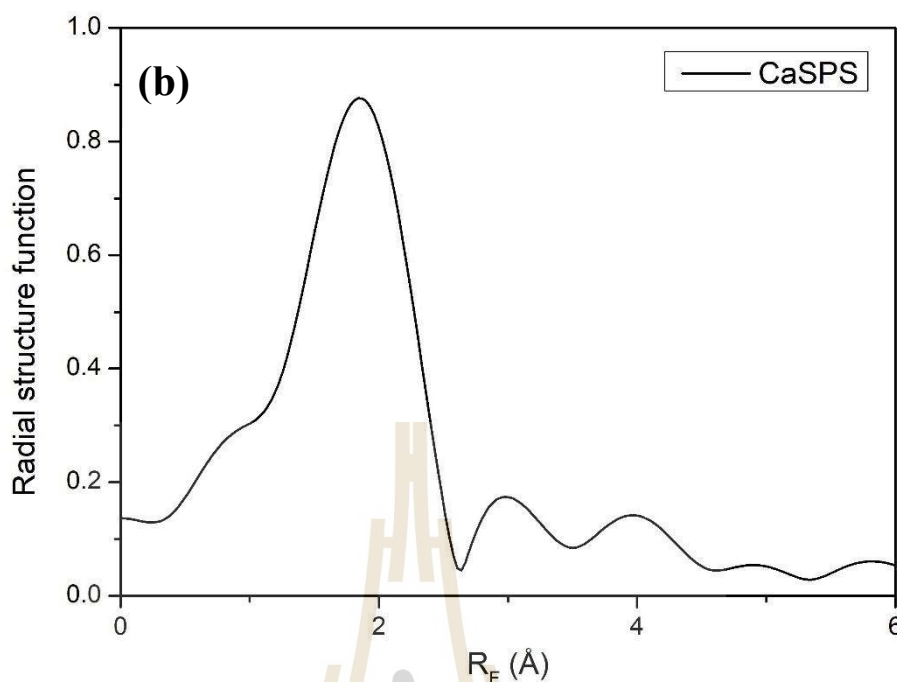


Figure 4.11 EXAFS spectra expressed in (a) k -space and (b) r -space for Ca-SPS ionomers (Continued).

In this work, calcium carbonate (CaCO_3) was adopted as the standard material for modeling the solvation structure of Ca-SPS. The chemical structure of CaCO_3 contains Ca^{2+} ion surrounded by three oxygen from one carbonated group, which is similar to the structure of the Ca-SPS sample. Also, the crystal structure of CaCO_3 (Persson, 2014), a simple cubic crystal structure with $a = 6.463^3$, was used as a reference known structure to fit with CaCO_3 from the EXAFS experiment. There are 6 oxygen atoms arranged equidistant from the probed Ca atoms in the CaCO_3 crystal structure. EXAFS spectra of CaCO_3 were fitted with the 6 pseudo-neighboring oxygen atoms of CaCO_3 crystal structure to determine the crude amplitude (S_0^2) of standard material. Then the fixed amplitude of standard material will be used to calculate the coordination number of Ca-SPS by fitting with referent crystal structure CaCO_3 following ratio method (Teo, 1986). The fitting results of CaCO_3 from the EXAFS experiment and crystal structure are presented in Figures 4.12(a) and 4.12(b) for k - and r -space, respectively. The fitting quality is quite good with an R-factor of 0.011 and an amplitude of 1.446.

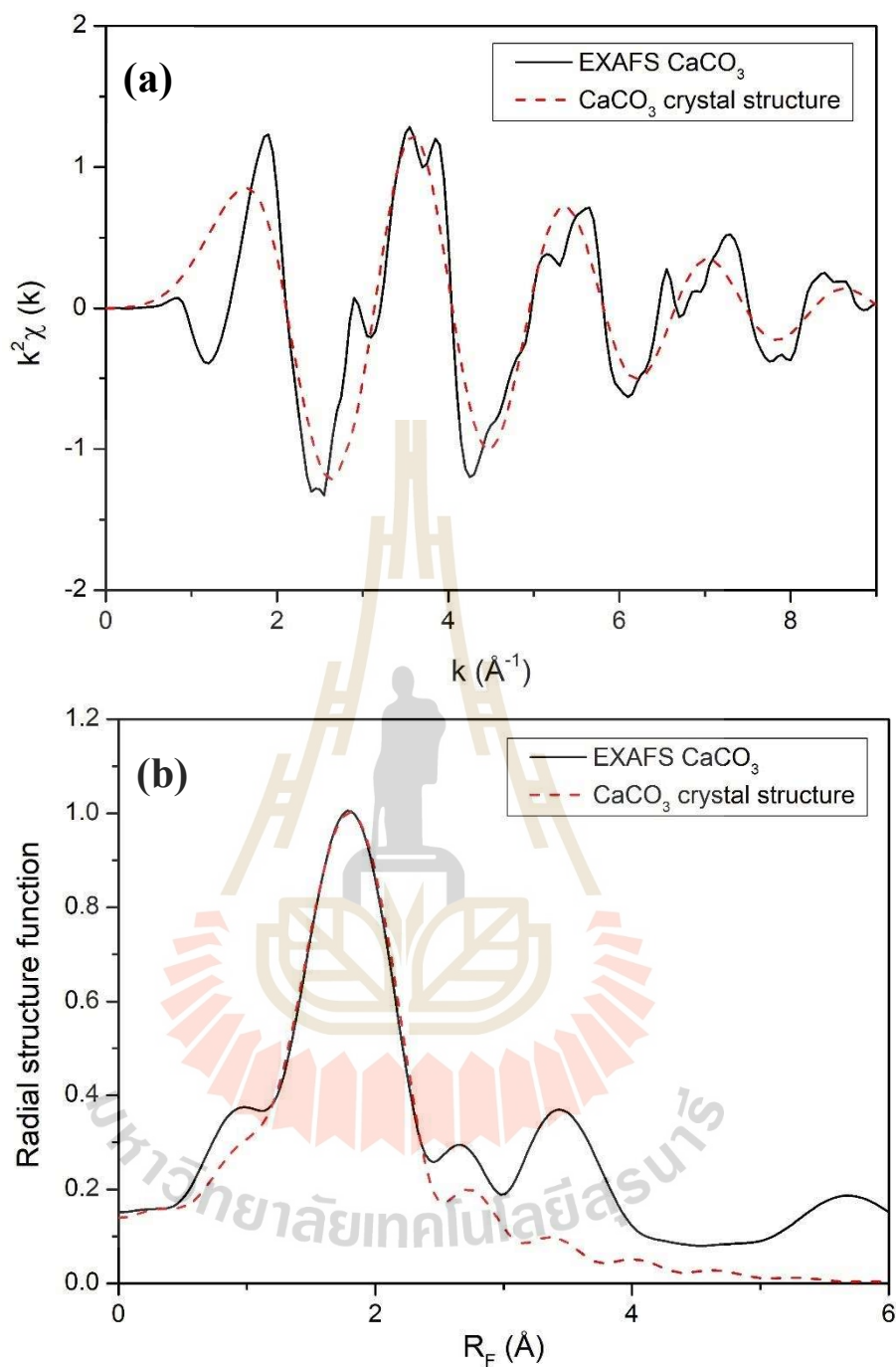


Figure 4.12 Fitting the first coordination shell of the calcium carbonate with CaCO_3 crystal structure (a) $k^2\chi$ and (b) radial structure function.

The coordination number of Ca-SPS can be determined from the fitting procedure with the known structure by fixing the amplitude (S_0^2) of the curve equal to the reference material. In this curve-fitting procedure the energy shift (E_0), the distance

shift (ΔR), and the first-shell oxygen Debye-Waller factors (σ^2), were adjustable. The best fit of Ca-SPS using the atomic positions of CaCO_3 crystal structure was presented in Figure 4.13(a) and (b) for k - and r -space, respectively. The quality of the fitting to the nearest-neighbor contribution of sulfonated ionomers is not quite good (R-factor around 0.045) and the fitting parameters are listed in Table 4.7. The best fit for the first coordination shell of Ca in Ca-SPS ionomer gives oxygen atoms at 2.389 Å, which is close to the Ca-O distance in CaCO_3 crystal. The coordination number for the first solvation shell is estimated to be 5 (4.81) atoms. The average Ca...O distance obtained from the fits agrees very well with the previous report for toluene diisocyanate-based polyurethane sulfonate ionomers neutralized with Ca^{2+} (Ding, 1989), which shows the Ca...O distance = 2.38 Å. While the coordination number from the fits and previous report are not agreed together, CN = 5 and 6, respectively. However, the local structure of calcium sulfonated polyurethane ionomers has slightly affected when the ionomers change from dry to a hydrated state.

Table 4.7 Fitting parameters of the first solvation shell: coordination number (CN), the amplitude reduction factor (S_0^2), the shift of energy (E_0), the shift of distance (ΔR), and the first-shell oxygen Debye-Waller factors of Ca-SPS.

Sample	CN	atom	S_0^2	E_0 (eV)	ΔR (Å)	R (Å)	σ^2 (Å ²)
Ca-SPS							
with CaCO_3	5.71	O	0.976	2.20	0.007	2.41	0.00855
	1	O-S	1.609	1.26	-0.071	2.38	0.00948
Ca-SPS	3	O-S	1.609	1.26	-0.071	2.49	0.00948
with MD	1	O-S	1.609	1.26	-0.071	2.89	0.00948
	1	O-W	1.609	1.26	-0.071	3.13	0.00948

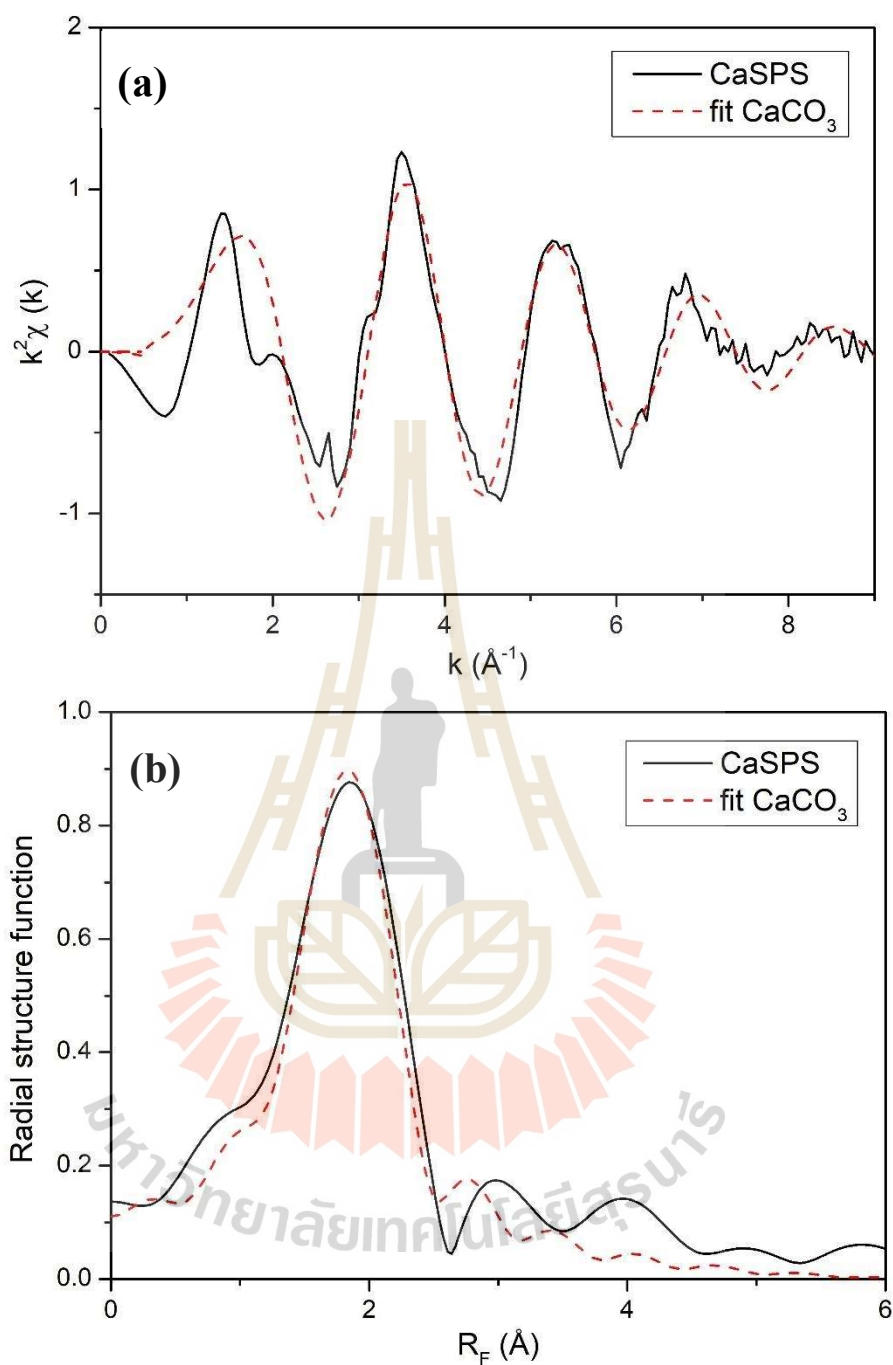


Figure 4.13 Fitting the first coordination shell of the Ca-SPS using CaCO_3 model (a) $k^2\chi$ and (b) radial structure function.

4.2.4 Solvation structure of calcium neutralized sulfonated polystyrene (Ca-SPS) by MD-EXAFS fitting

The atomic coordinates (Table 4.8) of calcium ion and oxygen atoms obtained from the MD simulation trajectories were also used to fit with experimental EXAFS data.

Four parameters were used in this fit including the amplitude reduction factor, the shift of energy, the shift of distance, and the first-shell oxygen Debye-Waller factors. Figure 4.14 shows the best fits of the molecular structure using the atomic coordinate from MD simulation of Ca-SPS with experiment, (a) and (b) for k- and r-space, respectively. The fitting parameters are listed in Table 4.7. The quality of the fitting is better than fitting with CaCO_3 crystal structure (R-factor around 0.017), this is maybe due to the structure of Ca-SPS being amorphous with a non-orderly structure. Using the mean-free-path value from the selected model from the MD snapshot (2.4 ± 0.4 Å), the coordination number for this shell is 6, including 5 oxygen atoms from the sulfonated group and 1 oxygen atom from water (list in Table 4.7). The shift of distance is quite small (~ 0.17 Å), this means that the distance of oxygen atom around Ca^{2+} ion from MD simulation agrees well with the experiment. The distance of Ca^{2+} ion is closer to the O atom from the sulfonated group than O atom from water. This is because Ca^{2+} ion should have anion close to the cation in order to neutralize the ions. The fitting result with MD hydrating system agrees well with the result from the TGA experiment, which showed the presence of 9% water in the Ca-SPS sample. The distance of oxygen atoms from the sulfonated group is in a large range from $2.36\text{-}2.84 \pm 0.4$ Å, this asymmetric oxygen position can be described to a broad peak of the experiment. The final coordination structure of Ca^{2+} ion solvated by O atom from both sulfonated group and water are summarized as in Figure 4.8(d).

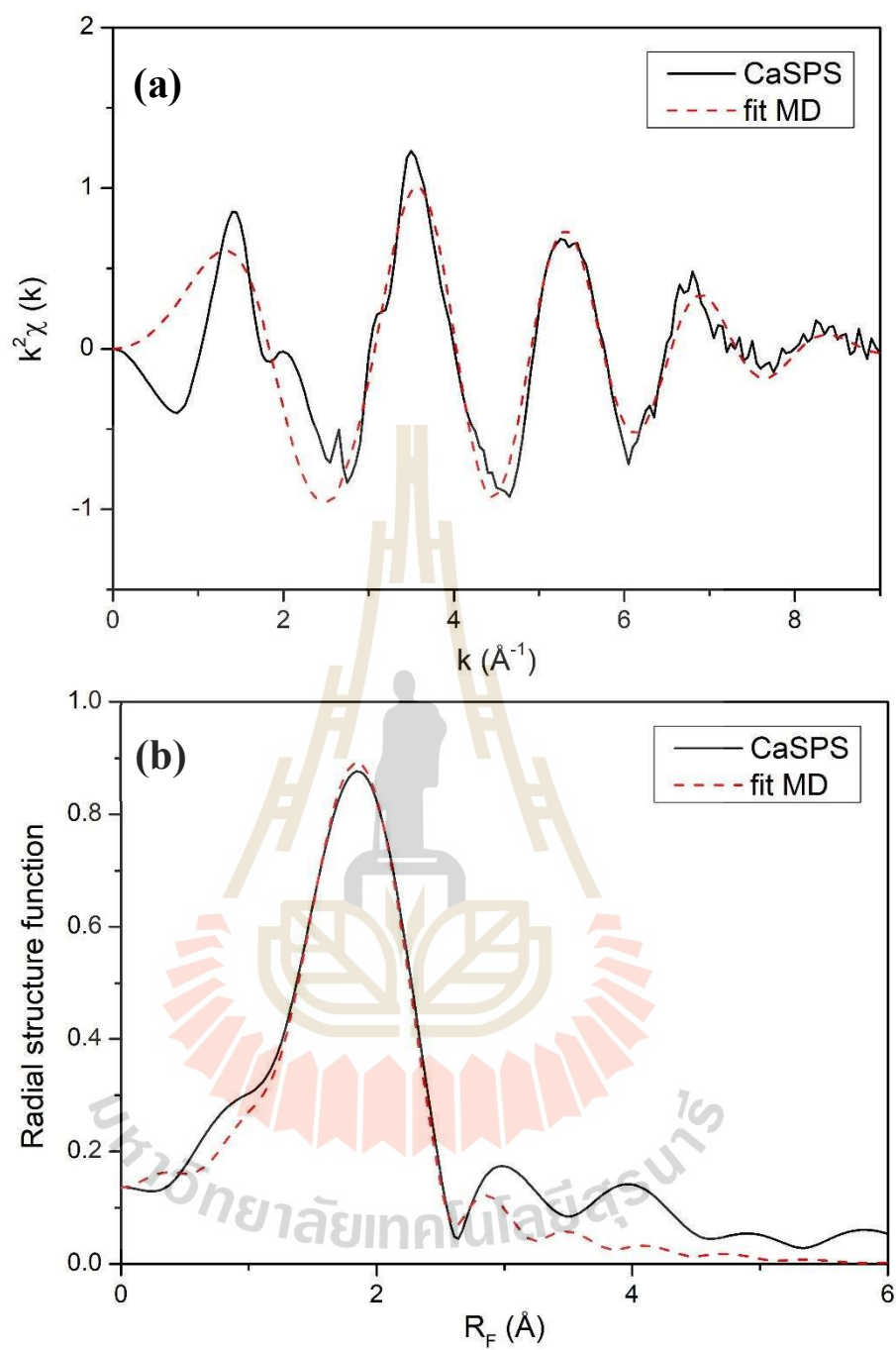


Figure 4.14 Fitting the first shell of the Ca-SPS using MD snapshot model (a) $k^2\chi$ and (b) radial structure function.

Table 4.8 Atomic coordinates from MD snapshot of Ca-SPS.

X (Å)	Y (Å)	Z (Å)	Atom type	distance
0	0	0	Ca	0
-1.81	-1.35	-0.76	OS	2.382
1.4	0.42	2.01	OS	2.485
-0.03	0.97	-2.3	OS	2.496
1.1	-2.09	0.82	OS	2.5
2.19	-0.98	-1.61	OS	2.889
-0.07	3.13	-0.02	OW	3.131
-0.09	0.34	-3.59	S	3.607
-2.32	-2.38	-1.63	S	3.702
-1.71	0.78	3.2	S	3.711
1.23	-3.5	-0.54	S	3.749
2.37	0.55	-3.08	S	3.925
-1.13	-0.39	3.81	OS	3.993
1.14	-3.85	-0.85	OS	4.104
-1.31	-3.21	-2.25	OS	4.133
-1.09	-3.48	2.02	C	4.169
3.47	-1.64	-1.63	S	4.17
3.46	2.23	1.22	C	4.293
-0.14	-4.26	1.35	C	4.471
4	-2.07	-0.36	OS	4.518
-3.24	-1.85	-2.59	OS	4.542
-1.35	1.98	3.9	OS	4.577
3.18	-0.62	3.31	OS	4.632
-1.11	0.89	-4.44	OS	4.662
3.5	1.8	2.55	C	4.69
-3.2	-3.49	-0.56	C	4.768
1.81	1.1	4.28	OS	4.775
1.35	0.76	-4.53	C	4.788
4.19	0.84	-2.23	C	4.82

Table 4.8 Atomic coordinates from MD snapshot of Ca-SPS (Continued).

X (Å)	Y (Å)	Z (Å)	Atom type	distance
2.37	-4.02	1.27	OS	4.836
1.64	3.77	-2.71	C	4.924
-4.32	2.33	0.6	C	4.945
-4.66	-1.67	0.58	C	4.984
-3.43	0.67	3.62	C	5.032
1.27	-3.64	-3.33	Ca	5.094
4.69	-0.46	-2.11	C	5.163
3.58	-2.54	-2.74	OS	5.175
-3.96	2.64	2.06	C	5.186
-4.25	-3.1	0.28	C	5.268
1.03	3.29	-4.03	C	5.303
-2.12	-4.08	2.75	C	5.358
1.75	2.1	-4.63	C	5.377
4.33	3.2	0.7	C	5.429
-4.35	1.54	3.02	C	5.515
-4.53	0.88	-3.05	OW	5.532
2.09	-0.21	-5.21	C	5.617

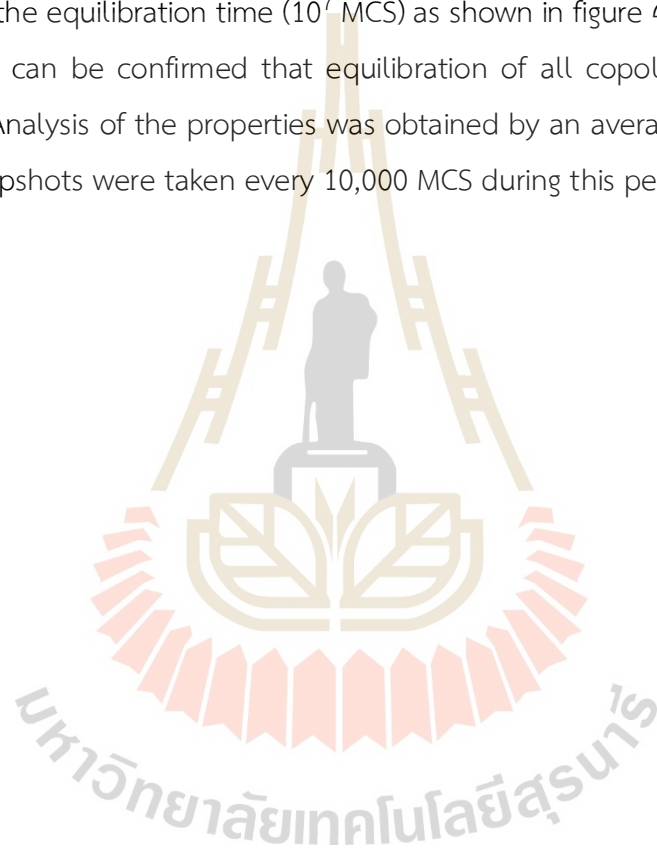
4.3 SPS thin film by coarse-grained random copolymer models

4.3.1 Equilibration

Free standing copolymer thin films can be formed quite easily from an equilibrated bulk structure. The equilibrated thin films were obtained within 10^7 MCS in order to obtain the structure with a uniform distribution of beads in the interior and constant system energy. A careful consideration of the extent of the equilibration achieved in the simulation is essential to a proper interpretation of the results. The equilibration of the conformations of random copolymer films was evaluated using the mean square displacements (*MSD*) defined as

$$MSD = \langle [R_{cm}(t) - R_{cm}(0)]^2 \rangle \quad \text{Equation 4.3}$$

The positions of the center of mass of a chain at an initial time and time t are denoted by $R_{cm}(0)$ and $R_{cm}(t)$, respectively. MSD for the simulation of some random copolymer thin film at 473 K are depicted in Figure 4.15(a). A chain can be considered to have relaxed from its initial conformation when MSD exceeds the mean square radius of gyration of copolymer chains. Equilibration of the conformations of the chains was also monitored using the normalized orientation autocorrelation functions (OACF) formulated from the end-to-end vector, $\langle R(t) \cdot R(0) \rangle / \langle R^2 \rangle$. OACF also decays to lower value within the equilibration time (10^7 MCS) as shown in figure 4.15(b). Based on MSD and OACF, it can be confirmed that equilibration of all copolymers thin films was completed. Analysis of the properties was obtained by an average of the subsequent 10^7 MCS. Snapshots were taken every 10,000 MCS during this period.



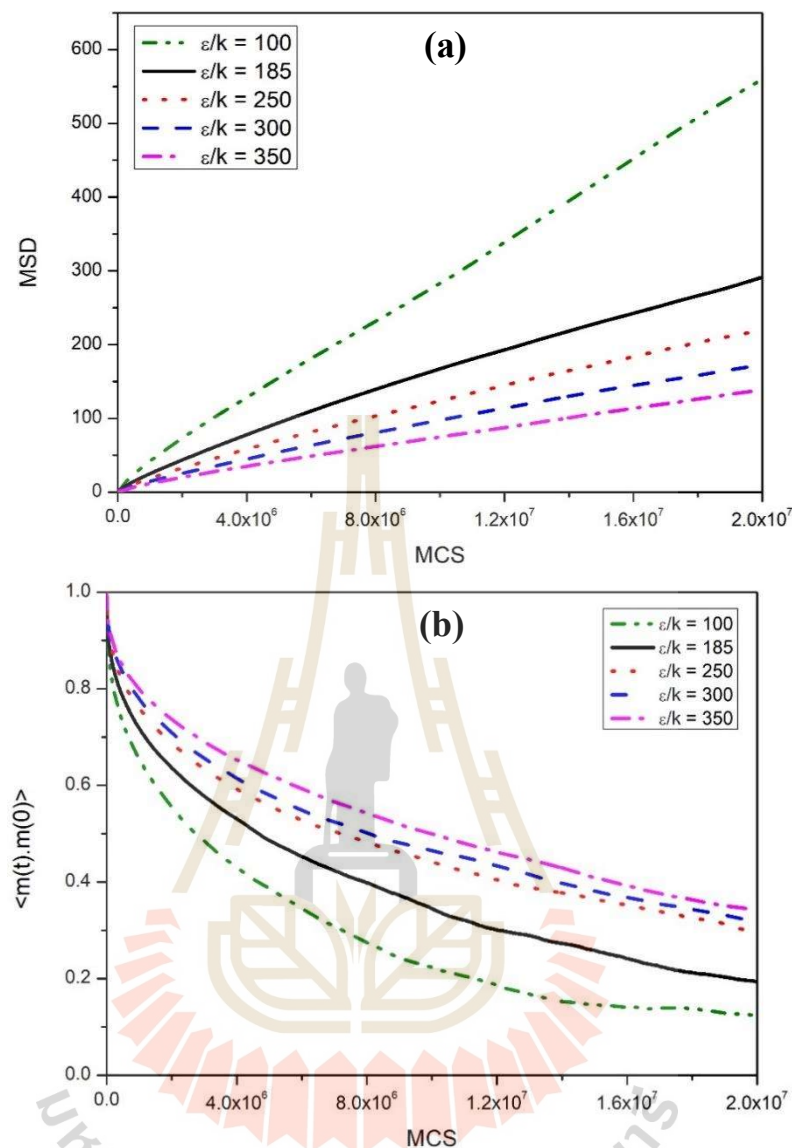


Figure 4.15 Equilibration of random copolymer thin film structure as illustrated by (a) the mean square displacement for the center of mass (MSD) and (b) the decorrelation function of the end-to-end vector of copolymer chains as a function of Monte Carlo Step.

4.3.2 Density profiles

Figure 4.16 shows the example thin-film structure of random copolymer with various LJ interaction parameters (ϵ/k) at 100, 185, 250, 300, and 350 K. The thickness of films was expanded as the LJ interactions increased. The density profiles of these thin films were investigated from the counting number of monomer beads in each

shell volume and averaging over all configurations as a function of distance from the center of the film along z-direction (Z). The densities of C and X beads were treated as the same that the density of bead was multiplied by the ethylene molecular weight. The density profiles of random copolymer thin film with different LJ interaction parameters (ϵ/k) were displayed in Figure 4.17. The middle of density profiles represented to the density at the bulk region of thin-film is strongly correlated with ϵ/k value. The bulk density increases as the LJ interaction parameter (ϵ/k) increased. The density profile of every system shows the same shape as having constant density value at bulk region and then rapidly decay at the interface region.

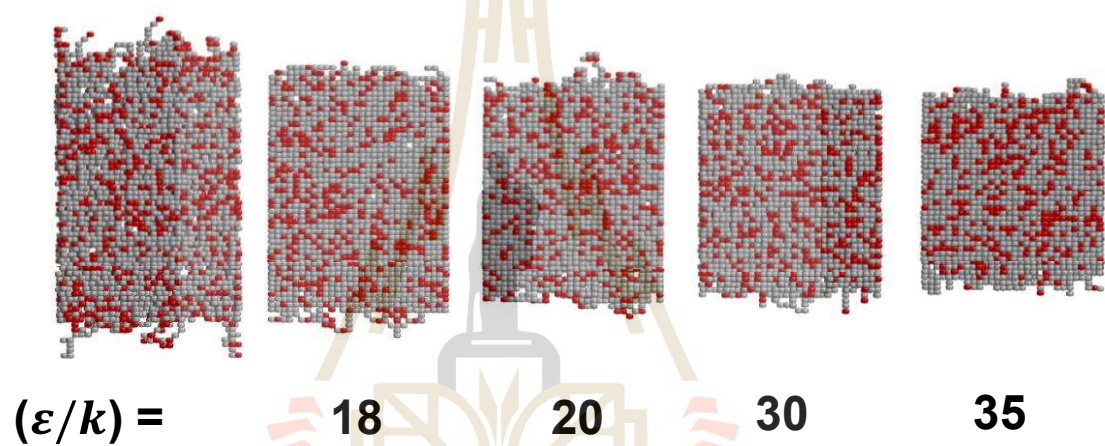


Figure 4.16 Example snapshots of random copolymer thin film structure for different LJ interaction parameters (ϵ/k) of 100, 185, 205, 300 and 350 K.

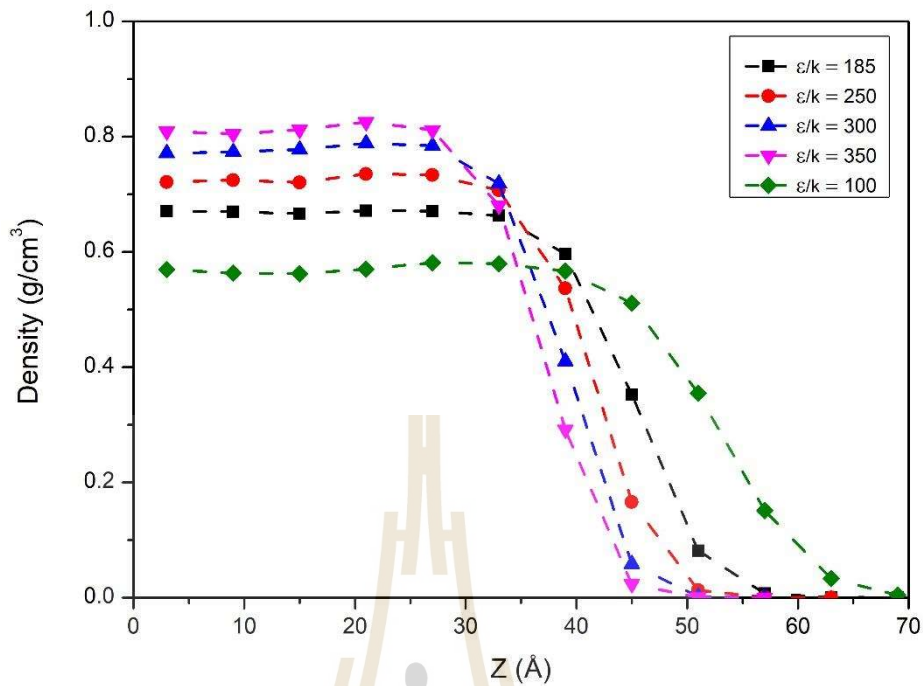


Figure 4.17 Density profile of random copolymer thin film structure for different LJ interaction parameters (ϵ/k) of 100, 185, 205, 300 and 350 K.

To quantitatively describe the density profiles parameter of random copolymer thin film as a function of ϵ/k , the density profile curves were fit with hyperbolic equation (Equation 4.4) that originally developed by Helfand and Tagami (Helfans. 1972).

$$\rho(r) = \frac{\rho_{bulk}}{2} \left[1 - \tanh \left[\frac{2(r-R)}{w} \right] \right] \quad \text{Equation 4.4}$$

Where the $\rho(r)$ represented the density profile as a function of distance from the center of the film, ρ_{bulk} is the bulk density, r is the distance from the midplane of the film along Z direction, R is the position of the interface at which the density drops to 50% of the bulk density, and w is the interface thickness. The equation fits well with the density profiles and the fitting parameters were displayed in Table 4.9. The bulk density increases linearly as the bead attraction increases as shown in Figure 4.18. The thickness of the film (R) becomes shrink with a stronger attractive force between each bead. Similarly, the interfacial thickness (w) become decreases as the LJ interaction parameters (ϵ/k) increase. Both the whole film and

interface thickness decreases as the attractive force increase and then convert to a constant value.

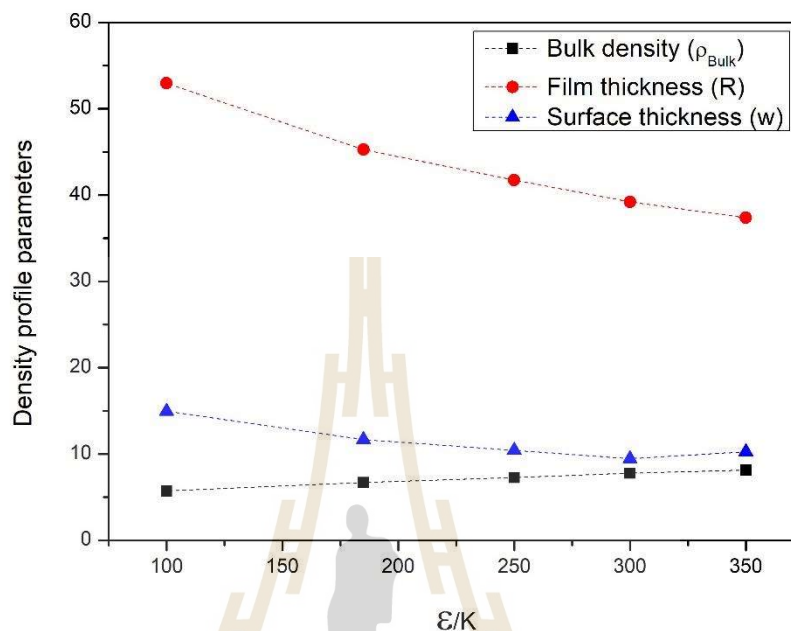


Figure 4.18 Density profile parameters of random copolymer thin film structure given by fitting the density profile curve with the hyperbolic equation.

Table 4.9 Density profile parameters of random copolymer thin films as a function of monomer interaction strength.

ϵ/K	Density bulk (Db) (g/cm^3)	Film thickness (R) (nm)	Surface thickness (w) (nm)
100	0.57	5.30	1.50
185	0.67	4.53	1.17
250	0.73	4.17	1.04
300	0.78	3.92	0.95
350	0.81	3.74	1.03

The normalized end bead and middle bead densities were calculated as a function of distance along Z direction and shown in Figure 4.19. The end bead densities clearly increase near the interface region, this means that the end bead prefers to stay

at the surface. The density of both the end bead and the middle bead of all systems are almost the same in the bulk region. While at the surface region, the end bead exhibits increasing in density value, but the middle bead decreases toward the surface. However, the magnitude of changes in density values in each system seems to be not much sensitive to ϵ/k but made the shorter distance at which the deviation from the bulk value. Because the middle of the film is denser packing, the end beads with high mobility tried to exclude from the bulk region. This makes the density of the end bead on the surface higher.

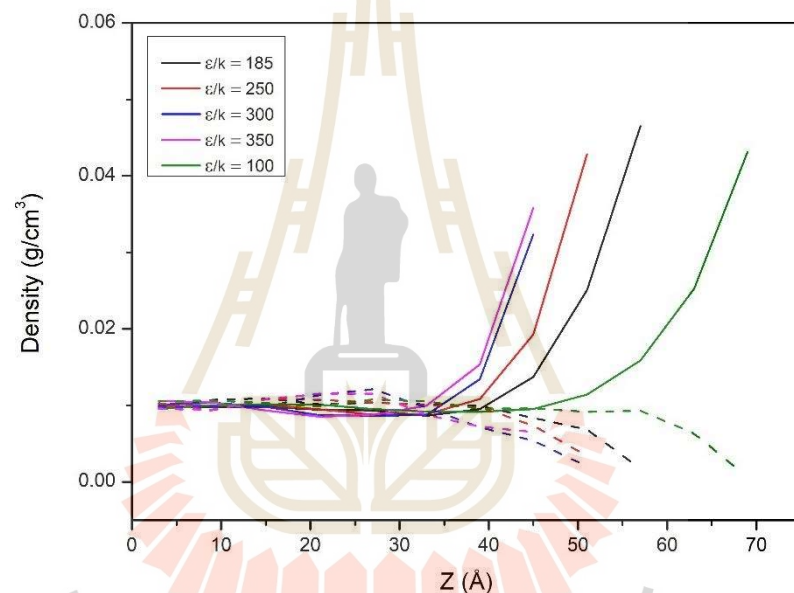


Figure 4.19 Normalized radial density profiles of the end beads (solid line) and the middle beads (dashed line) as a function of distance from the center of mass of the films.

Figure 4.20 shows the chain center of mass profile and its cumulative distribution as a function of distance along Z direction, which is represented the molecular packing of random copolymer chains. The copolymer thin film was distributed uniformly along a perpendicular direction to the film interface for the weakest interaction, $\epsilon/k = 100$ K, system. For higher LJ interaction parameters ($\epsilon/k = 185, 250, 300,$ and 350 K), the oscillating pattern was found in the chain centers, and the magnitudes are proportional to the strength of bead attraction. The characteristic

of the chain center of mass in the surface region is related to the energetic contribution. This differs from the behavior of the end bead profile complemented by the entropic effects. To reduce the effect of chain centers fluctuation inside thin-film, the cumulative distribution plot has been designed. In Figure 4.20(b), the cumulative chain center of mass distribution increases pattern as a function of ϵ/k .

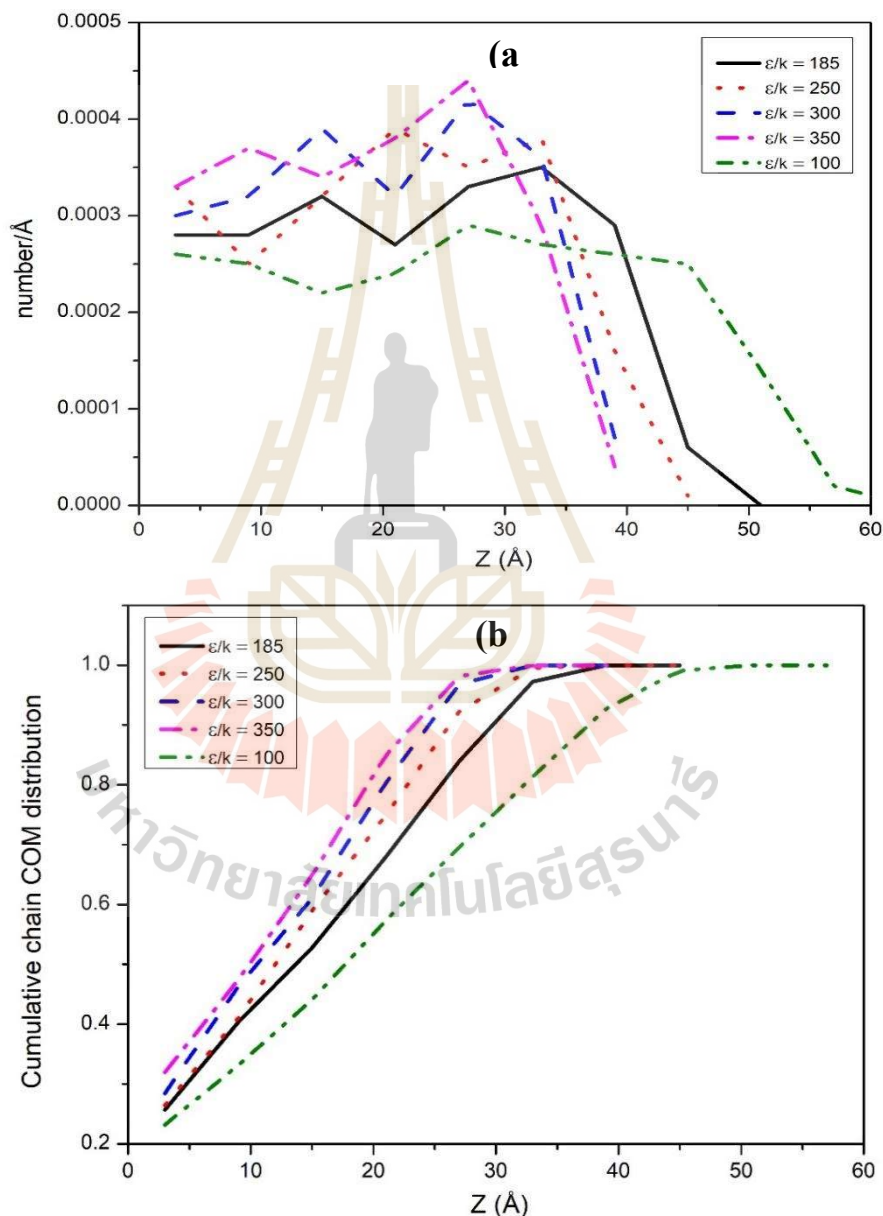


Figure 4.20 (a) center of mass and (b) cumulative chain center of mass distribution of random copolymer thin film structure for different LJ interaction parameters (ϵ/k) of 100, 185, 205, 300, and 350 K.

4.3.3 Bond arrangement

Local bond orientation, which is defined from the bond vectors of the backbone atom i to $i+2$, was studied using the definition of the order parameters as in equation 4.5.

$$S = \frac{1}{2} \langle 3(\cos^2 \theta) - 1 \rangle \quad \text{Equation 4.5}$$

Where θ is the angle between bond vectors and Z axis (the axis that is perpendicular to the film surface). The bond vectors that parallel to the film surface were defined as $S = -0.5$, while $S = 1.0$ is represented to the perpendicular of bond vectors to the interface. For $S = 0.0$ referred to the random orientation of bond vector to the film surface. The bond orientation parameter of middle and end beads is shown in Figures 4.21(a) and 4.21(b), respectively. The random orientation was clearly appeared for both middle and end bond vectors in the bulk region, observed from $S=0.0$. At the interface region, the middle and end bond vectors trend to parallel and perpendicular to the surface, respectively. For copolymers with stronger interactions between beads, the bond orientation was clearly more anisotropic.

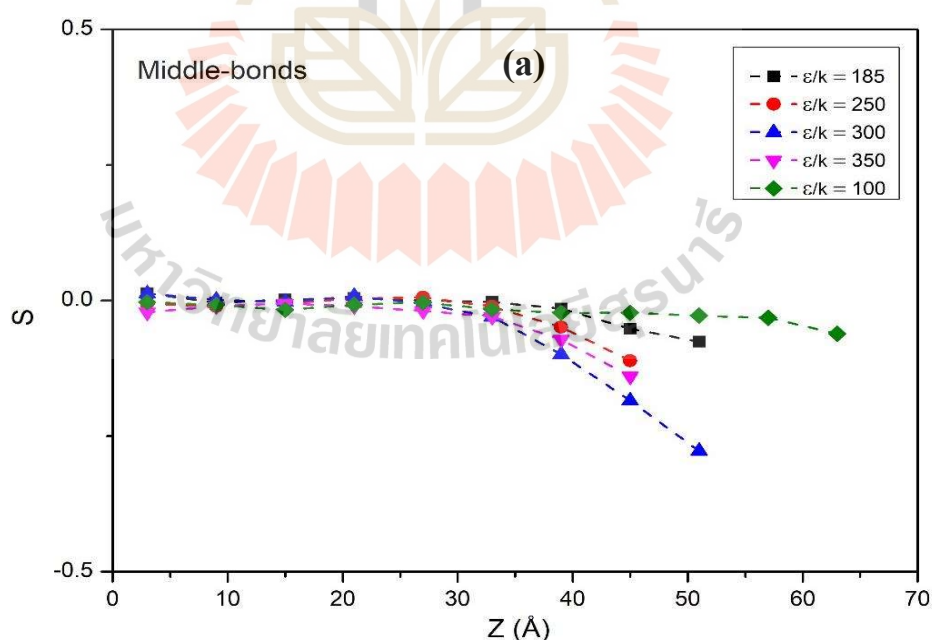


Figure 4.21 The orientation of bond vectors with respect to the distance from the center of mass of the films (a) middle bonds. (b) end bonds.

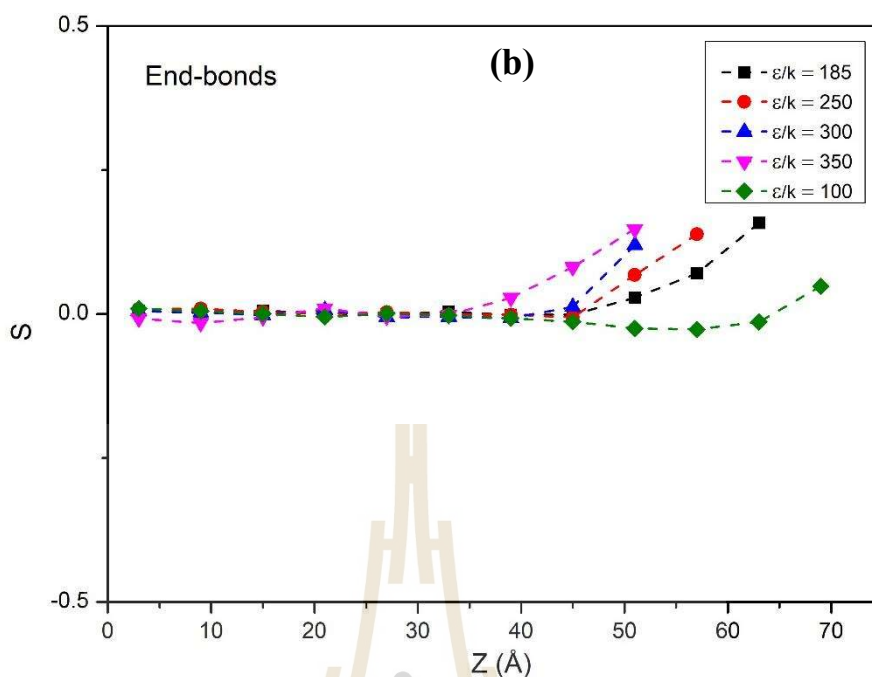


Figure 4.21 The orientation of bond vectors with respect to the distance from the center of mass of the films (a) middle bonds. (b) end bonds (Continued).

4.3.4 Chain properties

The molecular size of random copolymer thin film can be determined from the calculation of the mean square end-to-end vector ($\langle R_e^2 \rangle^{1/2}$) and mean square radius of gyration ($\langle R_g^2 \rangle^{1/2}$) as shown in Table 4.10. All these parameters are listed as a function of LJ interaction parameters. Both $\langle R_e^2 \rangle^{1/2}$ and $\langle R_g^2 \rangle^{1/2}$ parameters of thin-film decrease as the attractive interactions increase. This means that the copolymer chains are contracted well. Generally, the $\langle R_e^2 \rangle / \langle R_g^2 \rangle$ value of the PE model should be 6.5 but slightly smaller values have appeared in this simulation with the same degree of polymerization (Flory, 1969; Mattice, 1994). However, the $\langle R_e^2 \rangle / \langle R_g^2 \rangle$ value in this simulation is closer to 6 with increasing ϵ/k . Therefore, it is obvious that the chain approach the Gaussian limit (Cho, 1997) with increasing bead attraction.

Table 4.10 Root mean square radius of gyration $\langle R_g^2 \rangle^{1/2}$ and root mean square end-to-end vector $\langle R_e^2 \rangle^{1/2}$ for copolymer thin films.

ϵ/k	100	185	250	300	350
$\langle R_e^2 \rangle^{1/2}$	36.45 \pm	34.44 \pm	34.13 \pm	33.34 \pm	32.56 \pm
(nm)	31.31	29.59	29.70	29.02	27.97
$\langle R_g^2 \rangle^{1/2}$	14.48 \pm	13.82 \pm	13.67 \pm	13.43 \pm	13.25 \pm
(nm)	9.59	9.07	9.04	8.96	8.61
$\langle R_e^2 \rangle / \langle R_g^2 \rangle$	6.33	6.21	6.23	6.16	6.04

To determine the shape of polymer thin film, the equivalent ellipsoid with three principal components (L_1 , L_2 , and L_3) of the radius of gyration tensor (Solc, 1971; Solc, 1971) of polymer chains were approximated. In the theoretical formulation, the eigenvalue $L_1^2:L_2^2:L_3^2$ the ratio of the random flight chain model should be 11.7:2.7:1. Figure 4.22(a) and Table 4.11 represented the $L_1^2:L_2^2:L_3^2$ the ratio of random copolymer with various LJ interaction parameters in this work. For the $\epsilon/k \leq 185$ K, the eigenvalues are quite constant at the bulk region and then slightly change near the interface region. The L_1 parameter decrease while L_2 and L_3 increase in the surface region for copolymer with $\epsilon/k \leq 185$ K. These results are related to the distortion of chain conformation when the center of mass of the copolymer chain stayed near the interface. However, there is no significant change in the principal components (L_1 , L_2 , and L_3) despite the increased attraction force for $\epsilon/k > 185$ K. It can be clearly seen that the average chain shape changes as the attractive interaction of beads increases, and the chain assumes more compact ellipsoidal shapes.

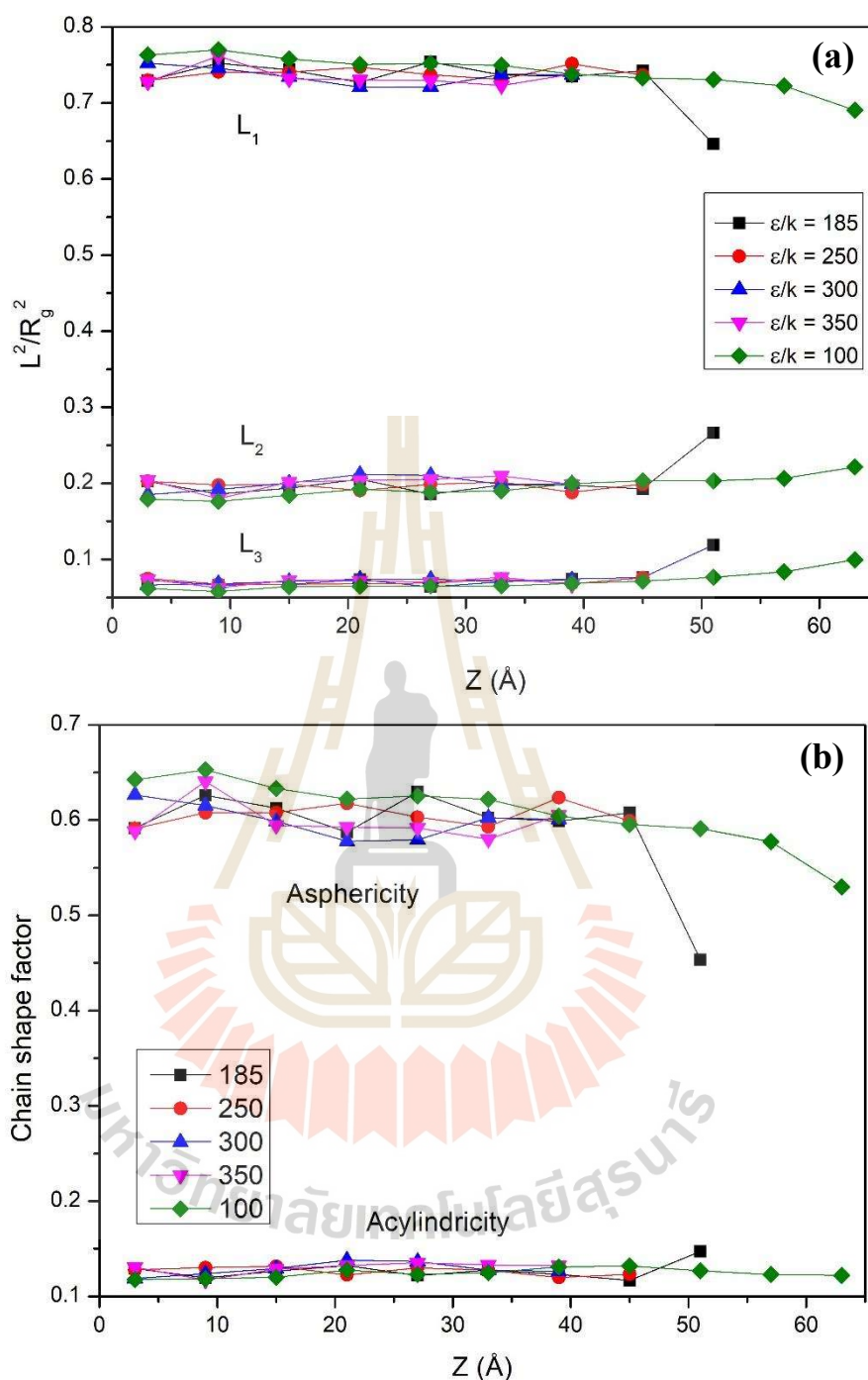


Figure 4.22 (a) The normalized principal moments (L_1 , L_2 , and L_3) of individual chains and (b) the normalized asphericity and acylindricity as a function of distance from the center of mass of thin film for various LJ interaction parameters.

The chain shapes were further investigated using acylindricity ($c = L_2^2 - L_3^2$) and asphericity ($b = L_1^2 - (L_2^2 + L_3^2)/2$). The acylindricity and asphericity were

normalized by the mean square radius of gyration to determine the extent of deviation from cylindrical and spherical shapes, respectively, and shown the results in Table 4.11 and Figure 4.22(b). From the result in Table 4.11., the acylindricity values were slightly increased in the range of 0.125 to 0.130, while the asphericity values were decreased from 0.621 to 0.599 as a function of LJ interaction parameter increases. This result can imply that the shape of random copolymers is more deviated from cylindrical shape to spherical shape for stronger bead attraction. There was no significant change in the copolymer chain shape as a function of distance from the film center for $\epsilon/k > 185$ K, the chain shape at the bulk and interface regions behave the same. Nevertheless, the shape of copolymers with $\epsilon/k = 100$ and 185 K have slightly decreased in asphericity and increased acylindricity near the surface. The distortion of the molecular size and shape in copolymer thin film is due to not only the strength of comonomer interaction but also the surface and confinement effect.

Table 4.11 The comparison of the principal components of the mean square radius of gyration and normalized average acylindricity and asphericity values for various LJ interaction parameters.

ϵ/k	$\langle L_1^2 \rangle : \langle L_2^2 \rangle : \langle L_3^2 \rangle$	$\langle c \rangle / \langle R_g^2 \rangle$	$\langle b \rangle / \langle R_g^2 \rangle$
100	11.33:2.89:1	0.125	0.621
185	10.49:2.77:1	0.125	0.607
250	10.49:2.80:1	0.127	0.605
300	10.35:2.81:1	0.129	0.600
350	10.41:2.84:1	0.130	0.599

The change in the radius of the gyration component of copolymer chains was calculated as a function of distance from the film center to observe the anisotropic change of chain dimension and shown the result in Figure 4.23. The solid line represented the square root of the 1/3rd of the total mean-squared radius of gyration (xyz), the dashed line represented the square root of the average of X-Y component (xy), and the dotted line represented the mean-squared radius of gyration in Z axis. In the middle region of the film, all three components (xyz , xy , and z) of copolymer

decrease when the ε/k increases and close to an average value of $(\langle R_g^2 \rangle / 3)^{1/2}$. Nevertheless, strongly decays in Z component and drops of $\langle R_g^2 \rangle^{1/2}$ value for xy and xyz components on the surface appeared. This means that the molecular size at the bulk region of random copolymer decreases due to strongly attractive force between beads, polymer chains packed well with high LJ interaction. The Z component that greatly reduced $\langle R_g^2 \rangle^{1/2}$ value at the surface was shown a change in the molecular shape, which corresponds to the result of the eigenvalue principal.

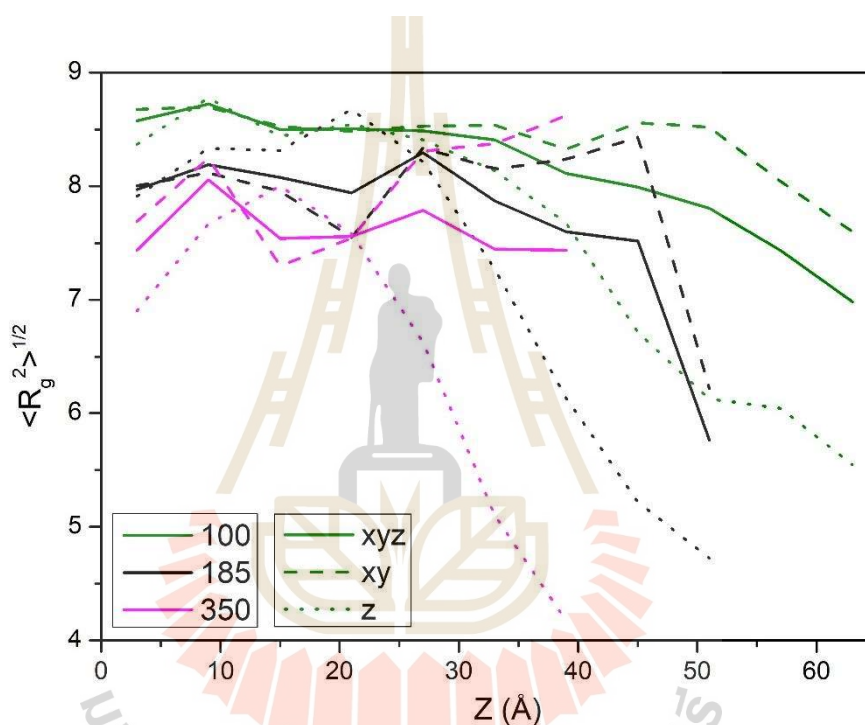


Figure 4.23 The components of the mean-squared radius of gyration in random copolymer thin films for various LJ interaction parameters.

The orientation of the polymer chain was determined using a similar principle with the bond arrangement as in equation 4.5. Figure 4.24 shows the orientations of the longest (L_1) and shortest (L_3) eigenvectors of copolymer chains with respect to the normal vector to the film interface. In the middle region of the film, both L_1 and L_3 are oriented in a random direction. While at the film surface, the L_1 tends to arrange perpendicular to the normal vector and the L_3 tends to parallel. The orientation of both L_1 and L_3 axis are anisotropic arrangements at the surface as a function of ε/k .

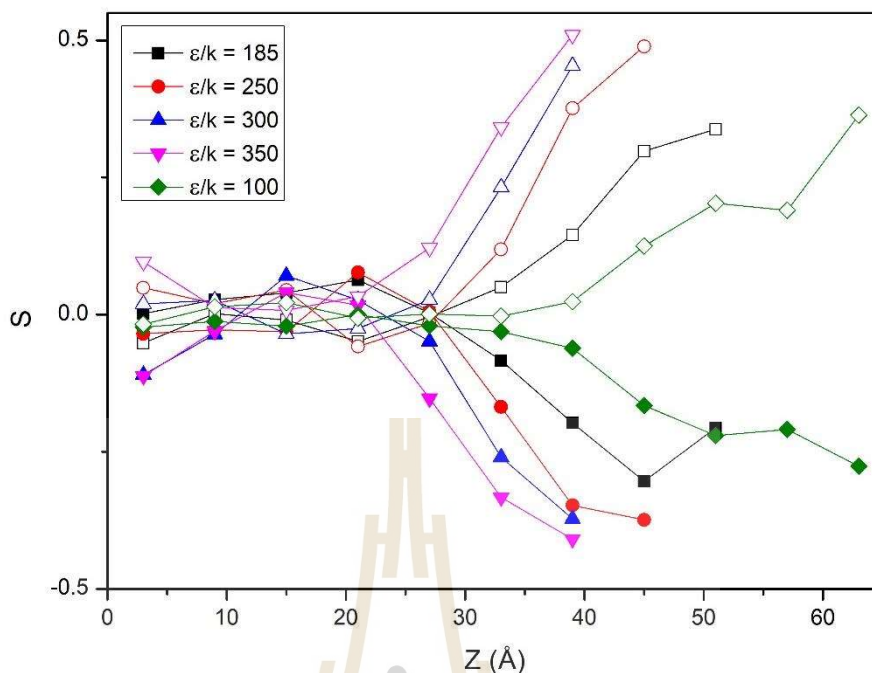


Figure 4.24 The orientation of the first and third principal axis of copolymer molecule (open symbol – L_3 , filled symbol – L_1).

4.3.5 Energetics

Figure 4.25 displays the intramolecular and intermolecular energies normalized by the number of beads in each bin as a function of distance from the film center along Z direction. The short-range intramolecular was calculated from the RIS model, long-range intermolecular was calculated from the Lennard-Jones potential, and the total energies combined from the short-range and long-range energy. Similar to other properties, the energies exhibited constant at the bulk region. The total and long-range energies increase, while short-range energy decreases as a function of LJ interaction parameters in the interface region. The decrease of short-range energy in the interface region can be explained by the highly *trans* conformation of the polymer chain. While an increase in long-range energy is related to better chain packing. Intermolecular energy exhibited more negative value in the middle region but shot up to a positive value near the film surface in the systems of high attractive force $\epsilon/k > 185$ K. For the slight increase of intramolecular energy in the bulk region can be interpreted that most polymers have more *gauche* conformation with increasing bead attraction.

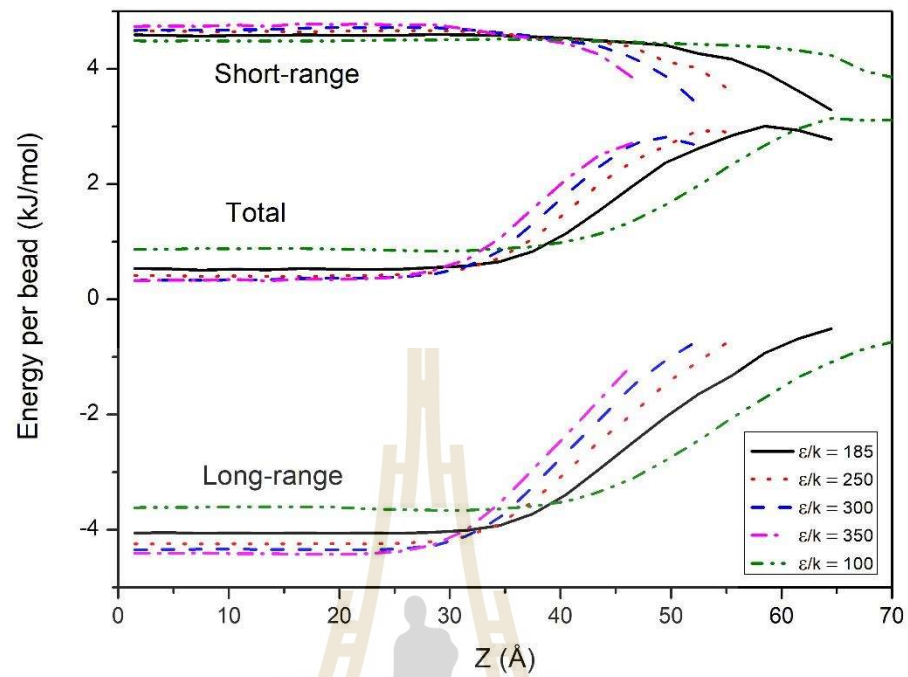


Figure 4.25 The average short-range, long-range, and total energy of polymer molecule (in 6 \AA) with $\epsilon/k = 100, 185, 250, 300,$ and 350 K along the Z-axis of thin film.



CHAPTER V

CONCLUSIONS

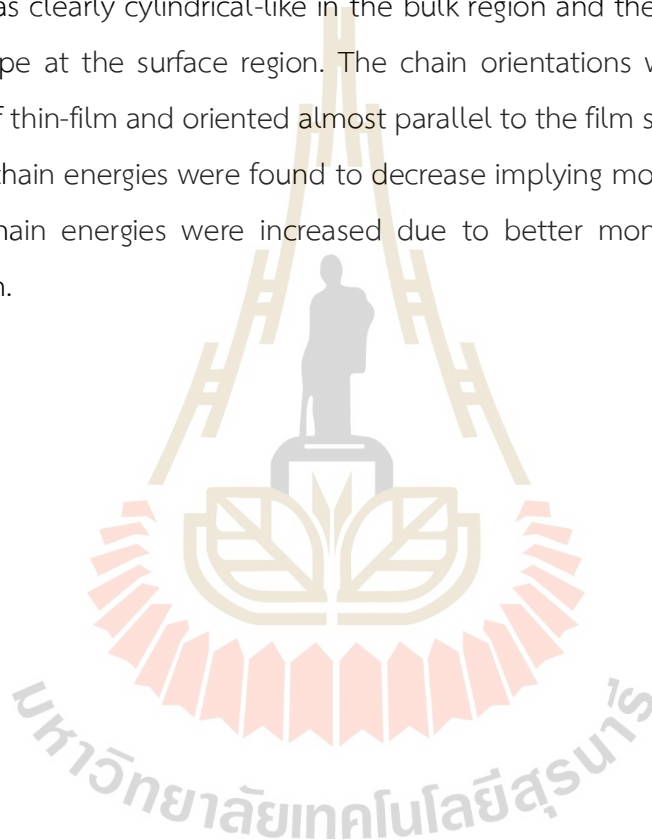
This work illustrates a multiscale molecular modeling technique to generate and equilibrate amorphous polymeric materials of polystyrene and sulfonated polystyrene. There are three main parts in this thesis: a multiscale simulation of polystyrene with different tacticity, coordination structure of salt doped sulfonated polystyrene by MD-EXAFS method, and interfacial property of random copolymer this film by Monte Carlo simulation.

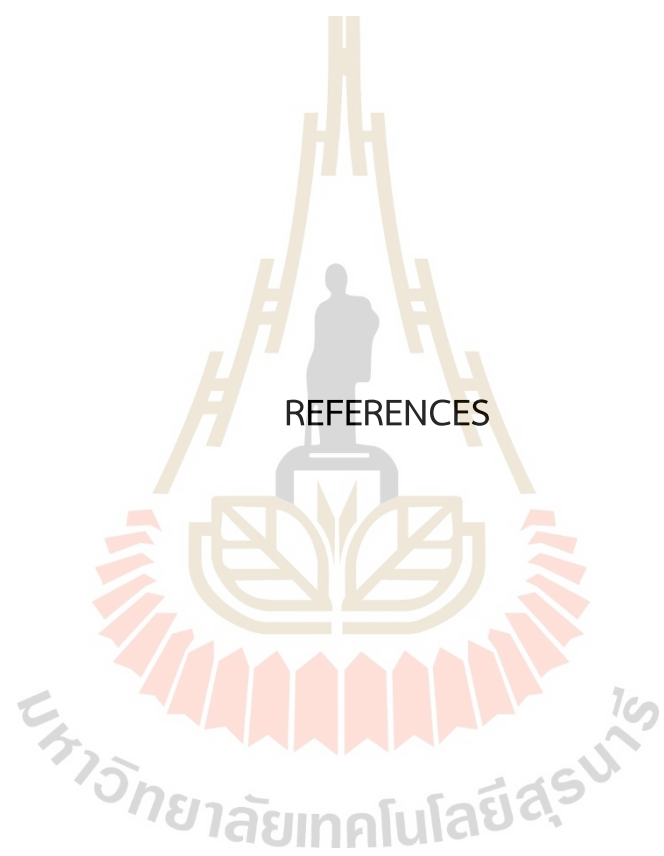
For the first part, amorphous polystyrene structures at the bulk density were investigated using a combination of lattice Monte Carlo simulation of coarse-grained polystyrene chains and energy minimization for reverse-mapping to fully atomistic models. The real polystyrene chains can be mapped into coarse-grained beads on the 2nd lattice using the RIS model. After that, the Monte Carlo simulation was used to equilibrate the bulk structure of coarse-grained polystyrene. The on-lattice properties including chain dynamics and statistics were investigated. Mobility of polystyrene with different tacticities can be determined from the autocorrelation function of the end-to-end vector and mean square displacement for the center of mass. The *syndiotactic* polystyrene showed the fastest diffusion rate and following by *atactic* and *isotactic* polystyrene, respectively. The diffusion rate decreases with the increasing probability of *meso*. The chain dimension and stiffness of *isotactic* polystyrene were smaller than those of others. The dynamics of polystyrene chains are more related to interchain packing than to intramolecular origin. The equilibrated polystyrene structures were then reverse mapped from coarse-grain beads to fully atomistic models. Conformation statistics, solubility parameters, radial distribution function, and neutron scattering were calculated at the atomistic level. The simulation results were in reasonable agreement with those obtained by the physical analysis. The effect of different tacticities polystyrene exhibited small differences on these properties.

In the second part, a combination of EXAFS spectroscopy and MD simulation was used to investigate the coordination structure of salt doped sulfonated polystyrene at an atomistic scale. The coordination structure investigated from MD simulation can be explained that the bivalent calcium cations were surrounded by six oxygen atoms from both sulfonated polystyrene and water. The number of sulfonation groups and water components has no effect on the coordination structure around calcium ions. Different from monovalent cation (Na^+ and K^+), the coordination number changed with a number of water components. The experimental EXAFS spectra were used to observe the coordination structure of CaSPS by fitting with a known standard structure. From the result of EXAFS spectra of CaSPS fitting with standard material (CaCO_3 crystal structure), the coordination number of calcium ions surrounded by 5 oxygen atoms on the first coordination shell. The fitting result is not quite good with a high R-factor and does not agree with the previous report. However, the EXAFS spectra from the MD simulation fitted very well with experimental data. The first coordination shell of calcium ion appeared in the range of $2.38\text{-}2.89 \pm 0.5 \text{ \AA}$, including 5 oxygen atoms from 5 sulfonated groups and 1 oxygen atom from water. The distance of oxygen atom from the sulfonated group is closer to calcium ion than oxygen from water, this is because calcium ions should have negative charges close to the cation to produce charge neutrality. The solvation structure of Ca-SPS with absorbed small amounts of water can be explained by the model in Figure 4.8(d), with only one oxygen from each sulfonated group near the cation while other oxygen atoms are from the same sulfonated group away from the nearest Ca^{2+} ion.

The final part, the Monte Carlo simulation of random copolymer thin film on a high coordination lattice were used to study the effect of the strength of comonomer attraction on the interfacial properties. The comonomer was treated with varying attractive forces which are described implicitly through the Lennard-Jones interaction parameter (ϵ/k). The effects of monomer attraction were studied on the monomer distribution, density profile, bond and chain orientation, chain dimension, chain shape, and change in energetics across copolymer thin films. The result shows that the chains were well distributed in thin-film structure for the comonomer with less attraction, and the chain in thin-film structure start to aggregate when the interaction parameter

was stronger. The random copolymer thin film became more compact with increasing comonomer attraction (increasing ϵ/k). The surface thickness also decreases with increasing interaction parameters. The bond vector orientations were randomly for the bulk region and prefer to parallel and perpendicular to the film surface for the middle and end bond vector near the interface region, respectively. This behavior became more clear with increasing comonomer attraction. The chain dimensions were slightly decreased as the comonomer attraction became stronger. The shape of copolymer molecules was clearly cylindrical-like in the bulk region and then slightly change to a spherical shape at the surface region. The chain orientations were randomly in the bulk region of thin-film and oriented almost parallel to the film surface in the interface region. Intra-chain energies were found to decrease implying more *trans* conformation while inter-chain energies were increased due to better monomer packing at the surface region.





REFERENCES

REFERENCES

- Abe, A., Jernigan, R.L., and Flory, P.J. (1965). Conformational Energies of n-Alkanes and the Random Configuration of Higher Homologs including Polymethylene. *Journal of the American Chemical Society*, *88*, 631–639.
- Antoniadis, S.J., Samara, C.T., and Theodorou, D.N. (1998). Molecular Dynamics of Atactic Polypropylene Melts. *Macromolecule*, *31*(22), 7944-7952.
- Antoniadis, S.J., Samara, C.T., and Theodorou, D.N. (1999). Effect of Tacticity on the Molecular Dynamics of Polypropylene Melts. *Macromolecules*, *32*(25), 8635-8644.
- Barra, G.M., Jacques, L.B., Orefice, R.L., and Carneiro, J. R. (2004). Processing, characterization and properties of conducting polyaniline-sulfonated SEBS block copolymers. *European Polymer Journal*, *40*(9), 2017-2013.
- Baschnagel, J., Binder, K., Doruker, P., Gusev, A., Hahn, O., Kremer, K., Mattice, W.L., Muller-Plathe, F., Murat, M., Paul, W., Santos, S., Suter, U.W., and Tries, V. (2000). Bridging the gap between atomistic and coarse-grained models of polymers: status and perspectives. *Advances in Polymer Science*, *152*, 41–156.
- Brandrup, J., and Immergut, E.H. (1989). *Polymer Handbook*. New York: Wiley-Interscience.
- Castagna, A.M., Wang, W., Winey, K.I., and Runt, J.P. (2010). Influence of the Degree of Sulfonation on the Structure and Dynamics of Sulfonated Polystyrene Copolymers. *Macromolecules*, *43*, 10498-10504.
- Castagna, A.M., Wang, W., Winey, K.I., and Runt, J.P. (2011). Structure and Dynamics of Zinc-Neutralized Sulfonated Polystyrene Ionomers. *Macromolecules*, *44*, 2791-2798.
- Castagna, A.M., Wang, W., Winey, K.I., and Runt, J.P. (2011). Influence of Cation Type on Structure and Dynamics in Sulfonated Polystyrene Ionomers. *Macromolecules*, *44*, 5420-5426.

- Chi, L., Register, R.A. and Cooper, S.L. (1989). Direct observation of ionic aggregates in sulphonated polystyrene ionomers. *Polymer*, 30(7), 1227-1233.
- Cho, J., and Mattice, W.L. (1997). Estimation of long-range interaction in coarse-grained rotational isomeric state polyethylene chains on a high coordination lattice. *Macromolecules*, 30, 637–644.
- Clancy, T.C., Jang, J.H., Dhinojwala, A., and Mattice, W.L. (2001). Orientation of phenyl rings and methylene bisectors at the free surface of atactic polystyrene. *Journal of Physical Chemistry B*, 105, 11493–11497.
- Ding, Y-P.S., Register, R.A., Yang, C.Z., and Cooper, S.L. (1989). Synthesis and Characterization of Sulfonated Polyurethane Ionomers based on Toluene Diisocyanate. *Polymer*, 30, 1204-1212.
- Doruker, P., and Mattice, W.L. (1997). Reverse mapping of coarsegrained polyethylene chains from the second nearest neighbor diamond lattice to an atomistic model in continuous space. *Macromolecules*, 30, 5520–5526.
- Doruker, P., and Mattice, W.L. (1998). Simulation of polyethylene thin films on a high coordination lattice. *Macromolecules*, 31, 1418–1426.
- Doruker, P., and Mattice, W.L. (1999). Mobility of the surface and interior of thin films composed of amorphous polyethylene. *Macromolecules*, 32, 194–198.
- Eisenberg, A. (1979). *Contemporary Topics in Polymer Science*. New York: Plenum Press.
- Eisenberg, A., and Kim J.S. (1998). *Introduction to Ionomers*. New York: Wiley-Interscience.
- Flory, P.J. (1969). *Statistical mechanics of chain molecules*. New York: Interscience.
- Grady, B.P., and Cooper, S.L. (1994). Extended X-ray Absorption Fine-Structure Studies of the Internal Aggregate Structure in Lightly Sulfonated Polystyrene. 1. Determination of the Coordination Environment about the Cation. *Macromolecule*, 27, 6627-6634.
- Grady, B.P. (2008). Review and critical analysis of the morphology of random ionomers across many length scales. *Polymer Engineering Science*, 48(6), 1029-1051.
- Grigoriadi, K., Westrik, J.B.H.M., Vogiatzis, G.G., van Breemen, L.C.A., Anderson, P.D., and Hutter, M. (2019). Physical ageing of polystyrene: Does tacticity play a role? *Macromolecules*, 52, 5948–5954.

- Haliloglu, T., and Mattice, W.L. (1999). Detection of the onset of demixing in simulations of polypropylene melts in which the chains differ only in stereochemical composition. *Journal of Chemical Physics*, *111*, 4327–4333.
- Hatakeyama, M., and Faller, R. (2007). Coarse-grained simulations of ABA amphiphilic triblock copolymer solutions in thin films. *Physical Chemistry Chemical Physics*, *9*, 4662–4672.
- Helfand, E., and Tagami, Y. (1972). Theory of interface between immiscible polymers. *Journal of Chemical Physics*, *57*, 1812–1813.
- Holliday, L. Ed. (1975). *Ionic Polymers*. London: Applied Science Publishers.
- Jalilehvand, F., Spangberg, D., Lindqvist-Reis, P., Hermansson, K., Persson, I., and Sandstrom, M. (2001). Hydration of the Calcium Ion. An EXAFS, Large-Angle X-ray Scattering, and Molecular Dynamics Simulation Study. *Journal of the American Chemical Society*, *123*, 431-441.
- Jang, J.H., and Mattice, W.L. (2000). A Monte Carlo simulation for the effect of compression of an amorphous polyethylene melt in very thin confined geometry. *Macromolecules*, *33*, 1467–1472.
- Kawahara, S., Suksawad, P., Yamamoto, Y., and Kuroda, H. (2009). Nanomatrix Channel for Ionic Molecular Transportation. *Macromolecules*, *42*, 8557-8560.
- Kim, J., Kim, B., and Jung, B. (2002). Proton conductivity and methanol permeability of membranes made from partially sulfonated polystyrene-block-poly (ethylene-ran-butylene)-block-polystyrene copolymers. *Journal of Membrane Science*, *207*(1), 129–137.
- Kotelyanskii, M., and Theodorou, D.N. (2008). *Simulation Methods For Polymers*. Boca Raton: CRS press.
- Lee, P.A., Citrin, P.H., Eisenberger, P., and Kincaid, B.M. (1981). Extended x-ray absorption fine structure—its strengths and limitations as a structural tool. *Reviews of Modern Physics*, *53*, 769-806.
- Logotheti, G.E., and Theodorou, D.N. (2007). Segmental and Chain Dynamics of Isotactic Polypropylene Melts. *Macromolecules*, *40*(6), 2235-2245.
- Ludovice, P.J. (1989). *Doctoral thesis*. Cambridge: Massachusetts Institute of Technology.

- Mansfield, K.F., and Theodorou, D.N. (1990). Atomistic simulation of a glassy polymer surface. *Macromolecules*, *23*, 4430–4445.
- Marrink, S.J., Vries, A.H., and Mark, A.E. (2003). Coarse grained model for semiquantitative lipid simulations. *Journal of Physical Chemistry B*, *108*, 750–760.
- Marrink, S.J., Risselada, H.J., Yefimov, S., Tieleman, D.P., and Vries, A.H. (2007). The MARTINI force field: coarse grained model for biomolecular simulation. *Journal of Physical Chemistry B*, *111*, 7812–7824.
- Meerwall, E.D., Waheed, N., and Mattice, W.L. (2009). Effect of stereochemistry on diffusion of polypropylene melts: comparison of simulation and experiment. *Macromolecules*, *42*, 8864–8869.
- Megyessy, T., Grosz, T., Radnai, T., Bako, I., and Palinkas, G. (2004). Solvation of Calcium Ion in Polar Solvents: An X-ray Diffraction and ab Initio Study. *Journal of Physical Chemistry A*, *108*, 7261–7271.
- Metropolis, N., Rosenbluth, A.W., Rosenbluth, M.N., Teller, A.H., and Teller, E. (1953). Equation of state calculations by fast computing machine. *Journal of Chemical Physics*, *21*, 1087–1092.
- Misra, S., Fleming, P.D., and Mattice, W.L. (1995). Structure and energy of thin films of poly-(1,4-cis-butadiene): a new atomistic approach. *Journal of Computer-Aided Material Design*, *2*, 101–112.
- Monnerie, L., and Suter U.W. (1994). *Atomistic modeling of physical properties (advances in polymer science, 116)*. Berlin: Springer.
- Monticeli, L., Kandasamy, S.K., Periolo, X., Larson, R.G., Tieleman, D.P., and Marrink, S.J. (2008). The MARTINI coarse-grained force field: extension to proteins. *Journal of Chemical Theory and Computation*, *4*, 819–834.
- Negash, S., Tatek, Y.B., and Tsige, M. (2018). Polystyrene adsorbed onto solid surfaces. *Journal of Chemical Physics*, *148*, 134705-1-134705–12.
- Overberger, C. (1985). Copolymerization: 1. general remarks; 2. selective examples of copolymerizations. *Journal of Polymer Science: Polymer Symposia*, *72*, 67–69.
- Pasztor, A.J., Landes, B.G., and Karjala, P.J. (1991). Thermal properties of syndiotactic polystyrene. *Thermochimica Acta*, *177*, 187-195.

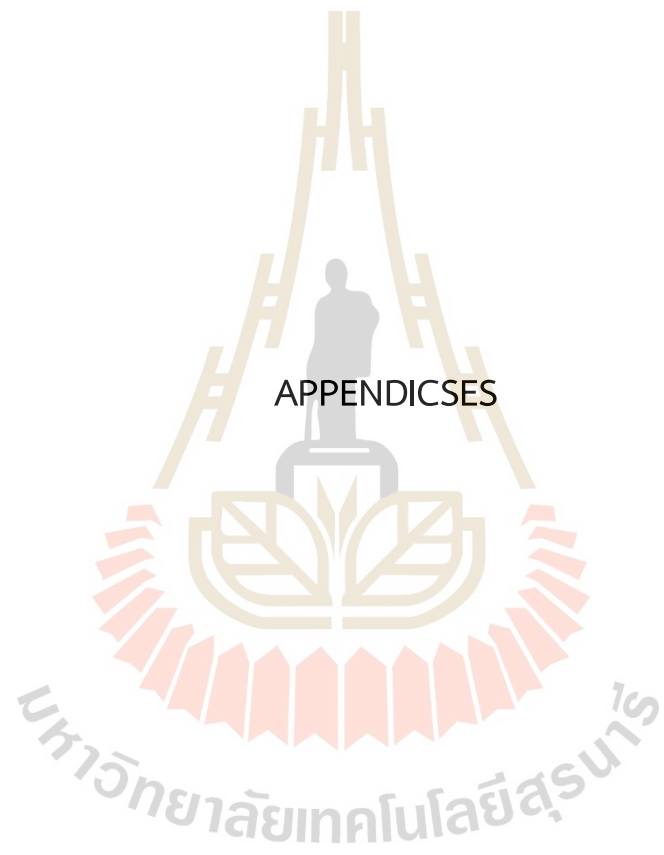
- Persson, K. (2014). *Materials Data on CaCO₃ (SG:167) by Materials Project*. The Materials Project.
- Poling, B.E., Prausnitz, J.M., and O'Connell, J.P. (2000). *The properties of gases and liquids, 5th edn. McGraw-Hill*. New York: Education.
- Rapold, R.F., and Mattice, W.L. (1995). New high-coordination lattice model for rotational isomeric state polymer-chains. *Journal of the Chemical Society Faraday Transactions, 91*, 2435–2441.
- Ravel, B., and Newville, M. (2005). ATHENA, ARTEMIS, HEPHAESTUS: data analysis for X-ray absorption spectroscopy using IFEFFIT. *Journal of Synchrotron Radiation, 12*, 537-541.
- Rehan, M., Mattice, W.L., and Suter, U.W. (1997). *Rotational isomeric state models in macromolecular systems (Advances in polymer science 131/132)*. Berlin: Springer.
- Rehr, J.J., Zabinsky, S.I., and Albert, R.C. (1992). High-order multiple-scattering calculations of x-ray-absorption fine structure. *Physical Review Letters, 69*, 3397-3400.
- Safronova, E.Y., Golubenko, D.V., Shevlyakova, N.V., D'yakova, M.G., Tverskoi, V.A., Dammak, L., and Yaroslavtsev, A.B. (2016). New cation-exchange membranes based on cross-linked sulfonated polystyrene and polyethylene for power generation systems. *Journal of Membrane Science, 515*, 196–203.
- Scheirs, J., and Priddy, D.B. (2003). *Modern Styrenic Polymers: Polystyrenes and Styrenic Copolymers*. New York: Wiley.
- Shaffer, J.S. (1995). Monte Carlo simulations of random copolymers near solid surfaces. *Macromolecules, 28*, 7447–7453.
- Sloan, J.M., Suleiman, D., Napadensky, E., and Craeford, D.M. (2008). *Thermo Stability of Highly Sulfonated Poly(styrene-isobutylene-styrene) Block Copolymers: Effects of Sulfonation and Counter-Ion Substitution*. Army Research Laboratory.
- Solc, K., and Stockmayer, W.H. (1971). Shape of random-flight chains. *Journal of Chemical Physics, 54*, 2756–2757.
- Solc, K. (1971). Shape of a random-flight chain. *Journal of Chemical Physics, 55*, 335–344.

- Stamm, M. (1992). Polymer interfaces on a molecular scale: comparison of techniques and some examples. *Advances in Polymer Science*, *100*, 357-400.
- Stern, E.A., Sayers, D.E., and Lytle, F.W. (1975). Extended x-ray absorption fine structure technique. III. Determination of physical parameters. *Physical Review B*, *11*, 4846.
- Takebe, T., Yamasaki, K., Funaki, K., and Malanga, M. (2009). In *Syndiotactic polystyrene: Synthesis, characterization, processing, and applications*. Hoboken: John Wiley & Sons.
- Tant, M., and Wilkes, G.L. (1987). "Viscoelastic behavior of ionomers in bulk and solution," in *Structure and Properties of Ionomers*. Reidel: Dordrecht.
- Teo, B.K. (1986). *EXAFS: Basic Principles and Data Analysis*. New York: Springer-Verlag.
- Vao-soongnern, V., Doruker, P., and Mattice, W.L. (1999). Simulation of an amorphous polyethylene nanofiber on a high coordination lattice. *Macromolecular Theory and Simulations*, *9*, 1-13.
- Vao-soongnern, V., and Mattice, W.L. (2000). Topological effects on static and dynamic properties in an amorphous nanofiber composed of cyclic polymers. *Macromolecular Theory and Simulations*, *9*, 570-577.
- Vao-songnern, V., Ozisik, R., and Mattice, W.L. (2001). Monte Carlo simulation of the structures and dynamics of amorphous polyethylene nanoparticles. *Macromolecular Theory and Simulations*, *10*, 553-563.
- Waheed, N., Mattice, W.L., and Meerwall, E.D. (2007). Enhanced diffusion at intermediate stereochemical composition in polypropylene by dynamical Monte Carlo. *Macromolecules*, *40*, 1504-1511.
- Wallace, E., and Sansom, M.S.P. (2007). Carbon nanotube/detergent interactions via coarse-grained molecular dynamics. *Nano Letters*, *7*, 1923-1328.
- Xenoview Visualization for atomistic simulations. (2002). Rensselaer polytechnic institute. Accessed 18 November 2020
- Yarusso, D. J., and Cooper, S. L. (1983). Microstructure of ionomers: interpretation of small-angle x-ray scattering data. *Macromolecules*, *16*(12), 1871-1880.
- Yoon, D.Y., Sundararajan, P.R., and Flory, P.J. (1975). Conformation characteristics of polystyrene. *Macromolecules*, *1*, 776-783.

Zho, N.C., Chan, C.D., and Winey, K.I. (2008). Reconciling STEM and X-ray Scattering Data to Determine the Nanoscale Ionic Aggregate Morphology in Sulfonated Polystyrene Ionomers. *Macromolecules*, 41(16), 6134-6140.



APPENDICES



APPENDIX A
INTERNATIONAL CONFERENCE I

The 21st International Union of Materials Research
Societies – International Conference in Asia
(IUMRS-ICA2020), 23-26 February 2021
The Empress Convention Center, Chiang Mai, Thailand

Development a method to generate the fully atomistic model of amorphous
polystyrene and prediction of material properties

Kamonthira Wichai^{a,b}, Visit Vao-soongnern^{b*}

^a Department of Macromolecular Science, Graduate School of Science, Osaka
University, Toyonaka Osaka, 560-0043, Japan.

^b Laboratory of Computational and Applied Polymer Science (LCAPS), School of
Chemistry, Institute of Science, Suranaree University of Technology, Nakhon
Ratchasima 30000, Thailand

[E-mail: kamonthira.mod@gmail.com](mailto:kamonthira.mod@gmail.com), visit@sut.ac.th*

Abstract

Recent development of multiscale simulation of amorphous polymeric materials at the bulk density is presented. Polystyrene (PS), $-\text{[CH}_2\text{-CH(C}_6\text{H}_5\text{)]-}$, with different chain tacticity was selected to illustrate the method. First, the original rotational isomeric state (RIS) model of polystyrene was modified to coarse-grained version and then mapped onto the second nearest neighbour diamond (2nd) lattice.

The average nonbonded interactions were represented by the discretized Lennard Jones (LJ) potential. Bulk amorphous PS was easily generated and equilibrated using lattice Monte Carlo method. On-lattice properties such as molecular size and conformational statistics agree well with the experiment. Then, fully atomistic amorphous PS models can be obtained by the reverse mapping procedure to recover the missing phenyl rings and C, H atoms. After an energy minimization step, material properties including torsional angle distribution, solubility parameter and static neutron scattering structure factor are in good agreement with experimental results. Static structure deformation was employed to determine the elastic constants. Calculated values for Young's modulus, Poisson's ratio, bulk modulus and shear modulus are also reported as a function of chain tacticities.

“Keyword: Polystyrene; Atomistic model; multiscale molecular simulation; tacticities”



มหาวิทยาลัยเทคโนโลยีสุรนารี

APPENDIX B
INTERNATIONAL CONFERENCE II

POLY-CHAR 2020 [Venice], April 12-14, 2021

Multiscale molecular simulation for amorphous polystyrene

Kamonthira Wichai^{1,2}, [Visit Vao-soongnern](mailto:visit.vao-soongnern@sut.ac.th)¹

¹ *Laboratory of Computational and Applied Polymer Science (LCAPS), School of Chemistry, Institute of Science, Suranaree University of Technology, Nakhon Ratchasima 30000, Thailand*

² *Department of Macromolecular Science, Graduate School of Science, Osaka University, Toyonaka Osaka, 560-0043, Japan.*

email: visit@sut.ac.th

Abstract

Recent development of multiscale simulation of amorphous polymeric materials at the bulk density [1] is applied to polystyrene (PS), $-\text{[CH}_2\text{-CH(C}_6\text{H}_5\text{)]-}$, with different chain tacticity and compared with the conventional ‘static’ method [2]. Coarse-grained PS chains are mapped onto the second nearest neighbor diamond (2nd) lattice incorporating short- and long-range interactions from the modified rotational isomeric state (RIS) model and the discretized Lennard-Jones (LJ) potential function, respectively. Bulk amorphous PS structures composed of 14 chains with 42 monomer units are easily generated and equilibrated on lattice Monte Carlo (MC) simulation. The on-lattice properties including molecular size, conformational statistics and chain dynamics are compared for each chain tacticity. The diffusion rates are

generally ordered as: *isotactic* < *atactic* << *syndiotactic* chains. The amplitude of diffusion is mainly related to the intermolecular effect *i.e.* chain packing among neighboring chains. Fully atomistic amorphous PS models at the bulk density can be obtained by the reverse-mapping procedure to convert the coarse-grained chains to recover the missing phenyl rings and C, H atoms. After energy minimization, molecular and material properties including torsional angle distribution, solubility parameter, radial distribution function and static neutron scattering structure factor are in good agreement with experimental results.

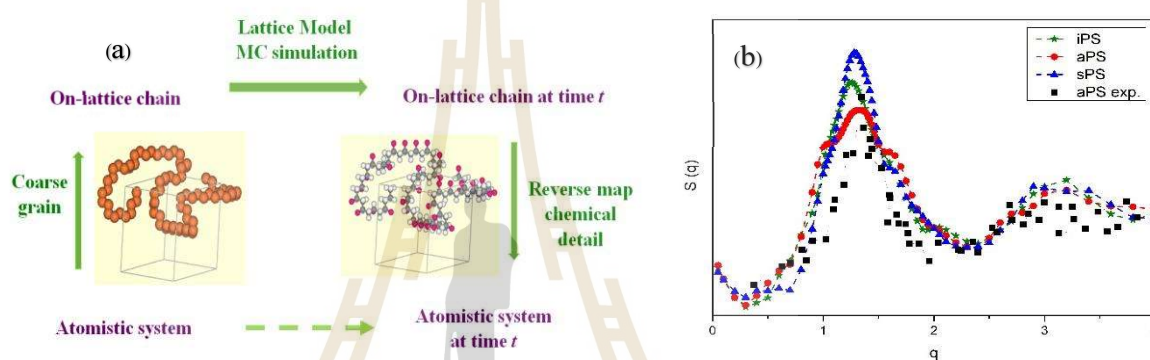


Figure 1. (a) Multiscale simulation to generate and equilibrate fully atomistic polystyrene model

Acknowledgements

Jointed research grant from National Research Council of Thailand (NRCT) and Suranaree University of Technology, SUT (NRCT5-RSA63009-07). KW thanks the Development and Promotion of Science and Technology Talented (DPST) scholarship.

(b) Static neutron scattering structure factor of polystyrene from simulation and experiment.

References

- [1] V. Vao-Soongnern, A multiscale simulation model for poly(ethylene oxide). *Polym. Sci. Ser. A* 2014, 56, 928–935.
- [2] R.F. Rapold, U.W. Suter, D.N. Theodorou, Static atomistic modelling of the structure and ring dynamics of bulk amorphous polystyrene, *Macromolecular Theory and Simulations*. 1994, 3, 19

CURRICULUM VITAE

Name: Kamonthira Wichai

Date of Birth: 10th January, 1997 at Khemmarat Ubonratchatani Thailand

Education:

2019–2022 M. Sc. Chemistry • School of Science • Suranaree University of Technology • with DPST scholarship Thailand and M. Sc. Macromolecule • School of Science • Osaka University • with JASSO scholarship • GPA 4.00

2015–2019 B. Sc. Chemistry • School of Science • Suranaree University of Technology • with DPST and Suranaree University scholarships • GPA 3.95

2012–2015 Science-Mathematics high school • Khemmarat Pittayakom School • GPA 3.91

Publications:

1. Wichai, K., and Vao-soongnern, V. (2021). A multiscale simulation of amorphous polystyrene. *J Polym Res* 28, 109.
2. Yokokoji, A., Kitayama, W., Wichai, K., Urakawa, O., Matsumoto, A., Vao-Soongnern, V., and Inoue, T. (2021). Viscoelastic Relaxation of Polymerized Ionic Liquid and Lithium Salt Mixtures: Effect of Salt Concentration. *Polymers*, 13, 1772.
3. Wichai, K., and Vao-soongnern, V. (2021). Monte Carlo simulation of molecular and structural properties of random copolymer thin films. *Journal of Molecular Modeling*, 27, 301.

Grants and Fellowships

1. Development and Promotion of Science and Technology Talents Project (DPST) scholarship, Thai government scholarship.
2. Scholarship Program in Honor of the 84th Birthday of Suranaree University of Technology.